TRIBHUVAN UNIVERSITY

INSTITUTE OF ENGINEERING

PULCHOWK CAMPUS

THESIS NO. 079/MSCCD/001

Black Carbon from Wildfires and Its Potential Impact on Surface Energy Balance of Khumbu Glacier, Nepal

by

Aashutosh Paudel

A THESIS

SUBMITTED TO THE DEPARTMENT OF APPLIED SCIENCES AND CHEMICAL ENGINEERING IN PARTIAL FULFILLMENT OF THE REQUIREMENTS FOR THE DEGREE OF MASTER'S IN CLIMATE CHANGE AND DEVELOPMENT

DEPARTMENT OF APPLIED SCIENCE AND CHEMICAL ENGINEERING

LALITPUR, NEPAL

MAY, 2025

COPYRIGHT

TRIBHUVAN UNIVERSITY

INSTITUTE OF ENGINEERING

PULCHOWK CAMPUS

DEPARTMENT OF APPLIED SCIENCES AND CHEMICAL ENGINEERING

The thesis titled "**Black Carbon from Wildfires and its Potential Impact on Surface Energy Balance of Khumbu Glacier, Nepal**" prepared and submitted by Aashutosh Paudel in partial fulfillment of the requirements for the degree of Master of Science (M. Sc.) in Climate Change and Development has been examined by us and is accepted for the award of M. Sc. in Climate Change and Development by Tribhuvan University.

The undersigned certify that they have read, and recommended to the Institute of Engineering for acceptance, a thesis report entitled "**Black Carbon from Wildfires and Its Potential Impact on Surface Energy Balance of Khumbu Glacier, Nepal"** submitted by Aashutosh Paudel in partial fulfillment of the requirements for the degree of Master in Climate Change and Development.

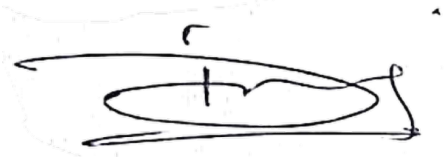

Supervisor

Asso. Prof. Dhiraj Pradhananga

Department of Meteorology,

Tri-Chandra Multiple Campus

Tribhuvan University

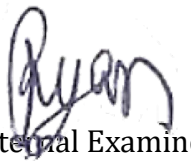

External Examiner

Prof. Rijan Bhakta Kayastha

Department of Environmental Science and Engineering

Kathmandu University

Program Coordinator

Prof. Dr. Rinita Rajbhandari

Climate Change and Development Program

Department of Applied Sciences and Chemical Engineering

Date: May, 2025

DECLARATION

I hereby declare that this study, titled "**Black Carbon from Wildfires and its Potential Impact on Surface Energy Balance of Khumbu Glacier, Nepal**"is based on my original research work. Related works on the topic by other researchers have been duly acknowledged. I owe all the liabilities relating to the accuracy and authenticity of the data and any other information included hereunder.

Aashutosh Paudel

079MSCCD001

MSc in Climate Change and Development

Date: May, 2025

ACKNOWLEDGEMENT

I would like to express my gratitude to Professor Rinita Rajbhandari, our program coordinator of the Applied Sciences and Chemical Engineering Department. I also thank Professor Dr. Khem Poudyal for providing me with this opportunity. I would also like to thank my friends and family who supported me and offered deep insight into the study.

I would like to express my deepest appreciation to my Supervisor, Dr. Dhiraj Pradhananga, who guided me throughout this project.

Special thanks are conveyed to Mr. Pramesh Karki and Ms. Apechhya Aryal for their unwavering support.

The love and goodwill of my family, which served as a continual source of inspiration for me during this time, is something I would also like to acknowledge.

Aashutosh Paudel

079/MSCCD/001

May 2025

ABSTRACT

Wildfires release significant Black Carbon (BC), which can be transported over long distances and deposited onto high-altitude Himalayan glaciers, altering surface albedo and accelerating melt. This study investigates potential transport pathways and seasonal patterns of wildfire-derived BC impacting the Khumbu Glacier in 2021, alongside the glacier's surface energy balance (SEB). Hybrid Single Particle-Lagrangian Integrated Trajectory (HYSPLIT) backward trajectory analysis, combined with Visible Infrared Imaging Radiometer Suite (VIIRS) fire data, identified key pre-monsoon (March-May) southwesterly transport pathways originating from fire-prone regions, particularly in Nepal and India. Potential BC emissions along these pathways, estimated using Intergovernmental Panel on Climate Change (IPCC) equations based on burned area derived from Convex Hull methods and satellite-based estimates, exhibited a pronounced seasonal peak, totaling approximately 134 tonnes over March-April 2021, with a peak of around 93.8 tonnes in April. However, considerable uncertainty exists due to challenges in accurately estimating burned areas. Independently, the glacier's SEB was calculated using High Asia Refined (HAR) analysis data, including time-varying albedo. This analysis identified the pre-monsoon onset as critical for melt initiation, driven primarily by net shortwave radiation (S_net) leading to a positive net energy balance (Qm). While direct quantification of BC deposition and its specific albedo impact was beyond the study's scope, the SEB was shown to be responsive to albedo reductions. The temporal coincidence of peak potential BC emissions/transport with the glacier's heightened sensitivity to albedo changes during the pre-monsoon suggests a plausible role for wildfire BC in modulating the surface energy balance and potentially enhancing melt. These findings underscore the significance of wildfire emissions for Himalayan cryosphere dynamics and highlight the need for further research integrating BC transport and deposition modeling to quantitatively evaluate this linkage.

Keywords: Black Carbon, Wildfires, HYSPLIT, Backward Trajectories, Atmospheric Transport, Khumbu Glacier, Surface Energy Balance (SEB)

TABLE OF CONTENTS

LIST OF TABLES

LIST OF FIGURES

ABBREVIATIONS

AOD	Aerosol Optical Depth
ARL	Air Resource Laboratory
BC	Black Carbon
CRB	Crop Residue Burning
DEM	Digital Elevation Models
DHM	Department of Hydrology and Meteorology
ECMWF	European Centre for Medium-Range Weather Forecasts
EF	Emission Factors
FINN	The Fire Inventory from NCAR
FIRMS	Fire Information for Resource Management System
FNL	Final Operational Global Analysis
FRP	Fire Radiative Power
GDAS	Global Data Assimilation System
GFAS	Global Fire Assimilation System
GFS	Global Forecast System
GIS	Geographic Information System
HAR	High Asia Refined
HTP	High Tibetan Plateau
HYSPLIT	Hybrid Single Particle-Lagrangian Integrated Trajectory
ICIMOD	International centre for Integrated Mountain Development
IGBP	International Geosphere Biosphere Program
IGP	Indo-Gangetic Plain
IPCC	Intergovernmental Panel on Climate Change
LAI	Light Absorbing Impurities
LULC	Land Use Land Cover
MODIS	Moderate Resolution Imaging Spectroradiometer
NCAR	National Center for Atmospheric Research
NCEP	National Centers for Environmental Prediction
NCOP	Nepal Climate Observatory Pyramid

NOAA	National Oceanic and Atmospheric Administration
OC	Organic Carbon
PBL	Planetary Boundary Layer
SEBM	Surface Energy Balance Model
TOA	Top of the Atmosphere
TP	Tibetan Plateau
VIIRS	Visible Infrared Imaging Radiometer Suite
WRF	Weather Research and Forecasting Model

CHAPTER 1. INTRODUCTION

1.1 Background

Black Carbon (BC) emissions are typically distinguished by their source, generated through the incomplete combustion of biomass (forest fires, grass burning, etc.), biofuels (firewood, charcoal, etc.), and fossil fuels (coal, petroleum products) (Kostrykin et al., 2021a).If BC is incorporated into snow, it can lead to additional warming due to its effect on the albedo of snow and ice, causing accelerated melting (Jacobi et al., 2015a). Due to its high light-absorbing efficiency over visible and infrared wavelengths, BC has been considered the second largest anthropogenic contributor to global warming after CO_2 (Gul et al., 2021). In addition, black carbon can be suspended as fine particles in the atmosphere for approximately one week, transported far from its emission sources, and then removed by both dry and wet deposition (Chen et al., 2018). Dry deposition is typically smaller in magnitude compared to wet deposition (He et al., 2017);(Han et al., 2020). Wet deposition is the primary process for removing BC, and it is responsible for over 90% of its total deposition in the Arctic (Dou & Xiao, 2016). Once deposited, BC remains in the upper layers of the snowpack, where it can persist until melting redistributes or removes it, leading to prolonged surface darkening and increased solar radiation absorption.

Understanding the transport pathways and seasonal variability of BC reaching the Khumbu Glacier is essential for assessing its impact on glacier melt. Since 2006, measurements taken at the Nepal Climate Observatory at Pyramid (NCO-P), located at 5079 meters above sea level, have confirmed that aerosols, including BC, can be effectively transported from their sources to high-altitude regions in the Himalayas (Marinoni et al., 2010) and has been similarly reported by (Bonasoni et al., 2010). This study utilizes Hybrid Single Particle-Lagrangian Integrated Trajectory (HYSPLIT) trajectory analysis to investigate the transport pathways of wildfire-induced BC and its seasonal impact on the Khumbu Glacier. By analyzing backward trajectories, key source areas, such as industrial zones, biomass-burning regions, and wildfire-affected areas, can be identified. Additionally, Visible Infrared Imaging Radiometer Suite (VIIRS) fire data is used to filter fire events along the trajectory pathways, providing insights into the role of seasonal wildfires in BC transport. Emissions from wildfires, particularly crown fires in the forest canopy, can easily rise to altitudes above 5 km, reaching up to 8-9 km in the mid-troposphere above the forest crown (Vadrevu et al., 2012) and (You & Xu, 2022). Wildfires emit massive volumes of BC particles into the

atmosphere, which can reach the lower stratosphere and generate significant radiative forcing(Ditas et al., 2018).

Wildfires are a growing concern in South Asia, significantly contributing to BC emissions that can be transported over long distances and deposited onto high-altitude glaciers. The Himalayan glaciers, including the Khumbu Glacier, are particularly vulnerable to such deposition due to their proximity to frequent biomass-burning events in Nepal, India, and China. During the pre-monsoon season**,** wildfires become more intense due to dry conditions, increasing the amount of BC in the atmosphere. Once deposited on glacier surfaces, BC reduces albedo, enhances heat absorption, and accelerates glacial melt rates**.** The real-time observations and simulation studies show that BC aerosols were transported substantially to the snow-capped Mt. Everest region. Surface glacier melt was affected by upwind wildfire activity by reducing surface albedo due to soot deposition on the glacier and by altering atmospheric conditions above the glacier through smoke (Aubry-Wake et al., 2022). The role of forest fires in contributing to snow and glacier melt is gaining greater recognition (Kaspari et al., 2015) by transfer and accumulation over the Himalayan area and its effect on snow albedo, leading to accelerated snow and ice melt has been a prominent topic of discussion in the research community (Gul et al., 2021). Because solar radiation is the primary source of heat for surface melting on nearly all mountain glaciers, their sensitivity to BC-induced changes in surface reflectance is critically important for their survival (Hodson, 2014).

1.2 Objective of the Study

General Objective:

To investigate potential atmospheric transport pathways of wildfire-derived BC towards the Khumbu Glacier, examine seasonal emission characteristics and air circulation patterns, and evaluate the sensitivity of the glacier's surface energy balance using regional climate data High Asia Refined (HAR)v2.

Specific Objectives:

1. Analyze seasonal transport pathways to Khumbu Glacier using the HYSPLIT model.
2. To identify significant biomass-burning regions potentially impacting the Khumbu Glacier during the pre-monsoon season.
3. To quantify potential BC emissions from fire sources along the transport routes.

4. To evaluate the seasonal surface energy balance sensitivity for Khumbu Glacier using HARv2 datasets.

1.3 Problem Statement

In Nepal, wildfire "season" comes into activity in December (Mangsir-Poush), and attains its highest point in April (Chaitra-Baishakh), and the rate subsequently declines with the monsoon in June (Jestha-Asar) (Matin et al., 2017).In spring 2021, Nepal experienced an unprecedented wildfire season, with the detection of active fires occurring at a rate 10 times higher than the average observed between 2001 and 2020 (Pokharel, 2022).In Nepal, the Tarai region, especially the western part, sees the most severe wildfires. The Siwalik region and the middle mountain areas follow, with the second and third-highest incidences of fires, respectively (Bhujel et al., 2019). The increasing emissions from Crop Residue Burning (CRB) in regions like the Indo-Gangetic Plain (IGP) have led to a rise in BC concentrations, significantly affecting air quality and contributing to accelerated glacier melt in nearby high-altitude areas, which poses both environmental and public health risks (Sarkar et al., 2018).

While numerous studies have quantified the amount of BC deposited in the Himalayan regions of Nepal, there is a notable gap in research specifically addressing the impact of wildfire-induced BC on snowmelt acceleration. Most existing research focuses on the overall contributions of black carbon from various sources, but the distinct influence of BC originating from wildfires on the rate of snowmelt remains underexplored. Despite glaciers in the Himalayan region retreating, it remains unclear whether this retreat is driven by rising temperatures or the deposition of BC and other Light Absorbing Impurities (LAI) (Kaspari et al., 2014a).

1.4 Significance of the Study

This work is important because it tackles the rising issue of BC transmission to Himalayan glaciers, especially the Khumbu Glacier, caused by wildfires. This study highlights possible origins and seasonal fluctuations by using HYSPLIT backward trajectory analysis to better understand how wildfire emissions from far-off sources contribute to BC transport along atmospheric routes into the Himalayas.

1. This study provides insights into the atmospheric transport mechanisms that carry BC from wildfire-prone regions in South Asia to high-altitude glaciers, also emphasizing the role of pre-monsoon southwesterly winds play in the long-distance movement of BC.

2. The study illustrates how emissions from burning biomass in South Asia might alter cryospheric systems by connecting regional wildfire events to more general climatic implications.
3. The results highlight the necessity of better wildfire management techniques and transboundary air pollution control in order to reduce BC emissions. In South Asia and the Himalayas, the study supports initiatives to create policies that address air quality, forest fire control, and climate adaptation.
4. It offers a platform for further research on BC deposition in other glaciated areas impacted by pollution from far-off sources.

This study is crucial for understanding the long-range transport pathways of wildfire-related BC to the Himalayas and the seasonal patterns influencing its movement. The findings provide valuable insights into atmospheric transport dynamics, contributing to scientific research on wildfire emissions and their potential implications for Himalayan glaciers.

1.5 Scope and Limitations

Scope:

1. This study focuses on the Khumbu Glacier in the Himalayas, analyzing the potential transport of wildfire-derived BC to this region in the year 2021 with a focus on seasonal variations, particularly during the pre-monsoon period.
2. Estimation of potential BC emissions originating from identified fire sources located along key atmospheric transport pathways leading towards the study region during the pre-monsoon period.
3. Wildfire events are identified using VIIRS satellite fire data, overlaying with the MODIS Vegetation data and back-trajectory pathways, helping to pinpoint potential BC sources contributing to long-range transport.
4. This study will characterize the daily and monthly SEMB components of the Khumbu Glacier during the 2021 pre-monsoon season, using meteorological data, including observed albedo, to establish baseline energy dynamics and identify the primary melt season.

Limitations:

1. Backward trajectory models like HYSPLIT rely on meteorological input data (e.g., GDAS, NCEP), which have their own spatial and temporal resolution limitations and inherent model inaccuracies.
2. The satellite-based fire detection system VIIRS has drawbacks. Cloud cover can mask active flames; minor or low-intensity fires may go undetected; and the data reflects snapshots in time, potentially missing peak burning periods or smoldering combustion, all of which generate BC.
3. Estimating BC emissions from identified fires poses high uncertainty. It takes assumptions regarding fuel types (derived from land cover), fuel loading, combustion efficiency, and acceptable BC emission factors, all of which can vary greatly and are sometimes inadequately limited for individual geographies or fire situations.
4. The study connects possible sources to the glacier region via trajectories, but it does not explicitly model the complicated processes of air movement, transformation (aging), and deposition (dry and wet) of BC onto the glacier surface. The exact volume and spatial distribution of BC reaching and depositing on the Khumbu remain unknown, and it is inherently challenging.
5. Because the neighboring fire event source regions from the trajectory might potentially aid in the transport of BC to the glacier, it is challenging to pinpoint the precise source region of the possible wildfire events.
6. Accurately quantifying burned area for emission estimates faces limitations across all methods. Satellite products (e.g., MODIS) and active fire inferences (e.g., VIIRS clustering/hulls) suffer from potential overestimation due to detection limits and algorithmic challenges.
7. The research utilizes trajectory analysis, HYSPLIT, and Surface Energy Balance Model (SEMB) sensitivity, methods effective for source identification and demonstrating potential melt impacts via albedo, but insufficient for fully simulating the complex interactions of BC transport, atmospheric processing, deposition, and snow physics. Accurately quantifying these coupled processes requires integrated chemical transport and sophisticated snow/ice models (e.g., WRF-Chem, SNICAR), the application of which was beyond the scope of this study due to resource and time constraints.

CHAPTER 2. LITERATURE REVIEW

The impact of BC on glacier melt has been a subject of increasing scientific inquiry due to its significant implications for water resources and sea-level rise. This literature review aims to synthesize existing research on the role of wildfire-induced BC in accelerating glacier melt, focusing on the Khumbu region of Nepal, an area highly vulnerable to both the transport of BC from wildfire events and following glacial retreat.

2.1 HYSPLIT Model for Trajectory Analysis

The Air Resource Laboratory (ARL) HYSPLIT model is a full-fledged system for simulating both simple air parcel trajectories and complex dispersion and deposition scenarios (Draxler & Rolph, 2010). The model uses a combination of the Lagrangian and Eulerian approaches, with the former assuming air parcel advection and diffusion from a starting point and the latter observing a fixed three-dimensional grid across time (Castagna et al., 2021). In this study, the Lagrangian technique within HYSPLIT is employed to compute backward trajectories for identifying potential source regions of BC.HYSPLIT has been previously used to compute 5-day backward trajectories for analyzing long-range atmospheric transport of BC, helping identify source regions influencing the Arctic air mass composition (Vinogradova & Vasileva, 2017). Additionally, the integration of fire data with HYSPLIT trajectories revealed that 52.5% of wildfire emissions detected at the monitoring station were due to long-range transport (Castagna et al., 2021). Similarly, HYSPLIT simulations during the 2019 Siberian wildfire season demonstrated that even short-duration fires can lead to significant BC movement toward the Arctic under favorable wind conditions (Kostrykin et al., 2021b). Back trajectory analysis over Pokhara revealed that aerosol transport to the Himalayan foothills is strongly influenced by transboundary air masses from the IGP and beyond, particularly during winter and pre-monsoon seasons (Regmi et al., 2020), while a similar study in Dhulikhel, Nepal, showed seasonal transport of organic and elemental carbon from both local and regional sources, including South Asia and the Middle East (Chaudhary et al., 2024) The model is used globally to simulate pollutant transport and dispersion for applications such as air quality and emergency response (Stein et al., 2015) and through spatial clustering of air parcel trajectories based on endpoint similarity, it helps identify dominant transport pathways with shared directional patterns (Draxler & Rolph, 2010).

2.2 Black Carbon and its Atmospheric Transport

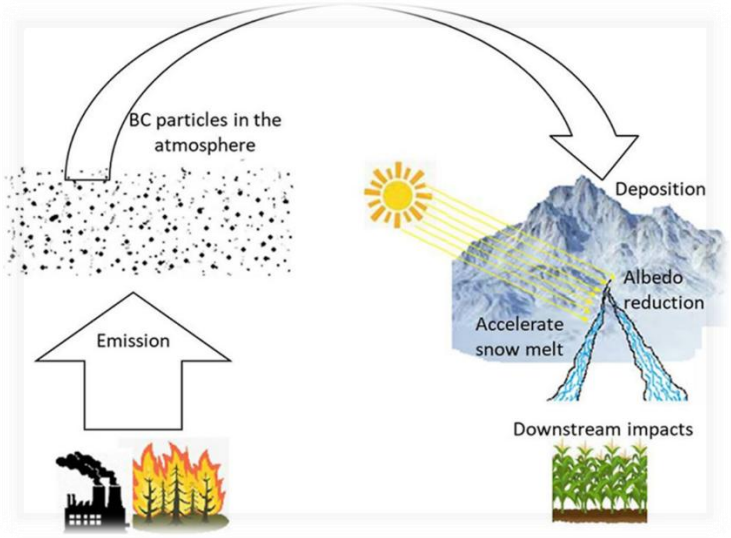

Figure 2-1 Visualization of BC transport from wildfire and industrial emissions, leading to atmospheric deposition on glaciers and potential downstream Impacts

Source: Black carbon impact on glacier melt and potential source contribution. (Gul et al., 2021).

2.2.1 Chemical and Physical Properties

Compared to Organic Carbon (OC), which accounts for approximately 80% of the total aerosol mass released from wildfires, BC makes up only about 10% of the emitted aerosol mass. However, BC is significantly more absorptive. As a result, BC plays a more critical role in influencing climate change factors, such as the aerosol-radiative forcing caused by wildfires (Veira et al., 2016). BC, also known as Soot, influences the atmosphere by changing the radiation balance, which in turn can lead to the formation of clouds (Kim et al., 2005). Several factors influence the increase in Top of Atmosphere (TOA) radiative forcing: (1) BC absorbs solar radiation reflected by the Earth's surface, atmosphere, and clouds, thereby lowering the planet's albedo; (2) soot deposited on snow and sea ice reduces surface albedo; and (3) when soot is embedded in cloud droplets and ice crystals, it enhances absorption, reducing the albedo of clouds (Ramanathan & Carmichael, 2008).

BC is a type of fine PM2.5 that results from incomplete combustion of fossil fuels, biofuel, and biomass. It is made up of pure carbon in several linked forms. According to the literature data, the size of aerosol particles containing BC ranges from 0.01 to 1 micron, which is significant in understanding their transport and climatic effects (Kostrykin et al., 2021a). Based on their optical properties,

aerosols are broadly classified into scattering and absorbing types. Scattering aerosols cool the Earth's surface by reflecting solar radiation, whereas absorbing aerosols heat the atmosphere by absorbing it. BC aerosols, which are carbonaceous, have the maximum absorption potential (Sandeep et al., 2022).

2.2.2 Long-Range Transport and Deposition

Wildfire smoke can drift to distant mountain ranges, darkening glacier surfaces, which leads to increased ice melting by up to 10% compared to simulations where the impacts of fire activity were removed (Aubry-Wake et al., 2022). The interaction of wildfire emissions with atmospheric circulation plays a critical role in determining the extent of BC deposition, with transport patterns shifting based on seasonal wind conditions. The atmospheric BC contribution from Nepal and India combined accounted for approximately 69% (ranging between 64% and 74% depending on the season). This was followed by contributions of 22% from China, 3% from Bangladesh, 2% from Pakistan, and 1% from Bhutan, with the remaining contributions coming from nearby regions (Gul et al., 2021). Though the High Tibetan Plateau (HTP) is generally cleaner and still maintains a relatively pristine environment, recent research has highlighted that atmospheric pollutants, including BC, can be carried across the Himalayas and reach the interior of the HTP (Neupane et al., 2019).Following wildfire events, BC concentrations in glacier snow and ice have been recorded at levels higher than 20 ng/g. This suggests that wildfires have played a substantial role in accelerating glacier melt in the Himalayas, contributing to the overall retreat of these glaciers (You et al., 2016). Additionally, the deposition of BC on glacier surfaces has been linked to changes in surface roughness, further modifying the glacier's melt dynamics and influencing runoff patterns.

During the pre-monsoon season, a significant atmospheric phenomenon emerged where strong brown cloud influence affected 20% of the days, resulting in a substantial 5-fold surge in BC and PM1 concentrations compared to the seasonal baseline (Bonasoni et al., 2010). Severe wildfires in East Siberia during 2019–2021 have surely contributed significantly to increased BC levels in the Khumbu region. Likewise, the PM generated by wildfires can accumulate to very high concentrations, travel vast distances, and threaten densely populated areas far from where the fires originated (Johnston et al., 2011). According to a study done by (Bali et al., 2017), results suggest the potential advection and deposition of BC and OC aerosols in the downwind direction from Uttarakhand to Nepal, as well as over the upper Himalayan glaciated region. The increase in aerosol concentration during the fire period also led to negative aerosol forcing at both the TOA and the

surface, with the effect being more pronounced in Nepal compared to the Uttarakhand region.

2.2.3 Wildfire Trends and Black Carbon Emissions

According to (Matin et al., 2017)From 2003 to 2013, MODIS detected 28,449 fire incidents, which were refined to 21,147 by excluding those with a confidence level below 50%. The fire season, which runs from March to June, accounts for 86.3% of all recorded fires, with the highest activity occurring in April, representing 43.6% of the total, followed by March at 16.31% and May at 15.63% (Vadrevu et al., 2012). In the 2023–24 season, India reported 203,544 forest fire hotspots. While this number indicates the frequency of fire incidents, the actual area burned is typically less than the number of hotspots. For example, in 2016, Haryana alone experienced stubble burning across over 208,000 hectares of land (TheTimesofIndia, 2024). Annually, in the Study done in the Yala Glacier (Gul et al., 2021) Wildfires influence atmospheric conditions across different spatial and temporal scales by releasing gases, particles, water, and heat, with emissions primarily composed of CO_2 (71% by mass), while OC and BC contribute approximately 0.24% and 0.02%, respectively (Liu et al., 2014). Since CO_2 emissions are significantly higher, BC may seem negligible in terms of mass; however, BC has a much higher absorption efficiency for solar radiation, making it a critical factor in reducing surface albedo and accelerating glacier melt.

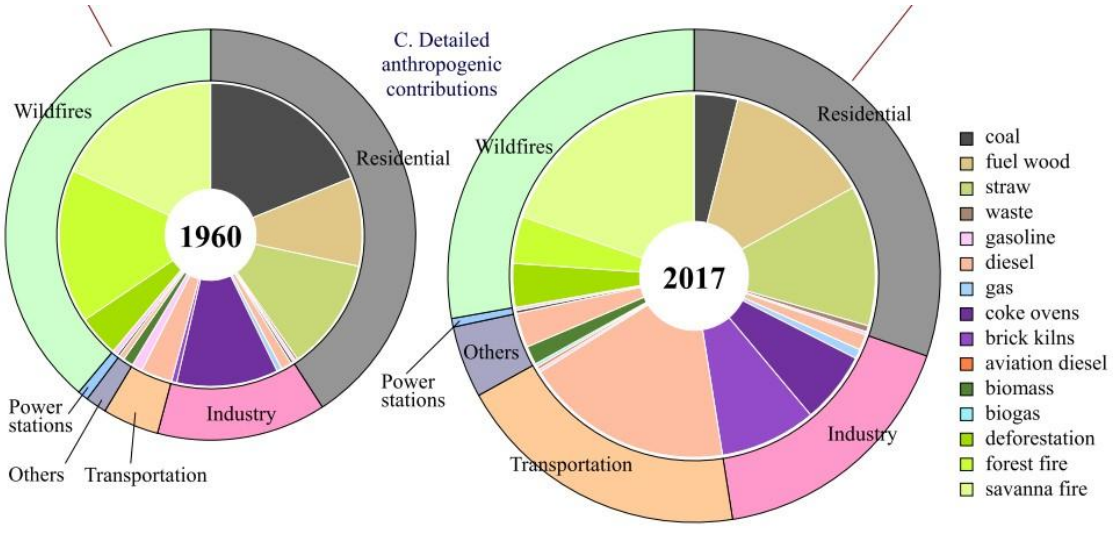

Figure 2-2 Stacked BC emissions from 1960 to 2017 show contributions from (A) wildfires (B) five anthropogenic sources and (C) fuel types (1960 and 2017)

Source from (Xu et al., 2021)

Figure 2-2 presents a comparative analysis of BC emissions in 1960 and 2017, highlighting changes in anthropogenic and wildfire contributions over time. The outer ring categorizes emissions by sector, including wildfires, residential, industry, transportation, power stations, and other sources, while the inner ring provides a detailed breakdown of fuel types such as coal, fuelwood, diesel, biomass, and deforestation. A notable shift is observed in the growing contribution of wildfires, particularly from forest and savanna fires, which have become more dominant in 2017 compared to 1960.

The levels of BC exhibit a temporal pattern closely aligned with that of PM1, displaying significant fluctuations during the pre-monsoon period (with peak minute concentrations exceeding 5000 ng m^{-3}) and markedly lower levels throughout the summer monsoon season (Bonasoni et al., 2010).Soon after being emitted, BC mixes with other aerosol components in the atmosphere. This mixing increases its light absorption, enhances its ability to form liquid-cloud droplets, alters its potential to create ice nuclei, and consequently influences its rate of removal from the atmosphere (Bond et al., 2013).

2.3 Regional BC Impact on Himalayan Glacier

Glaciers in the western Himalayas were predominantly impacted by long-range pollution transported from the Middle East and Central Asia (Gul et al., 2022).In contrast, glaciers in the central Himalayas were primarily influenced by emissions from local and South Asian sources, including Nepal, India, and China, particularly during the pre-monsoon season. The varying sources of BC deposition across different Himalayan regions highlight the complexity of transboundary pollution, necessitating a more region-specific approach to emission mitigation and climate adaptation strategies.(Kaspari et al., 2014b) found that BC and dust deposited in the winter-spring period can accelerate glacier melt if they remain exposed during the summer rather than being covered by fresh snowfall. Conversely, glacier ablation can be further enhanced if melting results in the re-exposure of these impurities. In situ measurements by (Rai et al., 2019) near Yala Glacier, Nepal revealed that BC mass concentrations reached their highest levels during the pre-monsoon season (707.9 ± 541.8 ng m^3), supported by elevated AOD values (0.058 ± 0.002). Mt. Everest could be regarded as a susceptible area under the influence of BC aerosols.(Chen et al., 2018).. BC transport and deposition in high-altitude glacier environments are strongly influenced by seasonal meteorological processes and dominant circulation patterns, as observed in the central-western Himalayas (Karakoti et al., 2023).

2.4 Wildfire BC Emissions Transported to Himalayan Glaciers

Studies indicate that only a small fraction of BC from wildfires actually reaches high-altitude Himalayan glacier regions like Khumbu. For example, observations in Nepal's central Himalayas suggest that on the order of 5% of aerosol pollution emitted in the IGP is transported up to glaciated areas during the pre-monsoon season (*Black Carbon and Glacier Melt - ICIMOD*, 2020).

This implies a low transport efficiency meaning only a few percent of BC emitted at lower elevations (whether from biomass burning or other sources) is lofted and carried to the elevation of glaciers such as Khumbu. One regional model study found that local biomass burning within South Asia contributed only 3–4% of the total BC depositing in the Himalaya Karakoram glaciers in the winter dry season (Alvarado et al., 2018).In summer, regional contributions drop further as long-range transport dominates (up to approx.87% of BC deposition came from outside South Asia during the monsoon). This indicates that while nearby wildfires have some impact, most BC on Himalaya snow originates from distant sources transported by atmospheric currents.

Notably, distant wildfire smoke can still reach the Himalayas given favorable winds. Adjoint sensitivity modeling by (He et al., 2017)showed that even sources as far away as African savanna fires can measurably contribute BC to the Himalayas and Tibetan Plateau (TP) (Kopacz et al., 2011).But overall, South Asian sources (including crop residue burning and forest fires in the Indo-Nepal region) remain the primary contributors in most seasons (Gul et al., 2024). A field study at Yala Glacier (central Nepal) combining in situ data with WRF-Chem modeling attributed approximately 28% of annual BC deposition to biomass-burning sources (forest fires and open burning), versus around 72% from fossil fuel emissions (Gul et al., 2024).This source split underscores that a significant share of the soot on Himalayan snow originates from biomass burning, but fossil fuel pollution is usually larger on an annual basis. Similarly, radiocarbon apportionment of Himalayan snow samples found biomass burning dominates around 64% of BC in the snow (despite contributing only ~39% of BC in the air), consistent with efficient transport and removal of wildfire smoke to the surface (Qi & Wang, 2019).In short, only a few percent of wildfire-emitted BC makes it to the high mountains, but biomass burning can still account for on the order of 20–30% of the soot deposited on glaciers when averaged annually(Gul et al., 2024)(higher during intense fire episodes).

2.5 Fraction of Transported BC Depositing on Glacier Surface

Once BC-laden smoke reaches a glacier region, a large fraction of the aerosol is likely to deposit, especially during precipitation events. Wet scavenging is extremely effective at removing atmospheric BC onto snow and ice. For instance, field measurements in the California Sierra found that snowfall efficiently removes almost all of the atmospheric BC into the snowpack (Hadley, 2008).In the Himalayas, the summer monsoon delivers heavy rainfall/snowfall that scrubs out transported aerosols. Modeling by (Zhang et al., 2015) showed that during monsoon, the BC removal timescale over the Himalayas is <1 day, meaning BC is rapidly scavenged and deposited almost as soon as it arrives.

In the Yala Glacier study, wet deposition was around 196 times larger than dry deposition annually (Gul et al., 2024), indicating that the vast majority of BC that reaches the area is eventually washed out onto the surface. In other words, nearly all transported BC particles will deposit on snow/ice given sufficient precipitation. Even in winter when precipitation is lower, some dry deposition occurs; Yala's measured dry fall-out was around 4.6 μg m^{-2} day^{-1}, totaling nearly 531 μg m^{-2} over the March–May pre-monsoon alone (Gul et al., 2024). This shows that a substantial surface loading of roughly hundreds of μg per m^2 can accumulate from a season of smoke transport.

Overall, studies imply that a large fraction on the order of 50–100% of BC aerosols that reach a glacier will ultimately deposit there rather than simply pass overhead. For example, a modeling analysis for Greenland's ice sheet found that 85% of simulated smoke BC deposition occurred via wet scavenging (Khan et al., 2023). Once smoke was in the vicinity, most of it fell out with snow/rain. In the Himalayas, precipitation efficacy is similar or higher. During one extreme fire season, deposition records from an ice core on Dasuopu (central Himalaya) spiked to "60 times" higher than average BC levels, directly linked to drought-driven forest fire smoke input (Barker et al., 2021).This dramatic case underlines that when dense wildfire smoke does arrive, the deposition efficiency is near-total, yielding massive BC loads in the snow. Thus, for estimation purposes, one can assume the vast majority of BC that is transported to a glacier will deposit onto it, especially under wet-deposition conditions.

2.6 Key Environmental Factors and Example Values

Atmospheric conditions and removal processes strongly modulate these transfer ratios. Seasonality is critical: pre-monsoon spring brings frequent regional

biomass burning and upslope transport, contributing ~50% of the annual BC deposition to Yala Glacier in just the spring months (Gul et al., 2024). By contrast, during the summer monsoon much of the incoming BC is scavenged quickly, and local emissions are lower; external contributions dominate deposition then. Meteorology thus controls both how much wildfire smoke reaches the glaciers (transport) and how efficiently it is deposited. In general, dry, windy conditions favor long-range transport, while precipitation events favor deposition. The Himalayas in spring often experience regional fire smoke influx, followed by snowfall that deposits the BC. For example, at Yala Glacier, about 25% of the entire year's BC deposition occurred in a single month (April)(*Black Carbon and Glacier Melt - ICIMOD*, 2020). When regional forest fires peak and intermittent snow showers efficiently remove the soot.

Modeled deposition fluxes provide a sense of magnitude: The WRF-Chem model estimated total BC deposition on Yala Glacier at ~531 μg m^{-2} over spring 2017 (dry + wet) (Gul et al., 2024).Over a full year (Sep 2016–Aug 2017), the model's dry deposition was ~1000 μg m^{-2}, whereas measured wet deposition would be on the order of 200 mg m^{-2} (given wet was 196× dry) (Gul et al., 2024)i.e. around 0.2 g m^{-2} of BC per year falling to the surface. This is comparable to observed BC concentrations in snow: surface snow samples from Yala contained hundreds of ng/g of BC, consistent with the modeled cumulative deposition. By comparison, an Alpine glacier site (Sonnblick, ~3100 m in Austria) provides a useful analog: in August 2013, an influx of North American wildfire smoke (mixed with Saharan dust) was detected at Sonnblick, markedly increasing BC and particle loadings aloft (Schauer et al., 2016). Such events illustrate that wildfire plumes can traverse continents and still deposit on distant mountain glaciers.

In summary, only a few percent of wildfire BC emissions are transported to Himalayan glaciers, but of that portion, nearly all can deposit given the efficient scavenging (especially via wet deposition). Quantitatively, one might assume the order of a 5% transport fraction (based on regional observations) and an 80–100% deposition fraction of the transported BC (given dominant wet removal) for rough estimates. These values are supported by peer-reviewed studies showing low transport efficiencies but very high removal efficiencies(Hadley, 2008). Applying such ratios, researchers can approximate BC deposition loads on glaciers from a known wildfire emission, and compare the modeled μg m^{-2} to mg m^{-2} deposition with field measurements of BC in snow. This approach is in line with evidence that biomass burning contributes a significant minority of Himalayan snow BC (roughly one-quarter to one-half), with the rest from anthropogenic pollution(Gul

et al., 2024), all subject to strong enhancement during episodic fire events (Barker et al., 2021). Each cited study's context (e.g. season, climate phase) should be noted when adopting transfer ratios, but collectively they reinforce that wildfire smoke can and does reach the Third Pole, and when it does, a substantial fraction deposits onto glacier surfaces.

2.7 Overview of the Surface Energy Balance Model

The Surface Energy Balance Model (SEMB) provides a physically-based framework to quantify glacier-climate interactions by solving for the energy fluxes at the glacier surface. BC from wildfires can deposit on glacier surfaces, darkening the snow/ice and reducing albedo. This has a direct impact on the shortwave radiation term in the Surface Energy Balance. (Kayastha et al., 1999) formulated a mass-balance model to calculate spatial and temporal variations of energy-balance components, and hence ablation, over a glacier, which they successfully applied to a small glacier in the Nepalese Himalaya. Similarly,(Rupper & Roe, 2008) developed an SEMB to calculate annual glacier mass balance by integrating energy fluxes and precipitation across the glacier surface. A physically-based SEMB was used to simulate the summer mass and energy balance of the Yala Glacier, revealing that net radiation was the primary energy source for melting, followed by sensible heat and ground heat conduction (Acharya & Kayastha, 2019). Net radiative energy (Rn) dominates energy exchanges at the glacier-atmosphere interface (governed primarily by the variation in net shortwave radiation), contributing on average 62% of the melt energy (Assessment, 2009). BC deposition on glacier surfaces plays a significant role in altering the radiation balance by reducing snow albedo, thereby enhancing the absorption of solar energy and accelerating melt processes (Ming et al., 2013).

2.7.1 Radiative forcing and BC

Radiative transfer modeling constrained by field measurements at Mera La indicated that BC concentrations in the winter–spring snow/ice horizons were sufficient to reduce snow albedo by 6-10% (Kaspari et al., 2014b) resulting in localized instantaneous radiative forcings of 75-120 $W\,m^{-2}$, highlighting the significant radiative impact of BC deposition on glacier energy balance. Estimated BC deposition over the Himalayan glaciers NCO-P site and Yala Glacier range from 5 to 23 $\mu g\ m^2\ day^1$**,** leading to a 2–5% reduction in snow albedo and contributing to radiative forcing between 1–3 $W\ m^{-2}$**,** which enhances glacier melt during the dry pre-monsoon season (Yasunari et al., 2013).

CHAPTER 3. STUDY AREA

The Khumbu region is situated in northeastern Nepal, within the Solukhumbu district of Koshi Pradesh, covering around 1,148 square kilometers (443 square miles) and bordering Tibet to the north. Encircled by the majestic Himalayas, the region is defined by snow-capped peaks, including Everest, Lhotse, Nuptse, and Ama Dablam, which dominate the landscape. The Khumbu Glacier (27°957′N, 86°823′E) covers an area of about 17 km^2, which includes its detached tributary glaciers, Changri Nup and Changri Shar. (Vincent et al., 2016) and (Gibson et al., 2018) and (Jacobi et al., 2015b) concluded that the concentrations of BC in the Khumbu Valley exhibit a seasonal pattern, with lower levels during the post-monsoon and winter seasons, and higher levels during the pre-monsoon, reaching peak concentrations just before the monsoon begins.

In the Khumbu region, the climate features a summer monsoon season when almost all of the annual rainfall, about 587 ± 34 mm, occurs. The winters are cold and dry with little precipitation (Zeller et al., 2024).Between 2000 and 2019, the Khumbu region experienced an approximate 34% expansion in the area of its glacial lakes, along with an estimated 42% rise in the total volume of liquid water contained within these lakes (O'Neill, 2021). The Khumbu Glacier, the highest in the world, is receding at about 30 meters per year (Writer, 2018).This study aims to determine how much BC from wildfires has accelerated the melting of the Khumbu Glacier, which is receding at a rate of approximately 30 meters per year.

The annual cycle can be divided into four distinct climatic periods instead of the traditional seasonal classifications: winter (December to February), pre-monsoon (March to May), Southwest monsoon (June to September), and post-monsoon (October to November) (Tartari et al., 1998).We thus define the period "March of May" as pre-monsoon and the period "end of May–September" as monsoon season (Bonasoni et al., 2010).

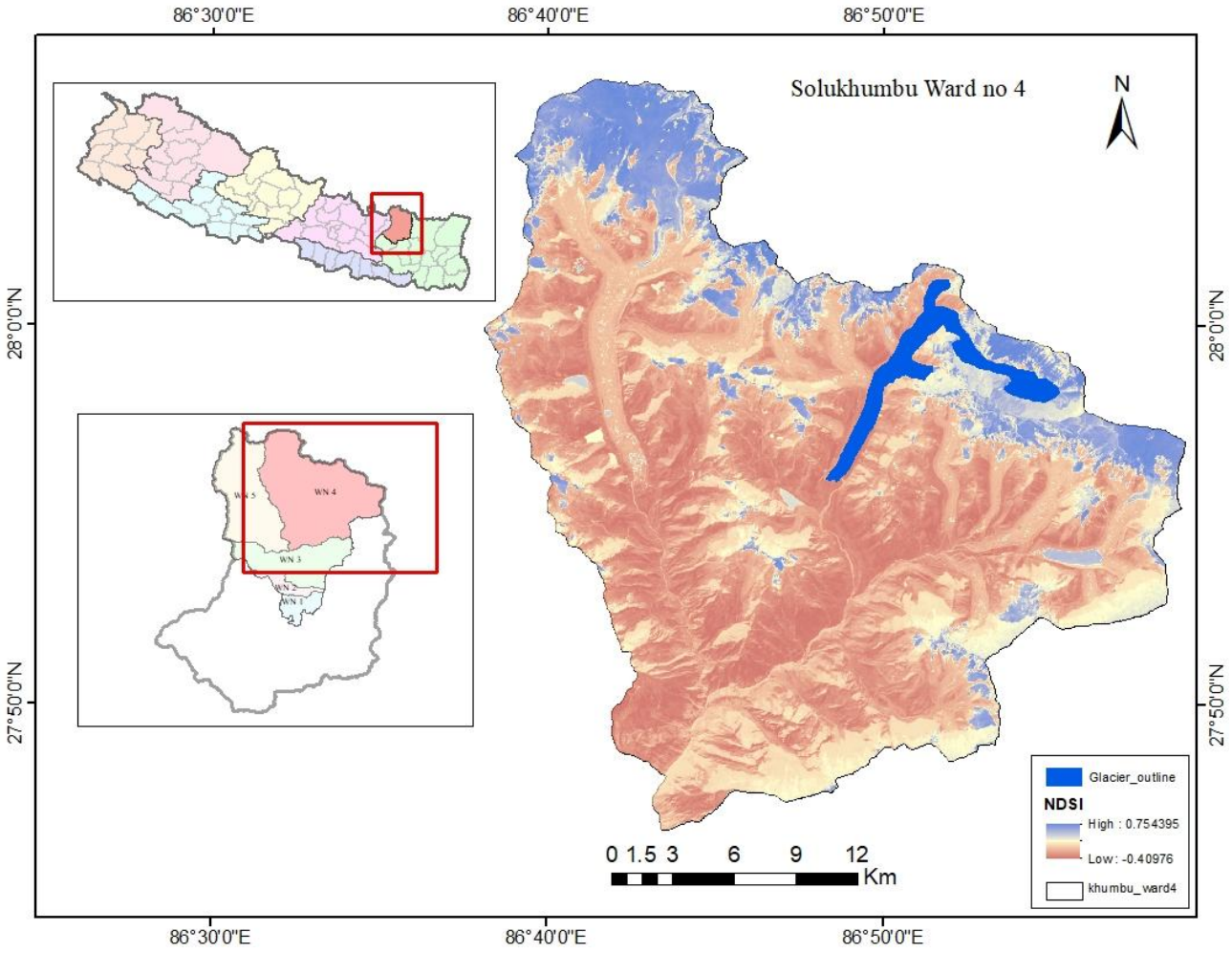

Figure 3-1 Location and topography of the Khumbu Glacier study area

CHAPTER 4. RESEARCH METHODOLOGY

This methodology integrates HYSPLIT backward trajectory analysis, driven by GDAS meteorological data to identify seasonal atmospheric pathways and potential source regions. Wildfire activity along these pathways is identified using VIIRS and FIRMS fire data, filtered by criteria such as brightness, confidence, and Fire Radiative Power (FRP). Corresponding land use Land Use Land Cover (LULC) information from GIS data allows for vegetation classification (e.g., temperate, tropical, agricultural residue). These trajectory, fire, and land use data are combined to estimate potential BC emissions originating along transport pathways using IPCC emission factors. Separately, the SEMB components (S_net, L_net, Qs, Ql, Qm) are calculated using variables obtained from the HARv2 dataset, incorporating HAR's time-varying surface albedo. The results and discussion synthesize the analysis of transport pathways, the seasonality of potential BC emissions, and the calculated SEMB components (particularly net shortwave radiation and energy available for melt), evaluating the glacier's sensitivity to albedo changes representative of potential BC deposition.

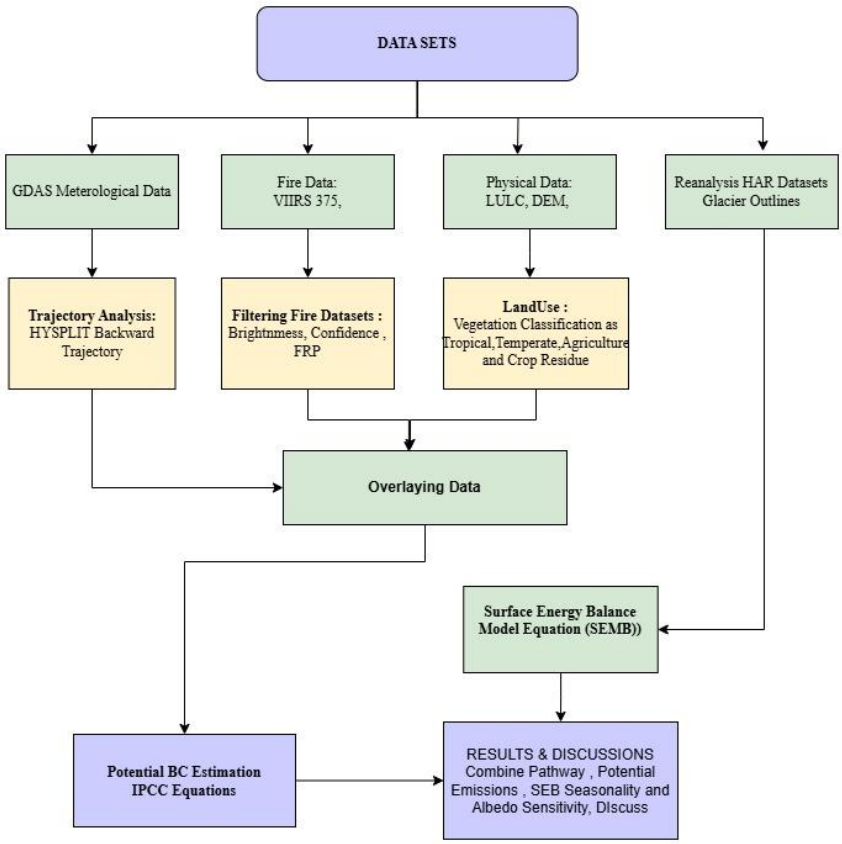

Figure 4-1 Flowchart illustrating the research methodology

4.1 Data Sources

4.1.1 HYSPLIT Meteorological Data

The HYSPLIT Ready System (https://www.ready.noaa.gov/HYSPLIT_traj.php) provides an online tool to calculate trajectories using global meteorological data. Data sources include Global Data Assimilation System (GDAS) with 1° spatial resolution (2006- present) and 0.5° (09/2007-06/2019), Global Forecast System (GFS) with 0.25° resolution (06/2019- present), and NCEP/NCAR Reanalysis (from 1948- present). The data used for this investigation is a 1° spatial resolution. While the vertical velocity of GDAS with 0.25° must be determined by vertically integrating the horizontal velocity, the vertical motion of the trajectory produced by GDAS with 1°can be computed directly from the model output vertical wind velocity (Su et al., 2015). Data objects with greater variability are grouped in distinct clusters, whereas clustering brings similar data objects together based on similarity (Cui et al., 2021). This study groups comparable data using clustering rather than classification. By identifying distinct trends in atmospheric transport, this clustering technique improves the study and offers a greater understanding of air parcel movements and their possible causes.

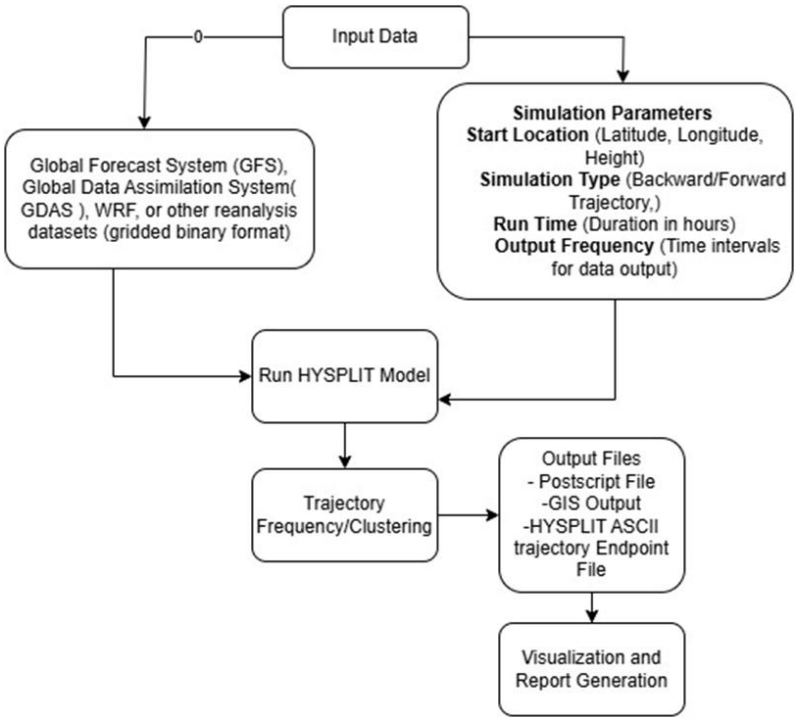

Figure 4-2 Schematic diagram of the HYSPLIT model Simulation process for backward trajectory analysis

This flow chart depicts the HYSPLIT model formulation method for trajectory analysis. It starts with input data, which can be meteorological datasets such as

the GFS, GDAS, or WRF model, all in gridded binary format. The user then sets the simulation parameters, including the starting point (latitude, longitude, and height), simulation type (backward or forward trajectory), run time(hours), and output frequency.

Once these parameters are established, the HYSPLIT model is run, resulting in atmospheric trajectory simulation. The obtained trajectories go through frequency or clustering analysis, which aids in finding dominant transport channels. The model then generates output files in various forms, including PostScript, GIS outputs, and HYSPLIT ASCII. The PBL was taken 500m above ground level. At 500 m above ground, within the Himalayan and Tibetan Plateau boundary layer, anthropogenic emissions increase significantly, as winter boundary layer heights typically range from 500 to 1000m (Ram & Sarin, 2010).The Meteorological Datasets used in this analysis are available from NOAA ARL's Archives (https://ready.arl.noaa.gov/archives.php).

Table 4-1 Datasets used for the HYSPLIT Model Simulation

	Datasets	Horizontal Resolution(km-)	Full-grid Dimensions	Temporal resolution (hrs)	Vertical levels	Period of each File	Size of Each File(GB)	Size of 1 month of data(GB)	Availability
Global Datasets	GFS - 0.25°	27	1440 × 721	3	56	1 day	2.7	82	Jun 2019 ->present
	GDAS - 0.5°	55	720 × 361	3	56	1 day	0.468	14	Sep 2007 -> Jun 2019
	GDAS - 1°	111	360 × 181	3	24	1 week	0.571	2.5	Dec 2004 -> present
	Global Reanalysis - 0.25°	278	144 × 73	6	18	1 month	0.11	0.11	1948 -> present

4.1.2 Satellite Imagery Analysis (VIIRS DATA)

The geographical coordinates and dates of fire occurrences were obtained from NASA's active fire data. The active fire data from the Fire Information for Resource Management System (FIRMS) was selected to analyze biomass burning emissions

across the region during various seasons. (https://firms.modaps.eosdis.nasa.gov). VIIRS provides high-resolution fire detection data, which includes FRP, brightness temperature, and confidence levels. The VIIRS 375 m fire data demonstrated notably better mapping accuracy than the existing Moderate Resolution Imaging Spectroradiometer (MODIS) fire detection data, offering greater consistency in delineating fire perimeters, especially for biomass-burning events that persist over multiple days (Schroeder et al., 2014). The dataset was filtered based on spatial and temporal criteria to identify fire events relevant to the study region. Fire occurrences were mapped to determine their proximity to the Khumbu Glacier and their potential contribution to BC deposition. Only high-confidence fire detections were included in the analysis to ensure data accuracy. The fire events were cross-checked with meteorological data to assess wind patterns and atmospheric transport pathways. Additionally, the VIIRS dataset was processed using GIS tools and Python scripts to overlay fire locations with HYSPLIT-derived back trajectories, allowing for the identification of likely source regions of BC emissions affecting the glacier. Further analysis included seasonal variations in fire activity, correlating FRP with emission estimates. The integration of VIIRS fire data with trajectory modeling provided insights into the transport and deposition of wildfire-induced pollutants in the Himalayan region.

Table 4-2 Summary of fire detection parameters from satellite observations

Parameter	**Description**	**Units**
Latitude	Geographical latitude of the detected fire	Degrees
Longitude	Geographical longitude of the detected fire	Degrees
Acquisition Date	Date when the fire was detected	YYYY-MM-DD
Acquisition Time	Time of fire detection (UTC)	HH: MM
Satellite	Identifies the satellite that recorded the fire (e.g., NOAA-20, Suomi-NPP)	N/A
Confidence Level	Confidence in fire detection (Low, Nominal, High)	Qualitative
Fire Radiative Power (FRP)	The energy emitted by the fire indicates its intensity.	Megawatts (MW)

Brightness Temperature (BT)	Temperature recorded at different thermal bands	Kelvin (K)
Scan	Width of the satellite swath used for fire detection	Kilometers (km)
Track	Length of the satellite swath used for fire detection	Kilometers (km)
Day/Night Flag	Indicates whether the fire was detected during the day or night	D/N

4.1.3 Physical Data (Geographical Data) DEM

The datasets for the landuse and landcover for vegetation types were extracted from the (https://developers.google.com/earth-engine/datasets/catalog/MODIS_061_MCD12Q1) dataset provides global land cover classification at a 500m resolution on a yearly basis. This dataset is derived from both the Terra and Aqua satellites and uses various classification schemes, including the IGBP and the University of Maryland (UMD). It includes data on land cover types, vegetation properties, and surface hydrology, offering critical insights for environmental monitoring and analysis of land use changes over time.

Table 4-3 Vegetation Classification based on MODIS MCD12Q1 datasets

ID	**Final Class**	**Mapped MODIS Land Cover Types (LC_Type1)**	**Latitude Rule (if needed)**
1	Tropical Forest	2 (Evergreen Broadleaf), 5(Mixed Forest)	If latitude between? 23.5° and +23.5°
2	Temperate Forest	1 (Evergreen Needleleaf), 3(Deciduous needleleaf), 4(Deciduous Broadleaf), 5 (Mixed forest)	If latitude < 50°, and not in tropics
3	Boreal Forest	1 (Evergreen needleleaf), 3(Deciduous needleleaf), 5(Mixed forest)	If latitude > 50°
4	Savanna & Grassland	6 (Closed Shrublands), 7 (Open Shrublands), 8 (Woody Savannas), 9	

		(Savannas), 10 (Grasslands), 11 (Wetlands), 14 (Cropland/natural mosaic), 16 (Barren)	No latitude condition needed
5	Agricultural / Crop Residue	12 (Croplands)	No lattitude condition needed
6	Unclassified	13 (Urban and Builtup lands), 15(Permanent Snow and Ice) 17(Water Bodies)	No Lattitude Condition needed

4.1.4 HAR Datasets

The HAR, a regional atmospheric dataset, is produced by downscaling the FNL with the WRF model and has been widely applied in scientific research (Wang et al., 2021). A new version, HAR v2, has a better domain of 10km grid spacing, which will be used in this research where ERA5 reanalysis data, provided by ECMWF, is used as forcing data. By using a Python script, these datasets were extracted and utilized for further analysis. The dataset variables used for this research are as follows;

Table 4-4 Variable used for the Surface Energy Balance Equations

Variable Name	**Variable Description**	**Type**	**Unit**
albedo	Albedo	2d	-
hfx	Upward Heat Flux at the Surface	2d	W m^{-2}
lh	Latent Heat Flux at the Surface	2d	W m^{-2}
lwdown	Downward Long Wave Flux at Ground	2d	W m^{-2}
psfc	Surface Pressure	2d	Pa
q2	Specific Humidity	2d	kg m^{-2}
swdown	Downward Shortwave Radiation	2d	W m^{-2}
t2	Air Temperature at 2m	2d	K
tsk	Skin Temperature	2d	K
v10	Wind Speed at 10m	2d	m s^{-1}
u10	U-component of Wind at 10m	2d	m s^{-1}

The analysis uses a grid-based approach with cell sizes of 500 meters, derived from the HAR dataset, to study the sensitivity of the Khumbu Glacier shown in Table 4-4 The glacier area, which spans 16.9 km^2, is covered by grid cells with varying cell weights, representing the influence of different environmental parameters on the glacier. The grid coverage is calculated as 0.17 cells, indicating how the glacier is represented within the grid.

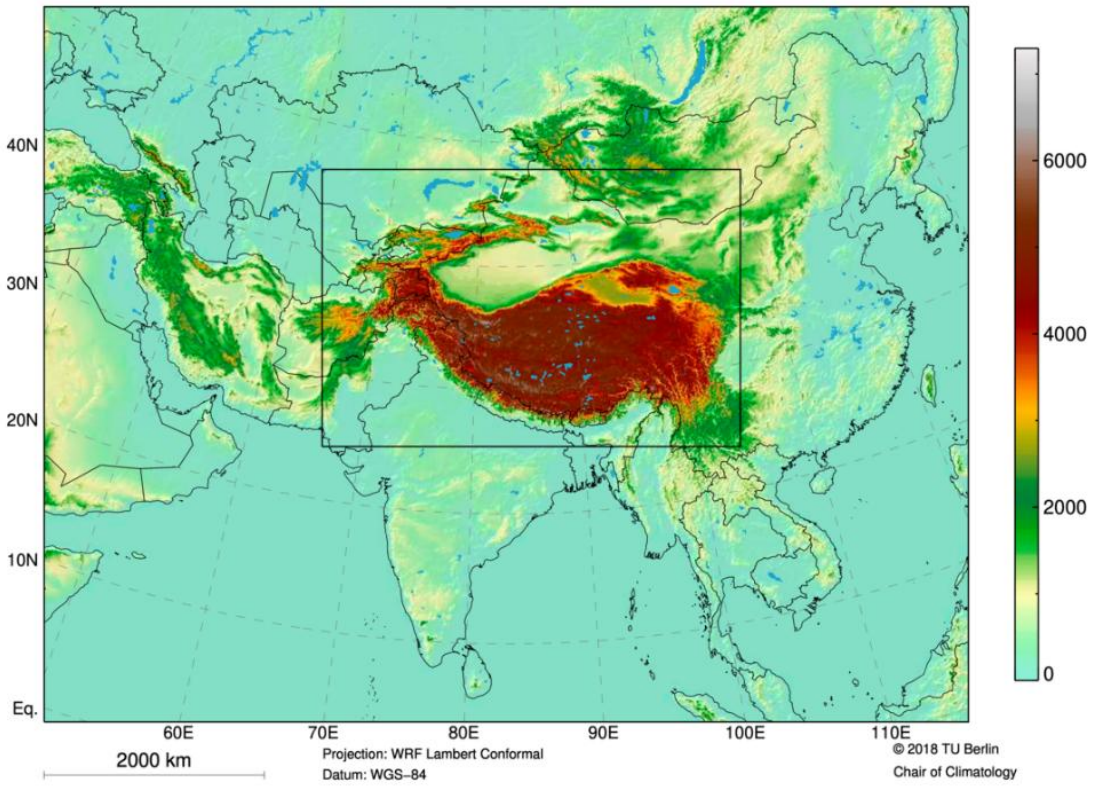

Figure 4-3 Calculated Model domains of HAR

Source : (https://www.tu.berlin/en/klima/research/regional-climatology/high-asia/har)

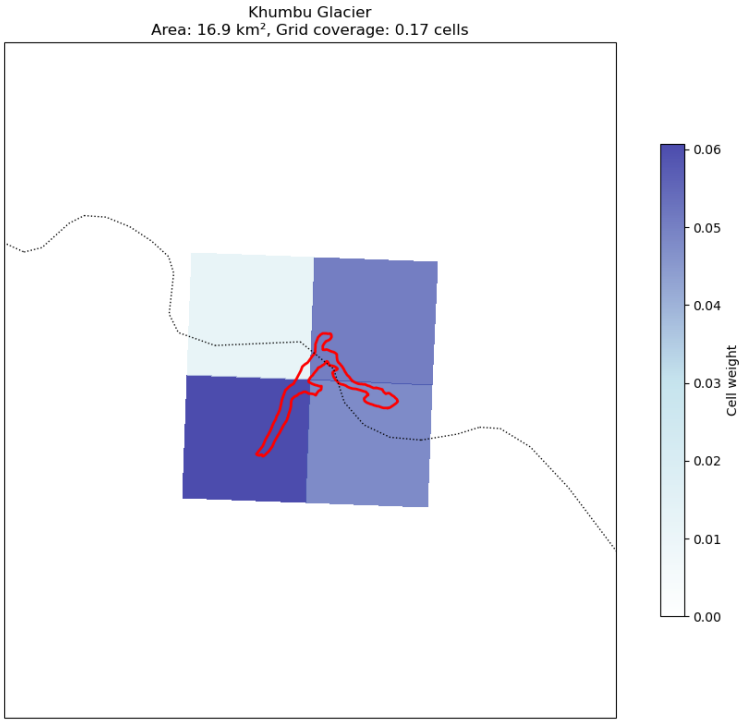

Figure 4-4 Spatial distribution of the Khumbu Glacier with grid cells of 500 meters, showing the glacier area (16.9 km^2) and the calculated grid coverage.

4.2 Estimating BC Emissions and Transport

4.2.1 Wildfire Source Identification

By tracing the trajectory backward, we can identify potential source regions where the air mass originated or passed through. These regions could be sources of BC or other pollutants. Suppose the trajectory passes over regions with active wildfires (e.g., northern India, Nepal, or Tibet). In that case, it suggests that BC from those fires could have been transported to the Khumbu Glacier.

The map provides a comprehensive visualization of potential sources of airborne pollutants reaching the Khumbu Glacier by integrating LULC data, backward trajectory pathways, and VIIRS fire detections. The LULC map serves as a backdrop, depicting different land cover types such as forests, savanna and grasslands, croplands, built-up areas, snow/glaciers, and barren land, which help identify potential emission sources. The backward trajectories**,** represented by black pathways, trace the movement of air parcels arriving at the glacier, revealing transport patterns from various regions. The VIIRS fire data**,** shown as red markers, indicates active wildfire locations, but only those that intersect with the air trajectories are displayed, highlighting potential sources of BC. Additionally, the map includes trajectory cluster percentages**,** illustrating the dominant transport pathways and their relative contributions. For instance, 33% of air

masses originate from Nepal and northern India, suggesting significant local emissions, while 44% come from the west, indicating long-range pollutant transport from regions such as Central Asia.

4.2.2 Assessment of Burned Area

VIIRS identifies fire hotspots but doesn't explicitly define burned areas. So, overlaying these fire points on vegetation data is subject to overestimation or underestimation of the burned area. Each fire detection pixel is initially assigned a square area corresponding to its sensor's nominal resolution (0.14 km^2 for VIIRS). The core idea is to aggregate nearby detections that likely represent a single, larger fire event rather than treating every pixel independently. Detections are grouped if they are in proximity (Wiedinmyer et al., n.d.). The method used to estimate the total burned area for a cluster of detections depends on the forest cover fraction, which is determined later using the (https://developers.google.com/earth-engine/datasets/catalog/MODIS_061_MCD12Q1). The model defines a slightly larger "detection rectangle" around each fire pixel (110% of the actual scan and track dimensions for that pixel). Clusters are formed where the detection rectangles overlap. Within a cluster, convex hulls are generated between pairs of detection rectangles that directly intersect. The union (combined area) of all these pairwise convex hulls forms the 'extended fire polygon'. The area of this extended fire polygon is used as the final burned area, for that fire cluster/event for that day. This method aims to fill gaps between detections in large, contiguous wildfires.

The comprehensive global validation from (Boschetti et al., 2019) found that MCD64A1 tends to significantly under-map burned area overall, but with a notable commission (overestimation) component. Commission errors averaged around 40% globally, meaning a substantial fraction of burned pixels detected by MODIS were unburned. MODIS MCD64A1 exhibited a 37.5% commission error in smallholder farms of Central India, falsely mapping unburned pixels as fire-affected (Deshpande et al., 2022). The VIIRS-inclusive FINNv2.5 version estimates ~25% more emissions than MODIS-only, primarily due to improved small fire detection. In this analysis, the burned area was calculated using the convex hull approach, similar to the methodology implemented in FINNv2.5 (Wiedinmyer et al., n.d.) to aggregate clustered fire detections into fire polygons. Upon comparison with MODIS-derived burned area data along the trajectory of interest, it is observed that MODIS significantly overestimated the actual burned area, a pattern consistent with prior findings that reported substantial commission errors in MODIS-based fire products.

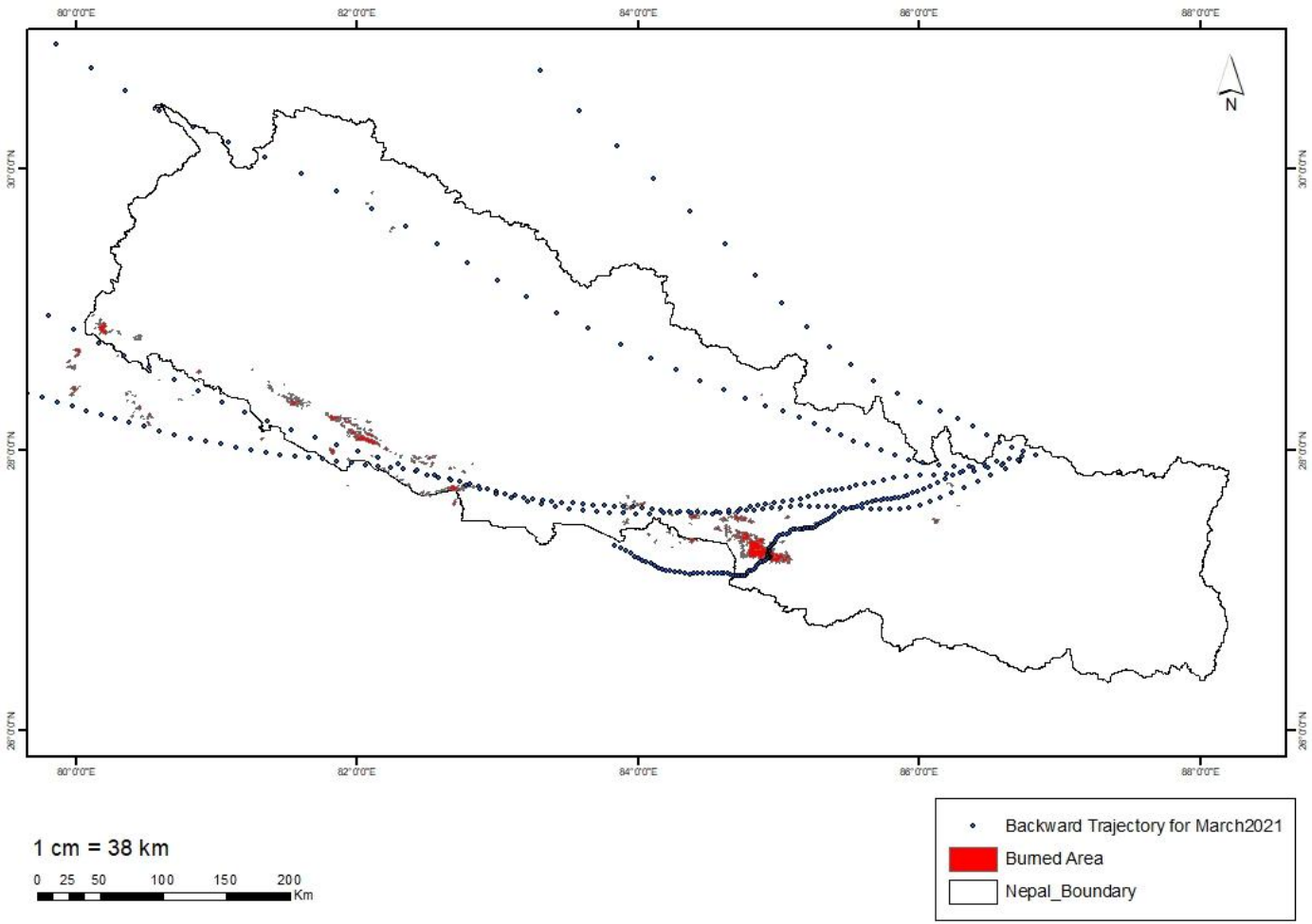

Figure 4-5 Fire occurrences across Nepal for March as detected by MODIS MCD64A1 burned area product (red dots). The black dotted lines representing backward air mass trajectories

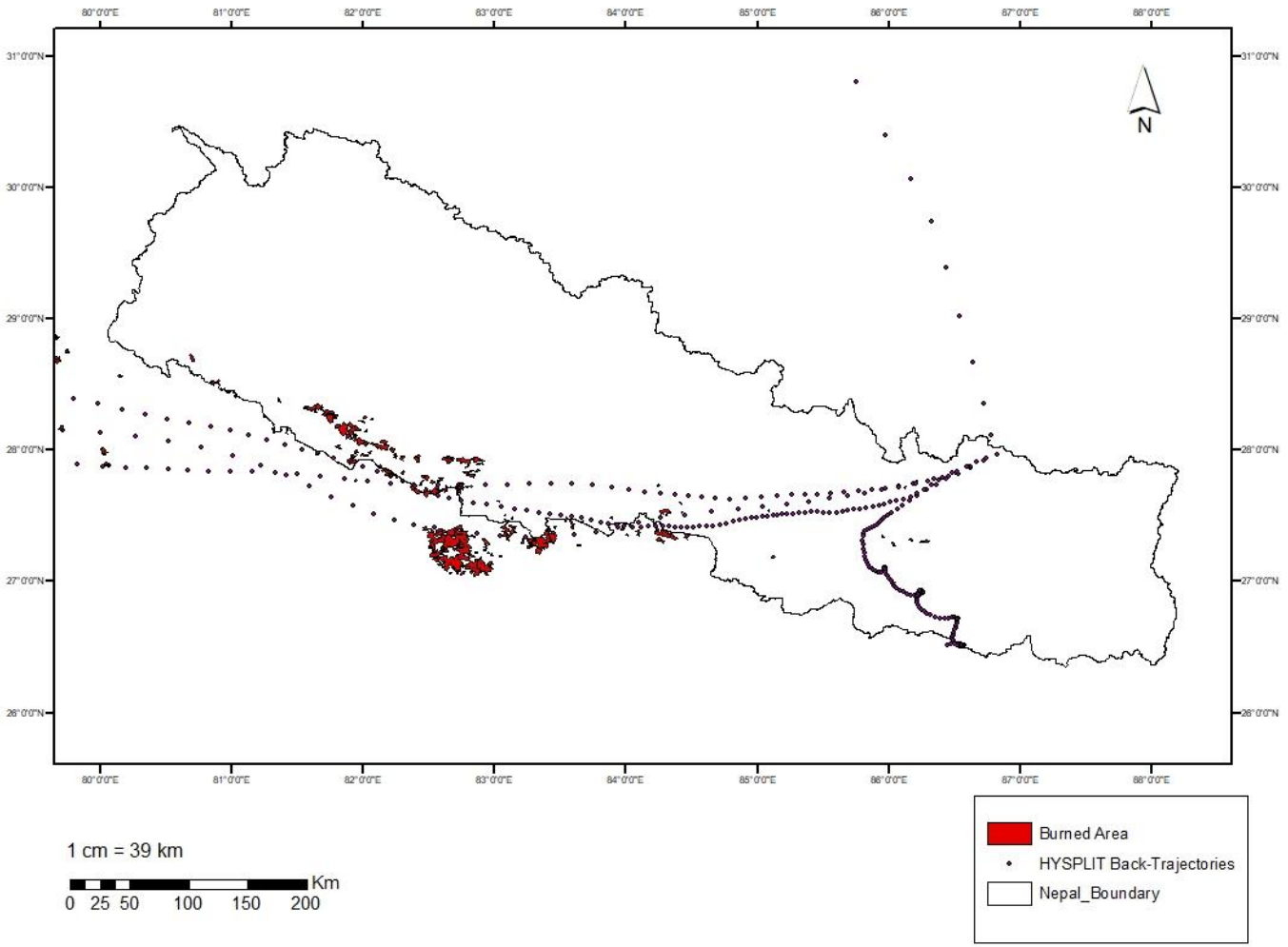

Figure 4-6 Fire occurrences across Nepal for April as detected by MODIS MCD64A1 burned area product (red dots). The black dotted lines representing backward air mass trajectories.

4.3 Estimating BC Emissions from Wildfires

The fundamental formula from the IPCC Guidelines can be used to determine the BC Emissions from wildfires. "Emission factors (EFs) for BC and other trace gases used in this study were extracted from the paper titled "Emission Factors for Open and Domestic Biomass Burning for Use in Atmospheric Models." This study provides an updated and comprehensive tabulation of EFs based on measurements taken in ambient-temperature smoke before significant photochemical processing. The EFs, expressed in grams of compound emitted per kilogram of dry biomass burned (g/kg), are categorized by vegetation and fuel type, ensuring consistency in biomass burning emissions estimation." Equation for Biomass Burning from the 2006 IPCC Guidelines for National Greenhouse Gas Inventories.

` $L_{fire} = A \times MB \times C_f \times G_{ef} \times 10^{-3}$ ……………………………………(1)

Where:

A = Area affected by fire (km^2), total area burned in ha.

L_{fire} = amount of greenhouse gas emissions from fire, tonnes of each GHG e.g., CH_4, N_2O, etc.

MB = mass of fuel available for combustion, tonnes ha^{-1}. This includes biomass, ground litter, and dead wood.

$C_{f\_}$ = Combustion factor for fire type (dimensionless)

G_{ef} = Emission factor for black carbon (BC) (g/kg) dry matter burnt

10^{-3} = Scaling factor to convert grams to kilograms

This equation estimates the BC emissions from fires in tons.

The BC estimate will be analyzed by categorizing wildfire emissions based on different vegetation types, including tropical forests, temperate forests, pasture maintenance, and crop residue burning. The values for the parameters in the BC emission equation such as biomass consumption **(**MB), combustion factor (C_f), and emission factor (G_{ef}) will be derived from the IPCC guidelines and supplemented with values from the relevant scientific literature to ensure accuracy and representativeness across different land cover categories (Akagi et al., 2011).

The EF is calculated by comparing the concentration of pollutants inside a fresh smoke plume (where the emissions from a fire are newly released) to the background air outside the plume (Urbanski, 2014). The idea is to measure how much a fire increases the levels of specific pollutants compared to the normal atmosphere. The difference in pollutant concentration between the smoke plume

and the background air helps estimate how much of a specific pollutant is emitted per unit of burned biomass.

4.4 Surface Energy Balance Model

The Surface Energy Balance (SEMB) model is a physical accounting of all energy gains and losses occurring directly at the glacier surface. It quantifies the key energy fluxes, primarily absorbed solar (shortwave) radiation, net infrared (longwave) radiation, and turbulent exchanges of sensible heat (due to temperature differences) and latent heat (due to evaporation/sublimation/condensation) with the atmosphere. By summing these incoming and outgoing fluxes, the model determines the net energy available (Q_m), which ultimately governs whether the surface temperature changes or if snow and ice melt occur.

The Surface Energy Balance Model Equation used in the Rupper and Roe (2008) study is:

$$Q_m = S + L + Q_s + Q_l + Q_g \quad \text{.....(2)}$$

Where:

Q_m = Energy available for melting snow/ice surface

S = Net shortwave radiation flux absorbed at the surface

L = Net longwave radiation flux

Q_s = Sensible heat flux

Q_l = Latent heat flux (evaporation/sublimation)

Q_g = Conductive heat flux into the glacier (often small and sometimes neglected and assumed to be zero in this study)

Shortwave Radiation Equation ;

$$S = (1-\alpha) \times SW\downarrow \quad \text{..... (3)}$$

(α from HAR Data)

Where,

S = Net Shortwave Radiation Absorbed (W/m^2)

α = Surface Albedo (unitless, 0-1)

SW↓ = Incoming Shortwave Radiation at Surface (W/m2)

For Longwave Radiation

$$L = LW\downarrow - LW\uparrow \quad \text{..... (4)}$$

Where:

L: Net longwave radiation (W/m^2)

LW↓: Incoming longwave radiation from the atmosphere (W/m^2)

LW↑: Outgoing longwave radiation emitted by the glacier surface (W/m^2)

Outgoing Longwave Radiation (LW↑)

$LW\uparrow = \varepsilon_s \times \sigma \times T^4$ ……(5)

Where:

Es = Emissivity of snow/ice surface (~0.97)

σ = Stefan-Boltzmann constant

T_s = Surface temperature (in Kelvin)

Incoming Longwave Radiation (LW↓)

$LW\downarrow = \sigma \times T_a{}^4 \times (C_1 + C_2 \times e_a)$……(6)

Where:

L↓: Incoming longwave radiation (W/m^2)

σ = Stefan-Boltzmann constant

Ta = Near-surface 2m air temperature (K)

ea = Near-surface vapor pressure (hPa or kPa, depending on units used)

C1, C2 = Empirical constants (dimensionless)

The Surface Energy Balance model utilized meteorological forcing data from the High Asia Refined analysis (HAR) dataset. Incoming longwave radiation, a key variable influenced by cloud cover, was taken directly from the HAR dataset output. As HAR is generated using a numerical weather prediction model that simulates cloud properties and their radiative effects, the influence of cloud conditions is implicitly included in the incoming longwave radiation values used in this study.

Sensible Heat flux (Q_s)

The sensible heat flux is given by the following equation:

$Q_s = D_s \times (\rho_0 / p_0) \times c_p \times (T_a - T_s)$……(7)

Where:

Ds= is the turbulent transfer coefficient for stable conditions,

(ρ_0 / p_0) = ratio of air density ($kg\ m^3$) to air pressure at standard sea level (hPa),

c_p = is the specific heat of air at constant pressure (J kg^{-1} K^{-1}),

T_a & T_s= are the air and surface temperatures, respectively (°C)

Latent Heat Flux (Q_l)

The latent heat flux is calculated as:

$Q_\gamma = D_s \times (\rho_0 / p_0) \times L \times (e_a - e_s)$……(8)

Q_l = is the latent heat flux (W m^2).

D_s= is the turbulent transfer coefficient for stable conditions.

ρ_0 = is the density of air at standard sea level (kg m^3).

p_0 = is the pressure of air at standard sea level (hPa).

L = latent heat of vaporization for melting (MJ kg^{-1}) or sublimation (MJ kg^{-1}), depending on surface temperature.

e_a = the vapor pressure of the air (hPa).

e_s =is the saturation vapor pressure at the surface (hPa), which depends on the surface temperature T_s

CHAPTER 5. RESULTS AND DISCUSSION

5.1 Atmospheric Transport and Deposition Pathways

5.1.1 BC Transport Pathways

The HYSPLIT model was used to simulate the monthly trajectories of black carbon particles transported to the Khumbu Glacier, originating from forest fire emissions. The following sections analyze the seasonal variability in air parcel transport patterns and their implications for black carbon deposition. A trajectory is the centerline of a dispersion and can be run both forward and backward. Forward trajectories will tell where the air will go, whereas backward trajectories will tell where the air came from. Back-trajectories are commonly used to help interpret air pollution measurements and answer the following questions:

1. Where did the air come from corresponding to any given sample time?
   - The backward trajectory model allows the tracking of air masses reaching the Khumbu Glacier at a specific time. This helps in identifying the source regions from which pollutants such as black carbon may have originated.
2. Where did the air come from when the concentrations of the pollutant were high?
   - High BC concentrations often correlate with air masses passing over regions experiencing intense biomass burning. During peak wildfire periods, trajectory density maps can be used to determine which regions contributed the most to BC transport. By comparing fire events from VIIRS satellite data with high BC deposition periods, it becomes possible to establish links between specific fire-prone areas and observed BC levels in the glacier.
3. Where did the air come from when the concentrations were low?
   - Lower BC concentrations are typically associated with air masses originating from cleaner regions or during monsoonal conditions, where wet scavenging reduces BC levels. During the monsoon season (June-September), most air parcels reaching the Khumbu Glacier come from the Bay of Bengal and Indian Ocean, regions with minimal wildfire emissions, leading to reduced BC transport. In contrast, during the dry season, air masses carry pollutants from densely populated and fire-prone areas, contributing to increased BC deposition.

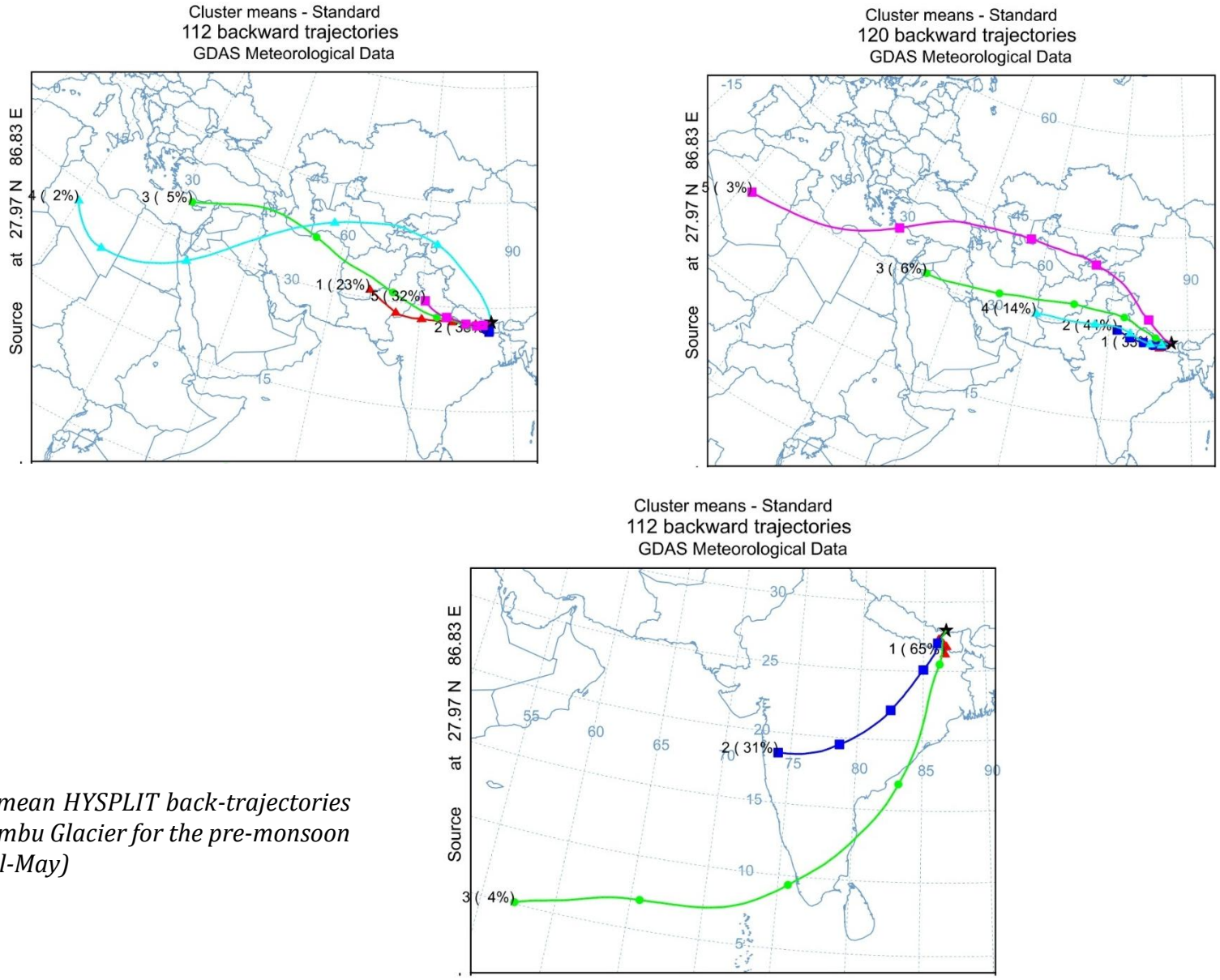

Figure 5-1 Cluster mean HYSPLIT back-trajectories arriving at the Khumbu Glacier for the pre-monsoon season(March-April-May)

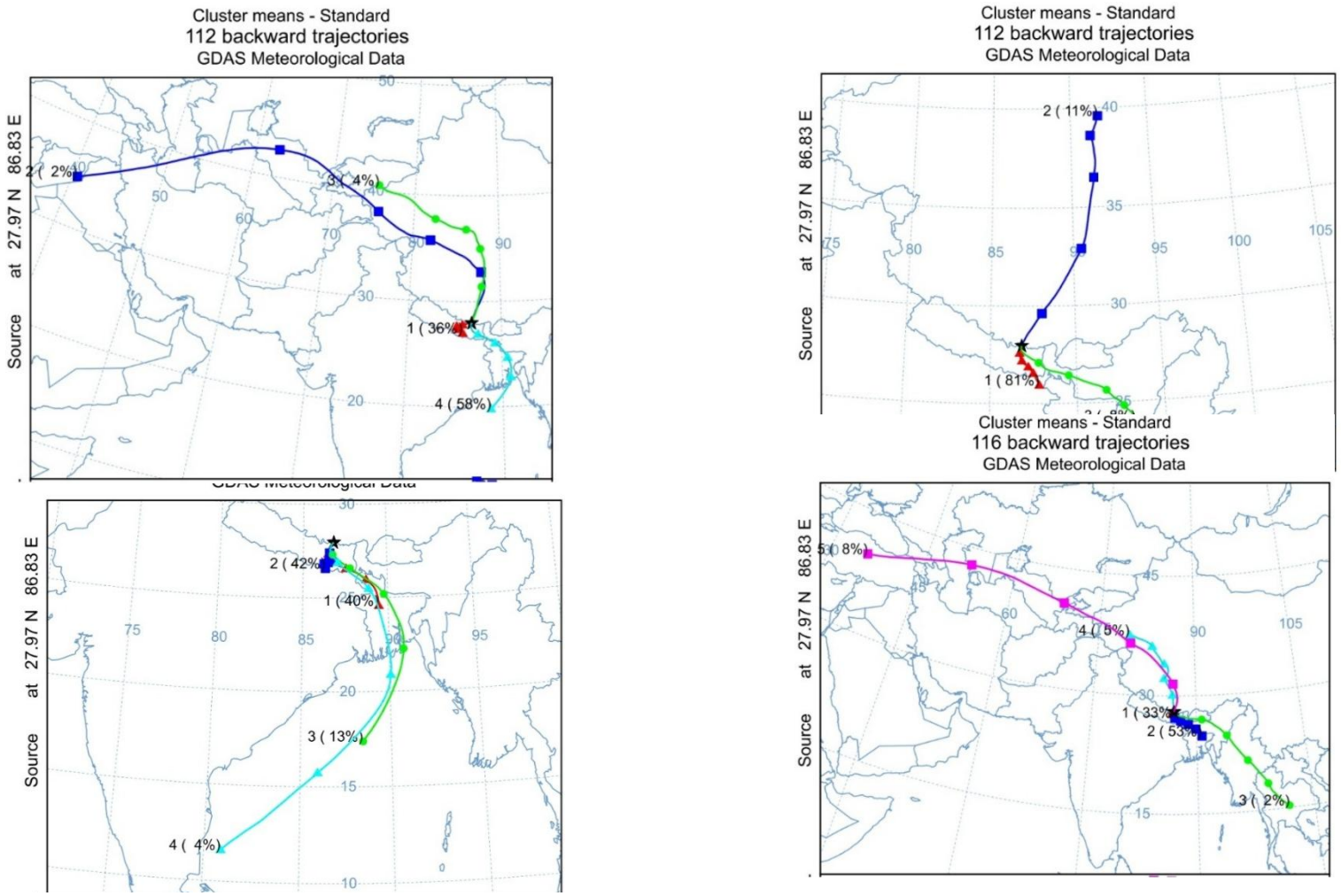

Figure 5-2 Cluster mean back trajectories arriving at the Khumbu Glacier for the monsoon season (June-July-August-September)

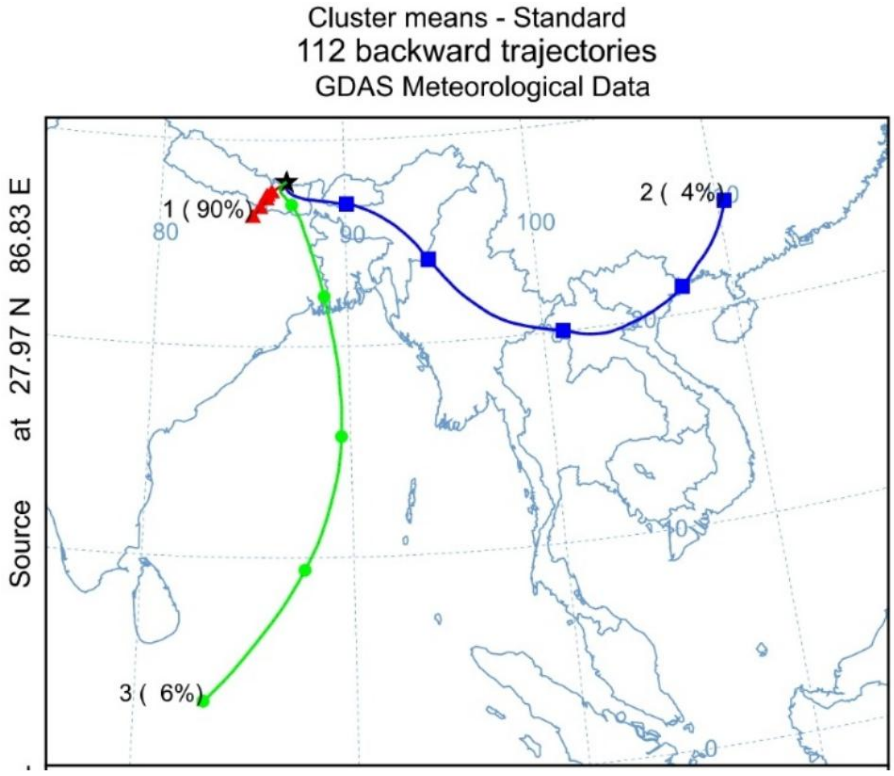

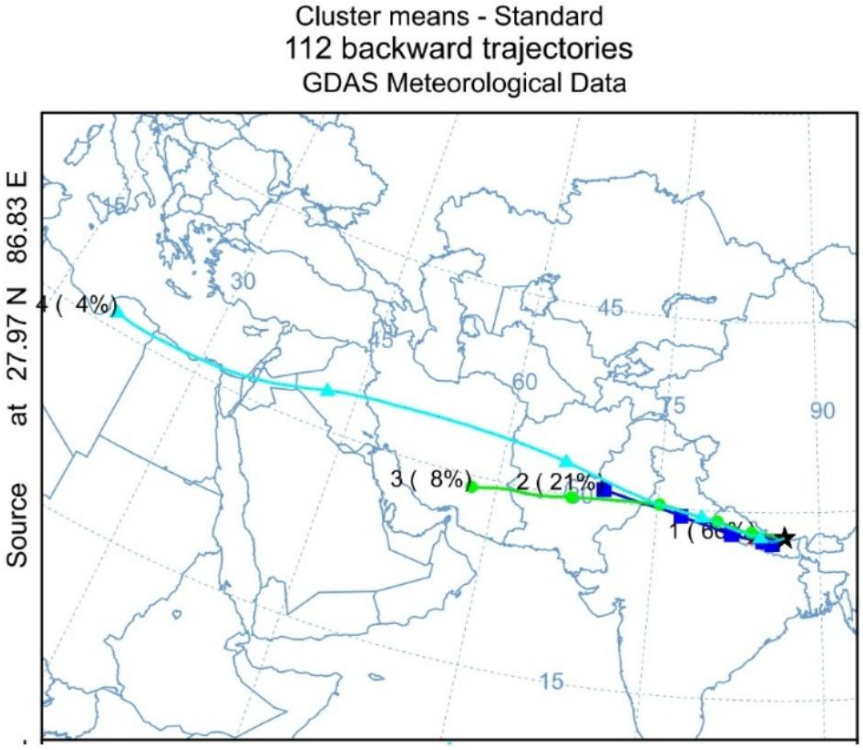

Figure 5-3 Cluster mean HYSPLIT back trajectories arriving at the Khumbu Glacier for the Post-monsoon season (October-November)

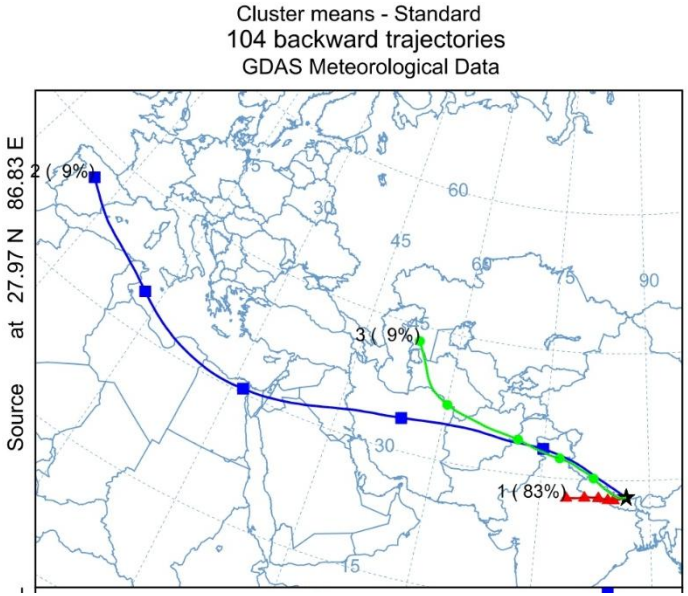

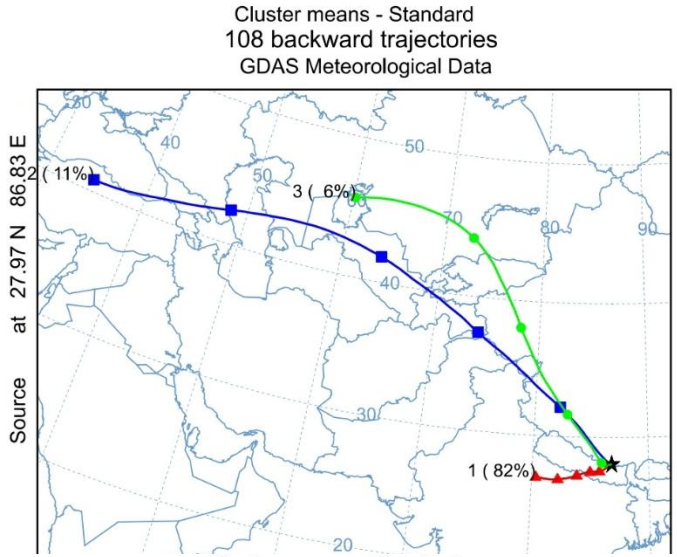

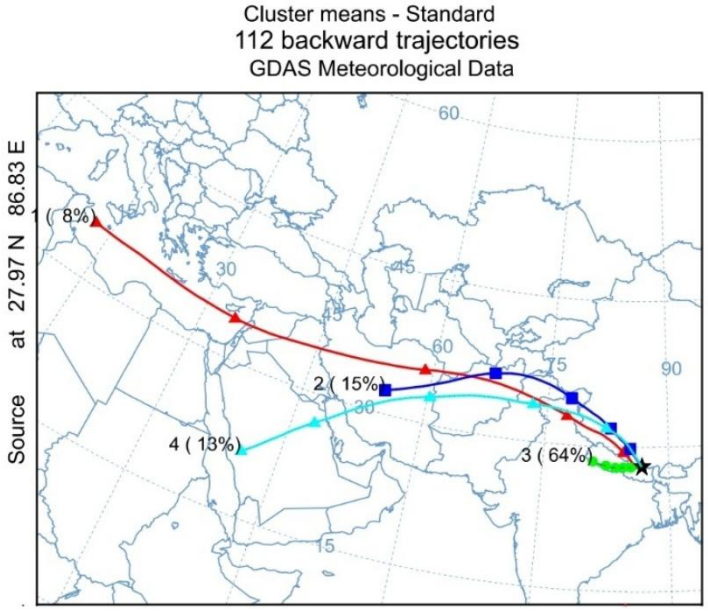

Figure 5-4 Cluster mean HYSPLIT back-trajectories arriving at the Khumbu Glacier for Winter season(December-January-Feburary)

During March, the backward trajectory analysis indicates that air masses reaching the Khumbu Glacier primarily originate from the southwest, with significant influence from forest fire emissions in the lowland regions where the Dominant Cluster 43% suggests strong air mass movement from a primary source following smaller clusters (33%,14%,6%,3%) shows the pre-monsoon atmospheric circulation facilitates the long-range transport of aerosols.

April exhibits similar trajectory patterns, with stronger southwesterly airflows due to the increasing influence of pre-monsoon convective activity. The rising temperatures and intensified biomass burning in South Asia may have contributed to an elevated BC load. In May, brings a noticeable shift, with air parcels arriving from the south. The pre-monsoon period is characterized by heightened transport potential, as increased surface heating enhances atmospheric instability. This results in deeper vertical mixing and a broader spatial extent of pollutant transport.

The onset of the monsoon season in June brings dispersed patterns in air parcel origins. Trajectories predominantly come from the Bay of Bengal with a dominant cluster of 58%, indicating a potential dilution effect due to monsoonal precipitation. This may reduce the efficiency of black carbon deposition over the glacier, despite ongoing emissions from regional fire activity of 36%. July and August are characterized by a strong monsoonal influence, with air masses primarily originating from the Bay of Bengal and the Indian Ocean. Heavy precipitation associated with the monsoon reduces atmospheric BC concentrations, leading to minimal deposition over the glacier. The wet scavenging effect dominates during this period. As the monsoon begins to retreat in September, there is a gradual re-emergence of southwesterly airflows. The weakening of precipitation allows for increased aerosol transport, potentially leading to a resurgence in black carbon deposition over the glacier.

October marks the transition to the post-monsoon season, with trajectories once again showing a dominant southwest influence. The drying of vegetation and resurgence of biomass burning events contribute to elevated BC emissions, increasing deposition risks in the Himalayan region. During November and December, air parcel trajectories indicate a strong influx from the IGP with 83% and 64% of dominant clusters in each month, a region known for extensive agricultural burning. The stable atmospheric conditions favor pollutant accumulation, leading to significant black carbon transport toward the Khumbu Glacier.

5.1.2 Trajectory Frequency

The trajectory frequency means it will start a trajectory from a single location and height every 6 hours and then sum the frequency that the trajectory passed over a grid cell and then normalize by either the total number of trajectories or endpoints. We should note that a trajectory may intersect a grid cell once or multiple times. The blue contour highlights areas contributing the highest BC concentrations reaching the receptor region. Additional contours represent varying transport probabilities, providing insight into dominant atmospheric pathways. This visualization underscores the importance of targeted regional mitigation measures to address BC sources and reduce deposition impacts on the glacier.

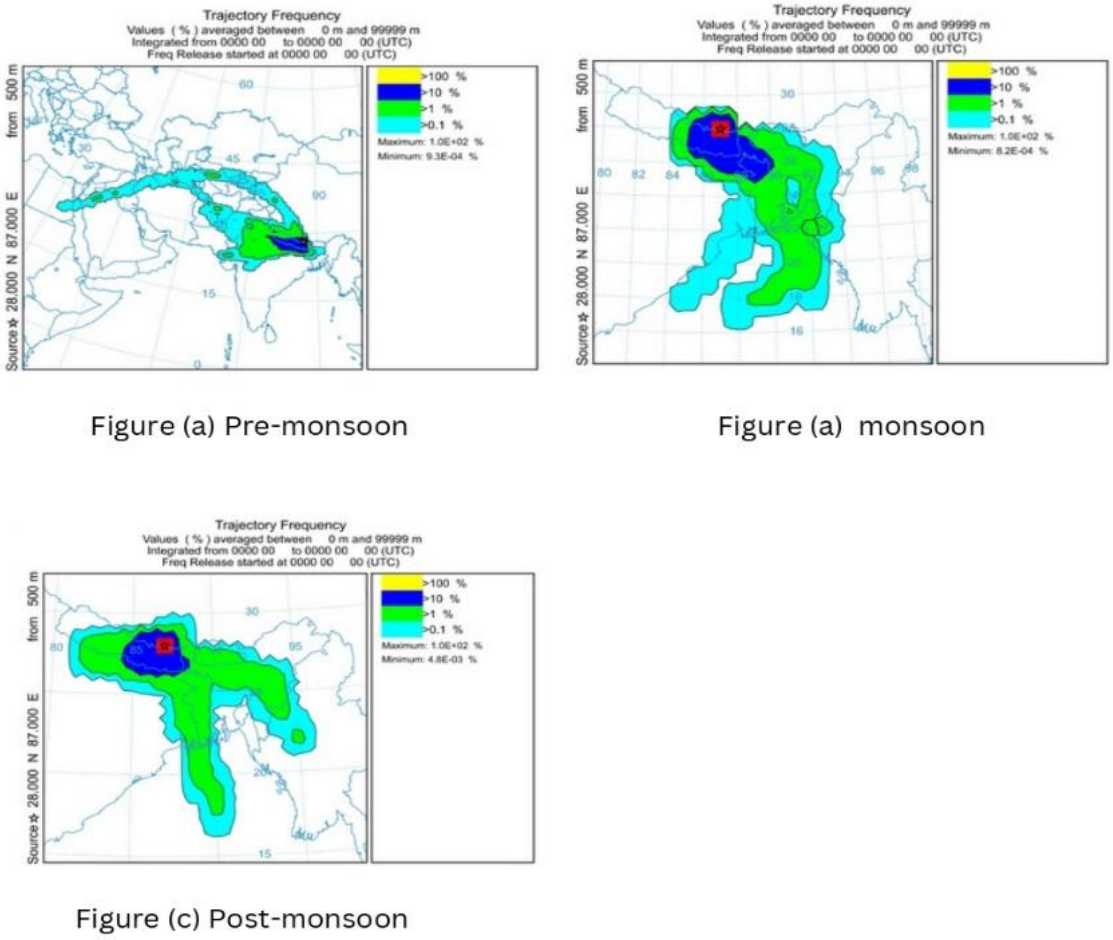

Figure 5-5 HYSPLIT frequency plot of five-day backward trajectories every 6 h at the Khumbu Glacier from 500 m in the year 2021

5.2 BC Emission Estimates

The analysis focused on estimating the potential BC emissions originating from wildfire sources located along identified atmospheric transport pathways leading towards the Khumbu Glacier during the pre-monsoon period (March-May) of the year 2021. Utilizing satellite fire detections (VIIRS/FIRMS) overlaid on HYSPLIT trajectories, combined with MCD12Q1.061 MODIS Land Cover Type Yearly Global 500m land cover data and IPCC emission factors, the total potential BC emission attributed to these trajectory-intersected sources was calculated to be approximately (tonnes). A distinct seasonal pattern emerged, with the highest potential emissions concentrated in April. This peak period aligns with the known seasonality of intensified agricultural burning in the IGP and increased forest fire activity in the Himalayan foothills, both of which occur before the summer monsoon. Along the trajectory, most of the burned vegetation that was filtered out consisted of agriculture and crop residue, followed by savanna and grassland, and tropical forest.

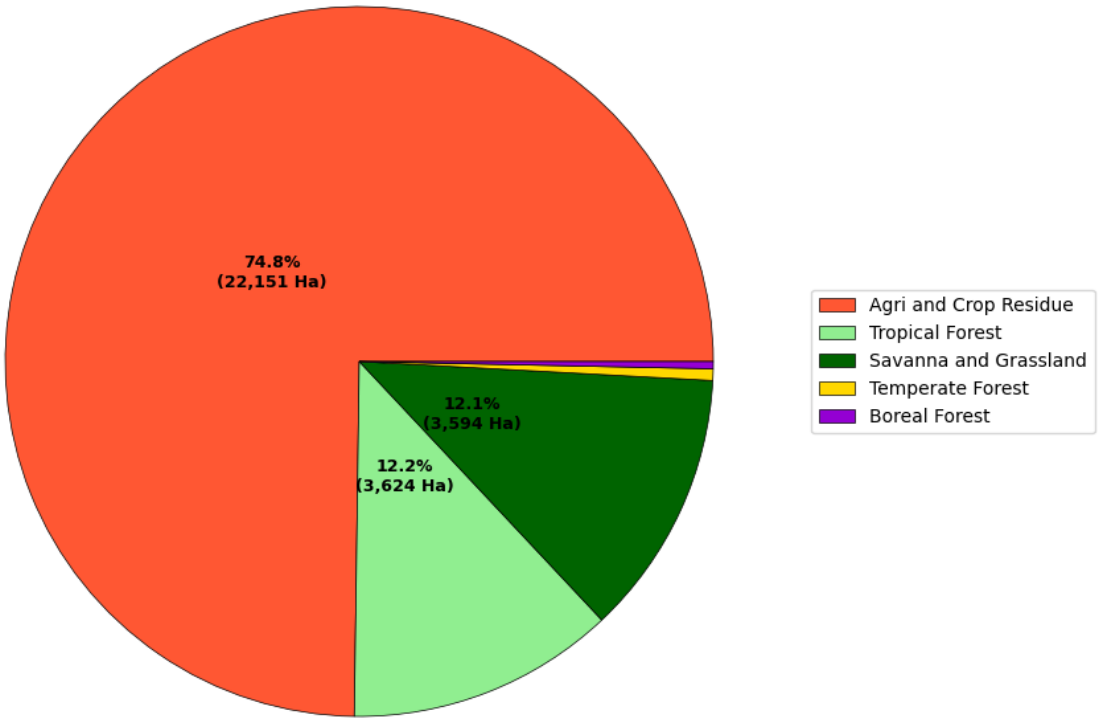

Figure 5-6 Contribution of different vegetation types to the total estimated area impacted by unique wildfire events along transport pathways during the Pre-Monsoon season.

Independent analysis focused on identifying potential Black Carbon (BC) sources impacting the Khumbu region during the 2021 pre-monsoon season (March-May). Utilizing HYSPLIT backward trajectories correlated with VIIRS active fire

detections, dominant atmospheric transport pathways originating primarily from the Indo-Gangetic Plain and Himalayan foothills were identified. Estimation of potential BC emissions associated with fires along these pathways, based on burned area derived from Convex Hull/MODIS approaches and IPCC emission factors, indicated a pronounced seasonal peak during March and April 2021 (calculated as approximately 39.6 tonnes and 93.8 tonnes respectively using the convex hull method, though considerable uncertainty exists due to burned area estimation challenges). This peak in potential BC emissions aligns temporally with known periods of heightened agricultural residue burning and forest fire activity in the identified source regions.

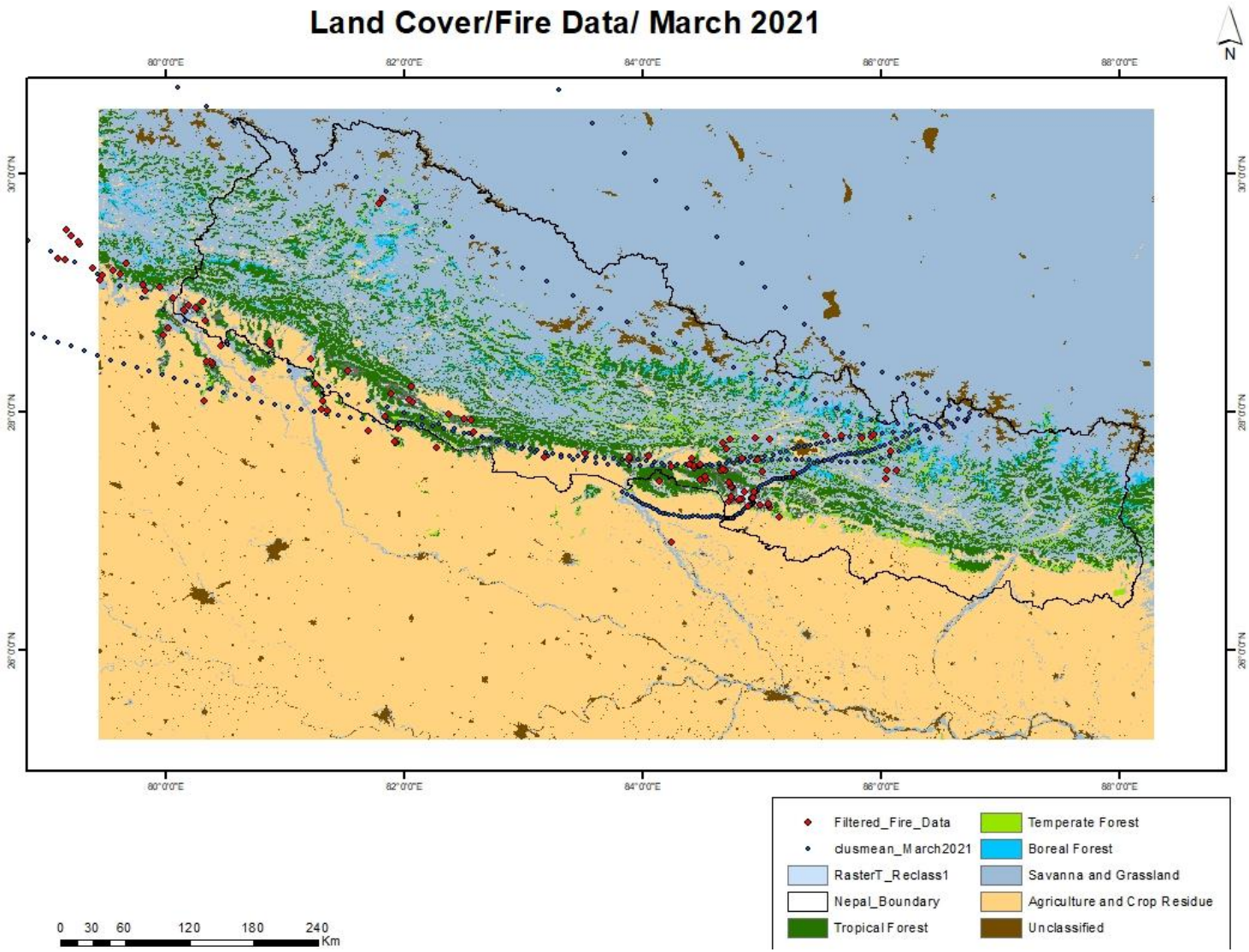

Figure 5-7 Spatial distribution of fire events and land cover types along the trajectory during March 2021

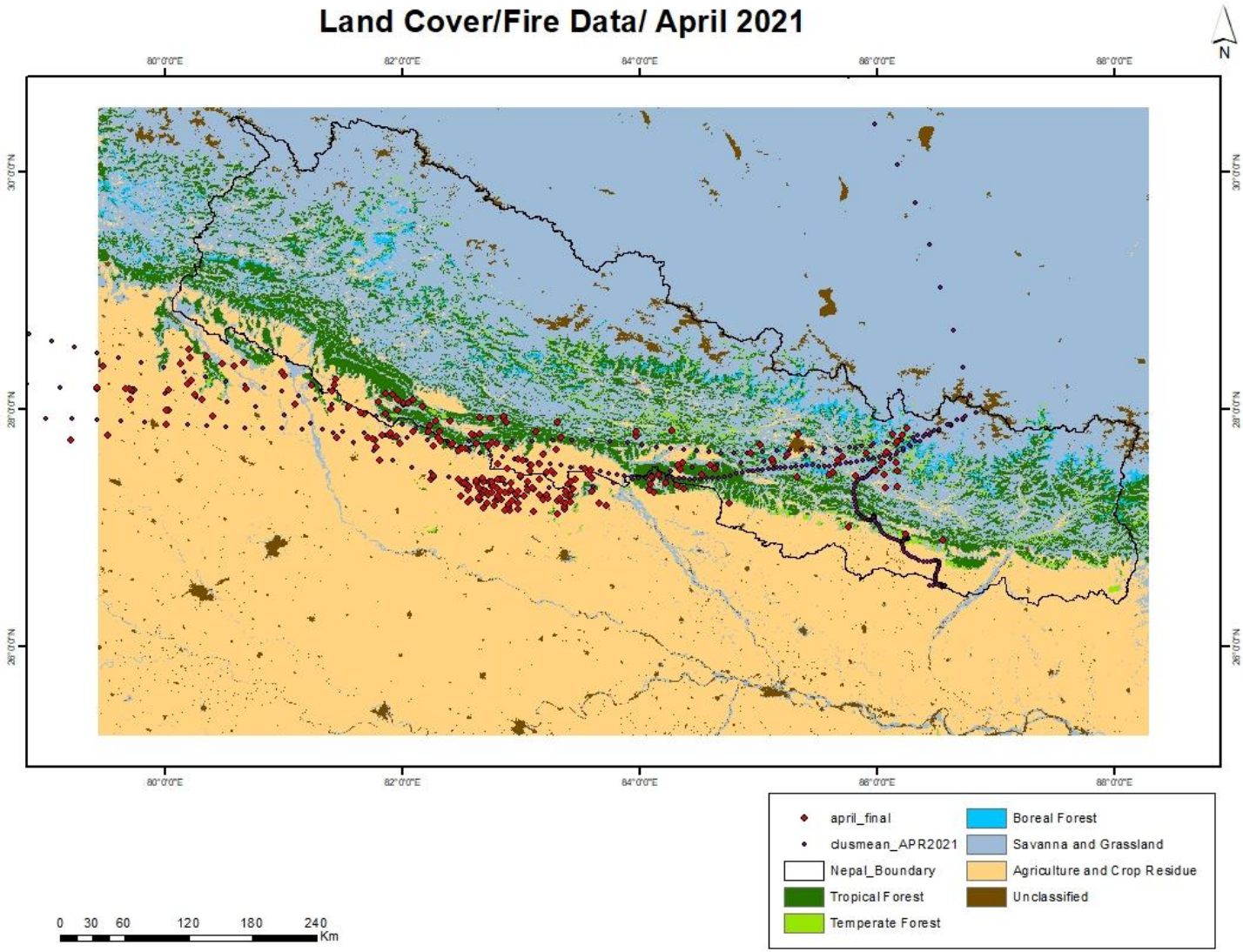

Figure 5-8 Spatial distribution of fire events and land cover types along the trajectory during April 2021

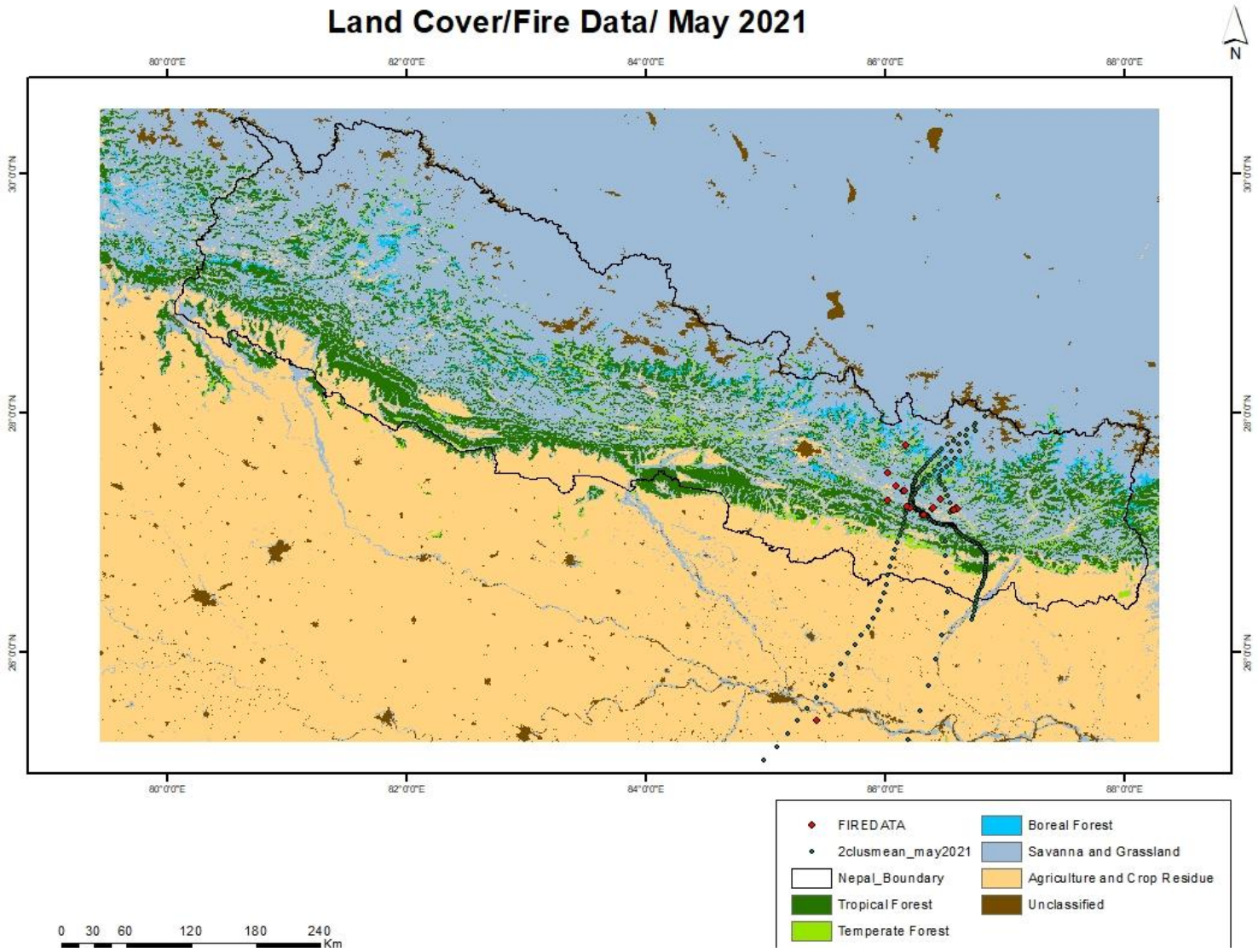

Figure 5-9 Spatial distribution of fire events and land cover types along the trajectory during May 2021

These figures illustrate the spatial relationship between land cover types, active fire locations (red markers), and representative HYSPLIT backward air mass trajectories (blue dotted lines) during the pre-monsoon months of March, April, and May 2021 for the region encompassing Nepal and its surroundings. Across all three months, a consistent pattern emerges where the calculated backward trajectories, indicating the pathways of air arriving at the study region, intersect with areas experiencing significant fire activity. Notably, these fire locations situated along the trajectories are predominantly concentrated within agricultural lands (including crop residue burning) and savanna/grassland areas, primarily located in the plains and foothills south and west of the main Himalayan range. This spatial overlap strongly suggests that biomass burning within these specific land cover types represents a major potential source contributing to aerosol loading, including BC, transported towards the Himalayan region during the critical pre-monsoon season.

5.3 SEB outputs

The daily output was created by first loading daily average meteorological data for the Khumbu Glacier region in 2021 from an Excel file. This data included variables like incoming solar radiation, incoming longwave radiation, air temperature, surface temperature, humidity, pressure, wind components, and importantly, surface albedo. The code then performed calculations using physical principles and constants (like the Stefan-Boltzmann law) to derive the key components of the surface energy balance: net shortwave radiation (S_net, considering albedo), net longwave radiation (L_net, based on incoming longwave and calculated outgoing longwave from surface temperature), sensible heat flux (Qs), and latent heat flux (Ql). These components were summed to find the total net energy available at the surface (Qm). Finally, these calculated daily energy fluxes, along with the potential melt energy (derived from Qm under specific conditions), were plotted against time over the year 2021 using Matplotlib, with melt energy shown on a separate right-hand axis for clarity.

In Figure (5.10) the same components as before are seen but plotted for each day of 2021. The lines are much "spikier" or "noisier" because they capture daily weather changes (sunny vs cloudy, warm vs cold spells, windy vs calm). However, the broad seasonal trends seen in the monthly plot are still visible underneath this daily variability.

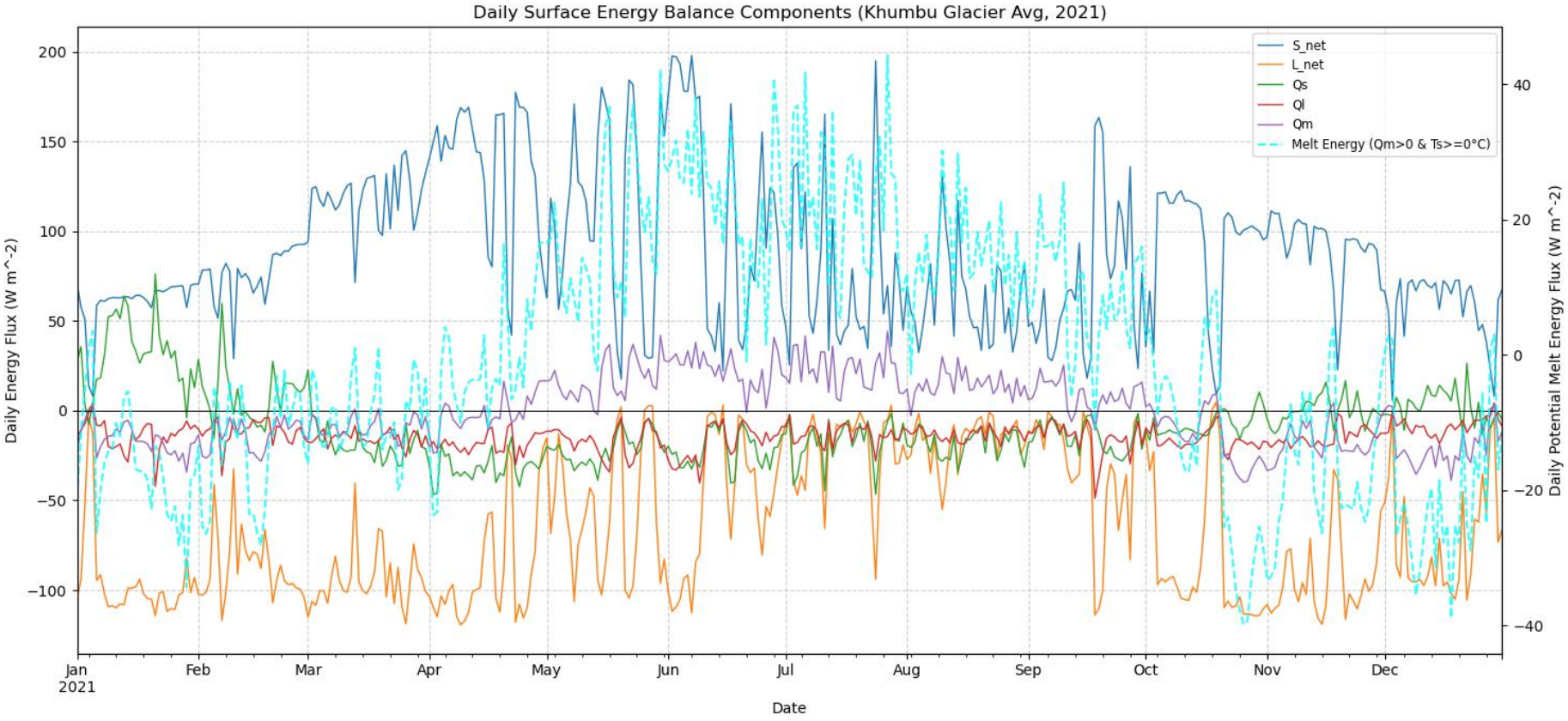

Figure 5-10 The daily evolution of energy fluxes contributing to the Surface Energy Balance and the resulting Potential Melt Energy Flux at Khumbu Glacier (Avg, 2021)

1. **S_net (Net Shortwave - Blue Line):**

Energy is gained from absorbed sunlight. This line shows huge daily fluctuations. On clear, sunny days, it shoots up high (reaching nearly 200 W/m^2 sometimes in spring/summer). On cloudy or snowy days, it drops significantly lower as clouds reflect sunlight away. Despite the daily ups and downs, you can still see the overall seasonal pattern: lower in winter, rising rapidly in spring (around March/April), staying high but variable in summer (May-Sept), and decreasing in autumn. This confirms sunlight is the main energy *input*.

2. **L_net (Net Longwave - Orange Line):**

Net balance of heat radiation (Outgoing minus Incoming). It's almost always negative (energy loss). It also varies daily. Clear nights allow strong heat loss (very negative values, down to -120 W/m^2). Cloudy conditions act like a blanket, trapping heat and making the net loss smaller (closer to zero, especially visible during the monsoon months June-August. The general trend of the largest losses in winter/early spring and the smallest losses in summer is still evident.

3. **Q_s (Sensible Heat - Green Line):**

Heat transfer due to air-surface temperature difference. Positive Qs means heat moves from warmer air to the colder surface. Negative Qs mean heat moves from the (relatively) warmer surface to colder air. (Calculated as -hfx).Highly variable day-to-day. It often fluctuates around zero. It might be positive when warm air moves over the cold glacier, and negative when the sun warms the surface even slightly above the air temperature, or during cold air outbreaks. It's generally a smaller term compared to radiation.

4. **Q_l (Latent Heat - Red Line):**

Energy is used for evaporation/sublimation (negative Q_l, cooling) or released by condensation/deposition (positive Q_l, warming). (Calculated as -lh). Mostly negative, indicating energy is primarily being used for sublimation or evaporation, acting as a consistent cooling term. The magnitude varies based on daily humidity differen132O][JP
B ces and wind speed. Dry, windy days might show larger negative values (more sublimation). It's also generally a smaller term.

5. **Q_m (Net Energy Balance - Purple Line):**

The total of all energy gains and losses (S_net + L_net + Qs + Ql). The overall energy surplus or deficit for the very dynamic surface. It jumps around daily, heavily influenced by the big swings in S_net (due to clouds).In the Winter season (Jan-

Mar), mostly below zero (energy deficit). Following Transition in (Apr-May): Starts having days where Qm crosses above zero. Similarly, in Summer (Jun-Aug), mostly above zero, often significantly so, indicating consistent energy surplus available for melt, but still with drops on cloudy/stormy days.The Transition in (Sep-Oct): Drops back below zero more frequently. In Late Autumn/Winter (Nov-Dec): Mostly below zero again.

6. **Melt Energy (Cyan Dashed Line - Right Axis):**

The energy available for melting (i.e., Qm when Qm > 0 and surface temp tsk >= 0°C). This line is zero most of the winter. It starts appearing as positive spikes around late April/May, mirroring the positive spikes in Qm. During the summer (June-Aug), it's frequently high, showing significant energy is available for melting on many days, but it still drops to zero or near-zero on days with poor weather (low S_net, low Qm). It fades out again in September/October. This perfectly highlights the intermittent nature of melt on a daily scale, even during the main melt season.

The daily plot shows the dramatic influence of daily weather (especially cloud cover affecting S_net) on top of the seasonal cycle. It confirms that while the *potential* for melt (Qm>0) starts around April/May, the period of most intense and frequent melt energy availability (Melt Energy line) is clearly concentrated in the summer monsoon months (June-July-August).

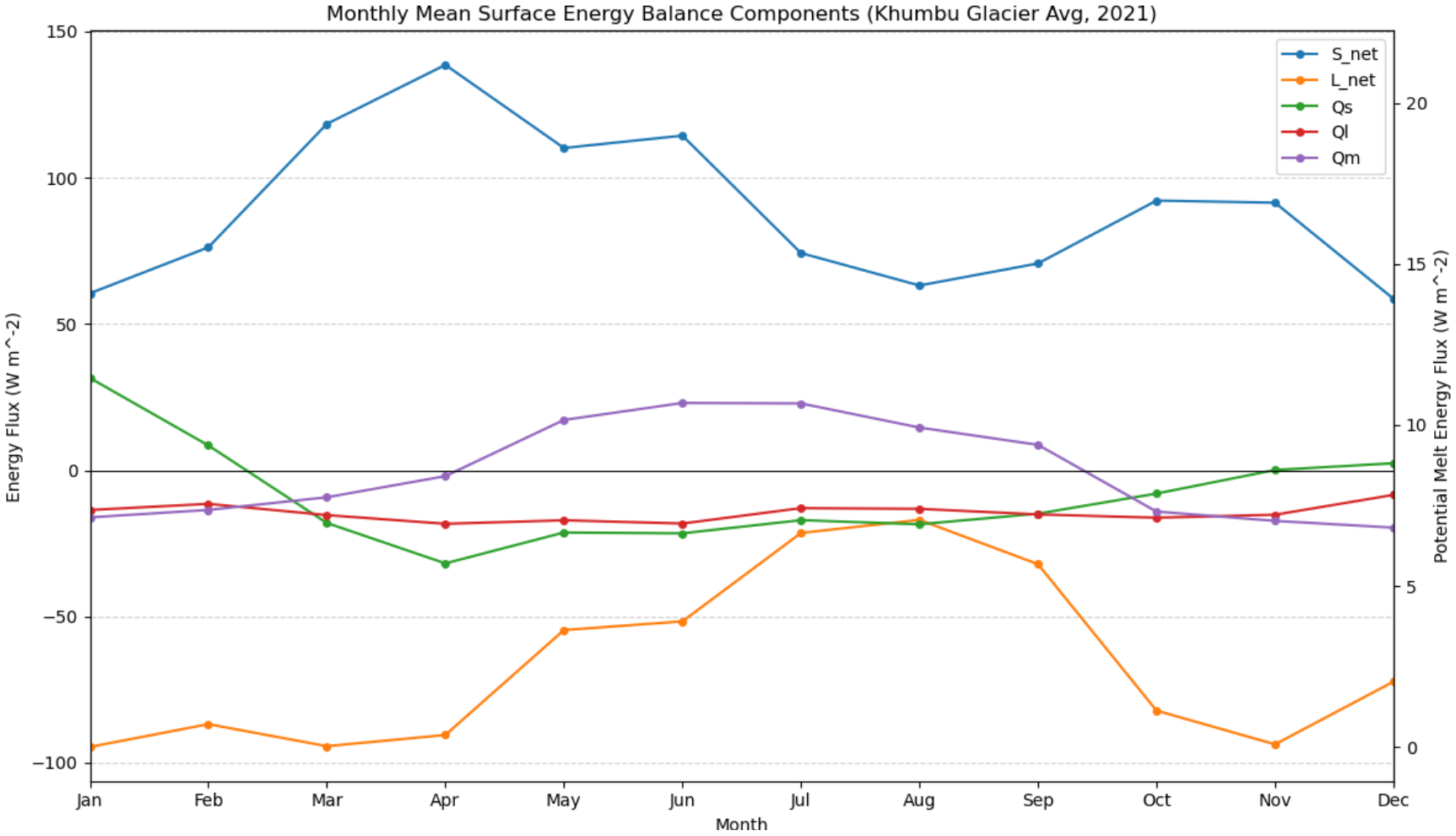

Figure 5-11 the average monthly surface energy balance components for the Khumbu Glacier region throughout 2021.

The net shortwave radiation (blue line) is the primary energy input. It has a seasonal pattern, peaking during the pre-monsoon and monsoon months (April to August) and hitting its lowest point in winter. On the flip side, net longwave radiation (the orange line) shows a steady and significant energy loss all year long. The biggest losses are seen in those clear winter months, and then it lessens a bit during the cloudier summer monsoon.

Looking at the turbulent fluxes, they're kind of playing a supporting role; the sensible heat flux (green line) usually adds a little energy gain in the warmer months (May to August) but shows a loss when it's colder. And then there's the latent heat flux (the red line), which indicates a continuous energy loss, mostly because of sublimation and evaporation, but it does get a bit less negative during the humid monsoon.

Now, the overall net energy balance (the purple line) is the total of all these components. It shifts from being in deficit during winter to showing a surplus during the summer months (from May to September). This indicates when we have energy available at the surface. The potential melt energy, which is shown with a red dashed line on the right axis, points out the part of that balance that's available for melting, especially when surface temperatures are at or above freezing. This highlights the main melt season, showing strong positive values mostly from May to September, with peaks in July and August pretty much aligning with that period of positive energy balance. Taking a monthly view like this helps smooth out those day-to-day weather variations. What stands out is that the summer monsoon season is when the glacier has the most energy available and the highest melt potential, all driven by high solar radiation, with longwave losses and turbulent fluxes kind of balancing things out. Q_m transitions from negative values (indicating heat loss from the subsurface in winter) to positive values (crossing zero around March/April and reaching approximately +10 W m^{-2} by May), signifying that sufficient energy is absorbed at the surface to begin warming the underlying snow and ice pack via conduction. This positive Q_m during the peak BC emission period contributes significantly to raising subsurface temperatures and priming the glacier for the onset of the main melt season, which is reflected in the increase of the potential melt energy flux (right y-axis).

The analysis of the surface energy balance (SEB) for the Khumbu Glacier in 2021, derived from High Asia Refined (HAR)v2 dataset variables including observed albedo, reveals distinct seasonal dynamics governing energy availability for melt. Calculation of the net energy flux (Q_m = S_net + L_net + Q_s + Q_l) indicates that the period encompassing the pre-monsoon and monsoon seasons (approximately

March/April through September) experiences the highest energy surplus available for melt. Examination of the individual SEB components during the critical pre-monsoon onset shows that increasing net shortwave radiation (S_net) is the dominant driver initiating positive Q_m values, often supplemented by contributions from sensible heat flux (Q_s). Notably, S_net is intrinsically linked to surface conditions via the relationship S_net = Incoming_SW × (1 - albedo), highlighting the critical role of surface albedo in modulating the primary energy input during this sensitive period.

5.4 Link Between Emissions and Glacier Energy Balance

While this study successfully characterized both the glacier's seasonal energy balance and the seasonality of potential BC emissions along relevant transport pathways, establishing a direct quantitative link between these calculated emissions and observed SEB changes (particularly the albedo effect on S_net and the resulting Qm) was precluded by the absence of atmospheric transport and deposition modeling. However, a compelling qualitative connection emerges from the temporal alignment of these independent analyses. The observed onset of the high melt-energy period (positive Qm) at Khumbu Glacier during the pre-monsoon is driven significantly by absorbed shortwave radiation, a flux highly sensitive to surface albedo. Concurrently, the analysis indicated a peak in potential BC input towards Khumbu from known source regions during this same pre-monsoon window. Given that BC is a potent light-absorbing particle known to reduce snow/ice albedo upon deposition, this seasonal coincidence strongly suggests a plausible contributing role for wildfire-derived aerosols in modulating the glacier's surface energy balance and potentially enhancing melt during this critical period in 2021. Although the literature indicates low overall transport efficiency to the high Himalayas, the timing supports the potential for deposited BC to act as a significant modulator of the surface energy budget alongside other primary drivers like incoming solar radiation and air temperature.

CHAPTER 6. CONCLUSION AND RECOMMENDATIONS

6.1 Conclusion

This research enhances the understanding of the complex interactions between Black Carbon (BC) pollution, particularly from wildfires, climate dynamics, and glacier retreats in the Himalayas. By employing a dual approach, the study characterized potential atmospheric transport pathways and associated BC emissions from wildfires using HYSPLIT, VIIRS, and IPCC methods, while independently analyzing the 2021 surface energy balance (SEB) of the Khumbu Glacier using HARv2 data.

The findings confirm dominant southwesterly transport pathways during the critical pre-monsoon season (March-May), originating largely from fire-prone regions in Nepal and India. Estimation of potential BC emissions associated with fires along these pathways indicated a pronounced seasonal peak, calculated as approximately 39.6 tonnes in March and peaking notably in April 2021 at 94 tonnes (using the convex hull method, though uncertainty remains in burned area estimation). Crucially, the SEB analysis identified this same pre-monsoon window as the onset period for significant melt potential (positive Qm), driven primarily by increasing net shortwave radiation (S_net) and thus highly sensitive to surface albedo changes. The compelling temporal alignment between the peak in potential BC transport/emissions and the glacier's heightened sensitivity establishes a strong plausible link suggesting wildfire BC contributes to modulating the SEB and enhancing melt during this critical period.

While quantifying the exact fraction of wildfire BC reaching and depositing remains complex due to transport/deposition uncertainties (atmospheric lifetime, scavenging, etc.) and the confounding influence of other BC sources (fossil fuels, biofuels), the estimated magnitude of potential wildfire emissions is significant, suggesting biomass burning may be an underrecognized contributor to Himalayan BC loading. This is further supported by the SEB analysis confirming that even modest BC deposition can meaningfully enhance glacier melt rates.

Therefore, this research highlights the potential importance of wildfire emissions in influencing Himalayan cryosphere dynamics. It provides an important step using physical modeling but underscores the critical need for future work integrating source-specific observational data (field measurements) with refined atmospheric transport and deposition modeling (e.g., WRF-Chem, SNICAR) to improve attribution and quantitatively assess this impact. Given the potential for

transboundary emissions to accelerate melt, policymaking efforts to mitigate regional biomass burning, especially pre-monsoon, alongside regional cooperation on fire management and air pollution control, appear critical for sustaining water security in Himalayan River basins.

6.2 Recommendations

Building upon the findings and identified limitations of this study, the following recommendations are proposed for future research and potential mitigation strategies:

- **Integrated Modeling**: The most critical next step is to quantitatively assess the impact of wildfire BC by employing coupled modeling systems. This involves integrating wildfire emission inventories (potentially refined beyond standard IPCC factors) with atmospheric chemical transport models (e.g., WRF-Chem, GEOS-Chem) to simulate BC transport and deposition onto the Khumbu Glacier, subsequently forcing a snow/ice energy balance model (like SEMB or incorporating a scheme like SNICAR) with dynamically calculated BC-induced albedo changes.
- **Refine Emission and Burned Area Estimates**: Improve the accuracy of potential BC emission calculations by utilizing region-specific fuel loading data, combustion factors, and emission factors where available, moving beyond generalized IPCC values. Further investigation into refining burned area estimates from satellite data (VIIRS, MODIS) specifically for Himalayan terrain and vegetation types is also warranted, addressing potential commission/omission errors.
- **Field Validation**: Conduct targeted field campaigns on the Khumbu Glacier, particularly during the pre-monsoon season, to measure actual BC concentrations in surface snow and atmospheric aerosols. Source apportionment techniques (e.g., using Aethalometer data or isotopic analysis) could help differentiate wildfire contributions from other sources, providing crucial data for model validation.
- **Transboundary Collaboration**: Given that identified source regions and transport pathways are transboundary, encourage regional cooperation focused on sustainable fire management practices (both forest fires and agricultural burning) and air quality control measures, particularly targeting the pre-monsoon season, as a potential strategy to mitigate BC impacts on sensitive Himalayan glaciers

REFRENCES

Acharya, A., & Kayastha, R. B. (2019). Mass and Energy Balance Estimation of Yala Glacier (2011–2017), Langtang Valley, Nepal. *Water*, *11*(1), Article 1. https://doi.org/10.3390/w11010006

Akagi, S. K., Yokelson, R. J., Wiedinmyer, C., Alvarado, M. J., Reid, J. S., Karl, T., Crounse, J. D., & Wennberg, P. O. (2011). Emission factors for open and domestic biomass burning for use in atmospheric models. *Atmospheric Chemistry and Physics*, *11*(9), 4039–4072. https://doi.org/10.5194/acp-11-4039-2011

Alvarado, M. J., Winijkul, E., Adams-Selin, R., Hunt, E., Brodowski, C., Lonsdale, C. R., Shindell, D. T., Faluvegi, G., Kleiman, G., Mosier, T. M., & Kumar, R. (2018). Sources of Black Carbon Deposition to the Himalayan Glaciers in Current and Future Climates. *Journal of Geophysical Research: Atmospheres*, *123*(14), 7482–7505. https://doi.org/10.1029/2018JD029049

Assessment, U. E. N. C. for E. (2009, March 15). *Radiation and energy balance dynamics over a rapidly receding glacier in the central Himalaya* [WEB SITE]. https://hero.epa.gov/hero/index.cfm/reference/details/reference_id/7299311

Aubry-Wake, C., Bertoncini, A., & Pomeroy, J. W. (2022). Fire and Ice: The Impact of Wildfire-Affected Albedo and Irradiance on Glacier Melt. *Earth's Future*, *10*(4), e2022EF002685. https://doi.org/10.1029/2022EF002685

Bali, K., Mishra, A. K., & Singh, S. (2017). Impact of anomalous forest fire on aerosol radiative forcing and snow cover over Himalayan region. *Atmospheric Environment*, *150*, 264–275.

Barker, J. D., Kaspari, S., Gabrielli, P., Wegner, A., Beaudon, E., Sierra-Hernández, M. R., & Thompson, L. (2021). Drought-induced biomass burning as a source of black carbon to the central Himalaya since 1781 CE as reconstructed from the Dasuopu ice core. *Atmospheric Chemistry and Physics*, *21*(7), 5615–5633. https://doi.org/10.5194/acp-21-5615-2021

Bhujel, K., Byanju, R., & Gautam, A. (2019). WILDFIRE DYNAMICS AND ITS EFFECTS ON THE FOREST RESOURCES AND PUBLIC PROPERTY IN NEPAL. *Journal of Institute of Science and Technology*, *23*, 61–68. https://doi.org/10.3126/jist.v23i1.22197

Black carbon and glacier melt—ICIMOD. (2020, August 14). https://www.icimod.org/success-stories/chapter-2/black-carbon-and-glacier-melt/

Bonasoni, P., Laj, P., Marinoni, A., Sprenger, M., Angelini, F., Arduini, J., Bonafè, U., Calzolari, F., Colombo, T., & Decesari, S. (2010). Atmospheric Brown Clouds in the Himalayas: First two years of continuous observations at the Nepal Climate Observatory-Pyramid (5079 m). *Atmospheric Chemistry and Physics*, *10*(15), 7515–7531.

Bond, T. C., Doherty, S. J., Fahey, D. W., Forster, P. M., Berntsen, T., DeAngelo, B. J., Flanner, M. G., Ghan, S., Kärcher, B., Koch, D., Kinne, S., Kondo, Y., Quinn, P. K., Sarofim, M. C., Schultz, M. G., Schulz, M., Venkataraman, C., Zhang, H., Zhang, S., … Zender, C. S. (2013). Bounding the role of black carbon in the climate system: A scientific assessment. *Journal of Geophysical Research: Atmospheres*, *118*(11), 5380–5552. https://doi.org/10.1002/jgrd.50171

Boschetti, L., Roy, D. P., Giglio, L., Huang, H., Zubkova, M., & Humber, M. L. (2019). Global validation of the collection 6 MODIS burned area product. *Remote*

Sensing of Environment, *235*, 111490. https://doi.org/10.1016/j.rse.2019.111490

Castagna, J., Senatore, A., Bencardino, M., D'Amore, F., Sprovieri, F., Pirrone, N., & Mendicino, G. (2021). Multiscale assessment of the impact on air quality of an intense wildfire season in southern Italy. *Science of The Total Environment*, *761*, 143271. https://doi.org/10.1016/j.scitotenv.2020.143271

Chaudhary, K., Khanal, S. N., & Shrestha, K. L. (2024). Potential Sources and Seasonal Transport Pathways of Organic and Elemental Carbon in the Lesser Himalayan Zone of Central Nepal. *Journal of Environment Sciences*, *10*, 19–33. https://doi.org/10.3126/jes.v10i1.66914

Chen, X., Kang, S., Cong, Z., Yang, J., & Ma, Y. (2018). Concentration, temporal variation, and sources of black carbon in the Mt. Everest region retrieved by real-time observation and simulation. *Atmospheric Chemistry and Physics*, *18*(17), 12859–12875.

Cui, L., Song, X., & Zhong, G. (2021). Comparative Analysis of Three Methods for HYSPLIT Atmospheric Trajectories Clustering. *Atmosphere*, *12*(6), Article 6. https://doi.org/10.3390/atmos12060698

Deshpande, M. V., Pillai, D., & Jain, M. (2022). Detecting and quantifying residue burning in smallholder systems: An integrated approach using Sentinel-2 data. *International Journal of Applied Earth Observation and Geoinformation*, *108*, 102761. https://doi.org/10.1016/j.jag.2022.102761

Ditas, J., Ma, N., Zhang, Y., Assmann, D., Neumaier, M., Riede, H., Karu, E., Williams, J., Scharffe, D., Wang, Q., Saturno, J., Schwarz, J. P., Katich, J. M., McMeeking, G. R., Zahn, A., Hermann, M., Brenninkmeijer, C. A. M., Andreae, M. O., Pöschl,

U., … Cheng, Y. (2018). Strong impact of wildfires on the abundance and aging of black carbon in the lowermost stratosphere. *Proceedings of the National Academy of Sciences*, *115*(50), E11595–E11603. https://doi.org/10.1073/pnas.1806868115

Dou, T.-F., & Xiao, C.-D. (2016). An overview of black carbon deposition and its radiative forcing over the Arctic. *Advances in Climate Change Research*, *7*(3), 115–122. https://doi.org/10.1016/j.accre.2016.10.003

Draxler, R. R., & Rolph, G. D. (2010). HYSPLIT (HYbrid Single-Particle Lagrangian Integrated Trajectory) model access via NOAA ARL READY website (http://ready. Arl. Noaa. Gov/HYSPLIT. php). NOAA Air Resources Laboratory. *Silver Spring, MD*, *25*(1). https://www.ready.noaa.gov/hysplit_metadata.html

Gibson, M. J., Irvine-Fynn, T. D. L., Wagnon, P., Rowan, A. V., Quincey, D. J., Homer, R., & Glasser, N. F. (2018). Variations in near-surface debris temperature through the summer monsoon on Khumbu Glacier, Nepal Himalaya. *Earth Surface Processes and Landforms*, *43*(13), 2698–2714. https://doi.org/10.1002/esp.4425

Gul, C., He, C., Kang, S., Xu, Y., Wu, X., Koch, I., Barker, J., Kumar, R., Ullah, R., Faisal, S., & Puppala, S. P. (2024). Measured black carbon deposition over the central Himalayan glaciers: Concentrations in surface snow and impact on snow albedo reduction. *Atmospheric Pollution Research*, *15*(9). https://doi.org/10.1016/j.apr.2024.102203

Gul, C., Kang, S., Puppala, S. P., Wu, X., He, C., Xu, Y., Koch, I., Muhammad, S., Kumar, R., & Dubache, G. (2022). Measurement of light-absorbing particles in surface snow of central and western Himalayan glaciers: Spatial variability,

radiative impacts, and potential source regions. *Atmospheric Chemistry and Physics*, *22*(13), 8725–8737. https://doi.org/10.5194/acp-22-8725-2022

Gul, C., Mahapatra, P. S., Kang, S., Singh, P. K., Wu, X., He, C., Kumar, R., Rai, M., Xu, Y., & Puppala, S. P. (2021). Black carbon concentration in the central Himalayas: Impact on glacier melt and potential source contribution. *Environmental Pollution*, *275*, 116544.

Hadley, O. L. (2008). *Black carbon transport and deposition to the California mountain snow pack* [UC San Diego]. https://escholarship.org/uc/item/4td6n0n8

Han, H., Wu, Y., Liu, J., Zhao, T., Zhuang, B., Wang, H., Li, Y., Chen, H., Zhu, Y., Liu, H., Wang, Q., Li, S., Wang, T., Xie, M., & Li, M. (2020). Impacts of atmospheric transport and biomass burning on the inter-annual variation in black carbon aerosols over the Tibetan Plateau. *Atmospheric Chemistry and Physics*, *20*(21), 13591–13610. https://doi.org/10.5194/acp-20-13591-2020

He, J., Gong, S., Yu, Y., Yu, L., Wu, L., Mao, H., Song, C., Zhao, S., Liu, H., Li, X., & Li, R. (2017). Air pollution characteristics and their relation to meteorological conditions during 2014–2015 in major Chinese cities. *Environmental Pollution*, *223*, 484–496. https://doi.org/10.1016/j.envpol.2017.01.050

Hodson, A. J. (2014). Understanding the dynamics of black carbon and associated contaminants in glacial systems. *WIREs Water*, *1*(2), 141–149. https://doi.org/10.1002/wat2.1016

Jacobi, H.-W., Lim, S., Ménégoz, M., Ginot, P., Laj, P., Bonasoni, P., Stocchi, P., Marinoni, A., & Arnaud, Y. (2015a). Black carbon in snow in the upper Himalayan Khumbu Valley, Nepal: Observations and modeling of the

impact on snow albedo, melting, and radiative forcing. *The Cryosphere*, *9*(4), 1685–1699.

Jacobi, H.-W., Lim, S., Ménégoz, M., Ginot, P., Laj, P., Bonasoni, P., Stocchi, P., Marinoni, A., & Arnaud, Y. (2015b). Black carbon in snow in the upper Himalayan Khumbu Valley, Nepal: Observations and modeling of the impact on snow albedo, melting, and radiative forcing. *The Cryosphere*, *9*(4), 1685–1699.

Johnston, F., Hanigan, I., Henderson, S., Morgan, G., & Bowman, D. (2011). Extreme air pollution events from bushfires and dust storms and their association with mortality in Sydney, Australia 1994-2007. *Environmental Research*, *111*(6), 811–816. https://doi.org/10.1016/j.envres.2011.05.007

Karakoti, I., Singh, N., Shukla, T., Gairola, A. C., & Dobhal, D. P. (2023). Characterization and source apportionment of black carbon over a valley glacier at transitional climatic zone of the central-western Himalaya. *Theoretical and Applied Climatology*, *151*(3), 1383–1397. https://doi.org/10.1007/s00704-022-04313-z

Kaspari, S., McKenzie Skiles, S., Delaney, I., Dixon, D., & Painter, T. H. (2015). Accelerated glacier melt on Snow Dome, Mount Olympus, Washington, USA, due to deposition of black carbon and mineral dust from wildfire. *Journal of Geophysical Research: Atmospheres*, *120*(7), 2793–2807. https://doi.org/10.1002/2014JD022676

Kaspari, S., Painter, T. H., Gysel, M., Skiles, S. M., & Schwikowski, M. (2014a). Seasonal and elevational variations of black carbon and dust in snow and ice in the Solu-Khumbu, Nepal and estimated radiative forcings. *Atmospheric Chemistry and Physics*, *14*(15), 8089–8103.

Kaspari, S., Painter, T. H., Gysel, M., Skiles, S. M., & Schwikowski, M. (2014b). Seasonal and elevational variations of black carbon and dust in snow and ice in the Solu-Khumbu, Nepal and estimated radiative forcings. *Atmospheric Chemistry and Physics*, *14*(15), Article 15.

Kayastha, R. B., Ohata, T., & Ageta, Y. (1999). Application of a mass-balance model to a Himalayan glacier. *Journal of Glaciology*, *45*(151), 559–567. https://doi.org/10.3189/S002214300000143X

Khan, A. L., Xian, P., & Schwarz, J. P. (2023). Black carbon concentrations and modeled smoke deposition fluxes to the bare-ice dark zone of the Greenland Ice Sheet. *The Cryosphere*, *17*(7), 2909–2918. https://doi.org/10.5194/tc-17-2909-2023

Kim, Y., Hatsushika, H., Muskett, R. R., & Yamazaki, K. (2005). Possible effect of boreal wildfire soot on Arctic sea ice and Alaska glaciers. *Atmospheric Environment*, *39*(19), 3513–3520. https://doi.org/10.1016/j.atmosenv.2005.02.050

Kopacz, M., Mauzerall, D. L., Wang, J., Leibensperger, E. M., Henze, D. K., & Singh, K. (2011). Origin and radiative forcing of black carbon transported to the Himalayas and Tibetan Plateau. *Atmospheric Chemistry and Physics*, *11*(6), 2837–2852. https://doi.org/10.5194/acp-11-2837-2011

Kostrykin, S., Revokatova, A., Chernenkov, A., Ginzburg, V., Polumieva, P., & Zelenova, M. (2021a). Black carbon emissions from the Siberian fires 2019: Modelling of the atmospheric transport and possible impact on the radiation balance in the Arctic region. *Atmosphere*, *12*(7), 814.

Kostrykin, S., Revokatova, A., Chernenkov, A., Ginzburg, V., Polumieva, P., & Zelenova, M. (2021b). Black carbon emissions from the Siberian fires 2019:

Modelling of the atmospheric transport and possible impact on the radiation balance in the Arctic region. *Atmosphere*, *12*(7), Article 7.

Liu, Y., Goodrick, S., & Heilman, W. (2014). Wildland fire emissions, carbon, and climate: Wildfire–climate interactions. *Forest Ecology and Management*, *317*, 80–96. https://doi.org/10.1016/j.foreco.2013.02.020

Marinoni, A., Cristofanelli, P., Laj, P., Duchi, R., Calzolari, F., Decesari, S., Sellegri, K., Vuillermoz, E., Verza, G. P., & Villani, P. (2010). Aerosol mass and black carbon concentrations, a two year record at NCO-P (5079 m, Southern Himalayas). *Atmospheric Chemistry and Physics*, *10*(17), 8551–8562.

Matin, M. A., Chitale, V. S., Murthy, M. S., Uddin, K., Bajracharya, B., & Pradhan, S. (2017). Understanding forest fire patterns and risk in Nepal using remote sensing, geographic information system and historical fire data. *International Journal of Wildland Fire*, *26*(4), 276–286.

Ming, J., Xiao, C., Du, Z., & Yang, X. (2013). An overview of black carbon deposition in High Asia glaciers and its impacts on radiation balance. *Advances in Water Resources*, *55*, 80–87. https://doi.org/10.1016/j.advwatres.2012.05.015

Neupane, B., Kang, S., Chen, P., Zhang, Y., Ram, K., Rupakheti, D., Tripathee, L., Sharma, C. M., Cong, Z., Li, C., Hou, J., Xu, M., & Thapa, P. (2019). Historical Black Carbon Reconstruction from the Lake Sediments of the Himalayan–Tibetan Plateau. *Environmental Science & Technology*, *53*(10), 5641–5651. https://doi.org/10.1021/acs.est.8b07025

O'Neill, A. (2021). *Analytical Hierarchical Modeling of Glacial Lake Outburst Flood Potential in the Khumbu Region, Nepal* [PhD Thesis, Appalachian State

University].
https://libres.uncg.edu/ir/asu/f/O'Neill_Alex_May%202021_Thesis.pdf

Pokharel, B. (2022). On the trend of amplified drought in Nepal that can enhance the potential for Himalayan wildfires. *AGU Fall Meeting Abstracts*, *2022*, NH56A-02.
https://ui.adsabs.harvard.edu/abs/2022AGUFMNH56A..02P/abstract

Qi, L., & Wang, S. (2019). Fossil fuel combustion and biomass burning sources of global black carbon from GEOS-Chem simulation and carbon isotope measurements. *Atmospheric Chemistry and Physics*, *19*(17), 11545–11557. https://doi.org/10.5194/acp-19-11545-2019

Rai, M., Mahapatra, P. S., Gul, C., Kayastha, R. B., Panday, A. K., & Puppala, S. P. (2019). Aerosol Radiative Forcing Estimation over a Remote High-altitude Location (~4900 masl) near Yala Glacier, Nepal. *Aerosol and Air Quality Research*, *19*(8), 1872–1891. https://doi.org/10.4209/aaqr.2018.09.0342

Ram, K., & Sarin, M. M. (2010). Spatio-temporal variability in atmospheric abundances of EC, OC and WSOC over Northern India. *Journal of Aerosol Science*, *41*(1), 88–98. https://doi.org/10.1016/j.jaerosci.2009.11.004

Ramanathan, V., & Carmichael, G. (2008). Global and regional climate changes due to black carbon. *Nature Geoscience*, *1*(4), 221–227. https://doi.org/10.1038/ngeo156

Regmi, J., Poudyal, K. N., Pokhrel, A., Gyawali, M., Tripathee, L., Panday, A., Barinelli, A., & Aryal, R. (2020). Investigation of Aerosol Climatology and Long-Range Transport of Aerosols over Pokhara, Nepal. *Atmosphere*, *11*(8), Article 8. https://doi.org/10.3390/atmos11080874

Rupper, S., & Roe, G. (2008). *Glacier Changes and Regional Climate: A Mass and Energy Balance Approach*. https://doi.org/10.1175/2008JCLI2219.1

Sandeep, K., Panicker, A. S., Gautam, A. S., Beig, G., Gandhi, N., Sanjeev, S., Shankar, R., & Nainwal, H. C. (2022). Black carbon over a high altitude Central Himalayan Glacier: Variability, transport, and radiative impacts. *Environmental Research*, *204*, 112017.

Sarkar, S., Singh, R. P., & Chauhan, A. (2018). Crop Residue Burning in Northern India: Increasing Threat to Greater India. *Journal of Geophysical Research: Atmospheres*, *123*(13), 6920–6934. https://doi.org/10.1029/2018JD028428

Schauer, G., Kasper-Giebl, A., & Močnik, G. (2016). Increased PM Concentrations during a Combined Wildfire and Saharan Dust Event Observed at High-Altitude Sonnblick Observatory, Austria. *Aerosol and Air Quality Research*, *16*(3), 542–554. https://doi.org/10.4209/aaqr.2015.05.0337

Schroeder, W., Oliva, P., Giglio, L., & Csiszar, I. A. (2014). The New VIIRS 375 m active fire detection data product: Algorithm description and initial assessment. *Remote Sensing of Environment*, *143*, 85–96. https://doi.org/10.1016/j.rse.2013.12.008

Stein, A. F., Draxler, R. R., Rolph, G. D., Stunder, B. J., Cohen, M. D., & Ngan, F. (2015). NOAA's HYSPLIT atmospheric transport and dispersion modeling system. *Bulletin of the American Meteorological Society*, *96*(12), Article 12.

Su, L., Yuan, Z., Fung, J. C. H., & Lau, A. K. H. (2015). A comparison of HYSPLIT backward trajectories generated from two GDAS datasets. *Science of The Total Environment*, *506–507*, 527–537. https://doi.org/10.1016/j.scitotenv.2014.11.072

Tartari, G., Verza, G., & Bertolami, L. (1998). Meteorological data at the pyramid observatory laboratory (khumbu valley, sagarmatha national park, nepal). *Mem. Ist. Ital. Idrobiol*, *57*, 23–40.

TheTimesofIndia. (2024, December 22). Forest fires down to 2.03 lakh in 2023-24 from 2.23 lakh in 2021-22. *The Times of India*. https://timesofindia.indiatimes.com/india/forest-fires-down-to-2-03-lakh-in-2023-24-from-2-23-lakh-in-2021-22/articleshow/116548462.cms?utm_source=chatgpt.com

Urbanski, S. (2014). Wildland fire emissions, carbon, and climate: Emission factors. *Forest Ecology and Management*, *317*, 51–60. https://doi.org/10.1016/j.foreco.2013.05.045

Vadrevu, K. P., Ellicott, E., Giglio, L., Badarinath, K. V. S., Vermote, E., Justice, C., & Lau, W. K. M. (2012). Vegetation fires in the himalayan region – Aerosol load, black carbon emissions and smoke plume heights. *Atmospheric Environment*, *47*, 241–251. https://doi.org/10.1016/j.atmosenv.2011.11.009

Veira, A., Lasslop, G., & Kloster, S. (2016). Wildfires in a warmer climate: Emission fluxes, emission heights, and black carbon concentrations in 2090–2099. *Journal of Geophysical Research: Atmospheres*, *121*(7), 3195–3223. https://doi.org/10.1002/2015JD024142

Vincent, C., Wagnon, P., Shea, J. M., Immerzeel, W. W., Kraaijenbrink, P., Shrestha, D., Soruco, A., Arnaud, Y., Brun, F., Berthier, E., & Sherpa, S. F. (2016). Reduced melt on debris-covered glaciers: Investigations from Changri Nup Glacier, Nepal. *The Cryosphere*, *10*(4), 1845–1858. https://doi.org/10.5194/tc-10-1845-2016

Vinogradova, A. A., & Vasileva, A. V. (2017). Black carbon in air over northern regions of Russia: Sources and spatiotemporal variations. *Atmospheric and Oceanic Optics*, *30*(6), 533–541. https://doi.org/10.1134/S1024856017060161

Wang, X., Tolksdorf, V., Otto, M., & Scherer, D. (2021). WRF-based dynamical downscaling of ERA5 reanalysis data for High Mountain Asia: Towards a new version of the High Asia Refined analysis. *International Journal of Climatology*, *41*(1), 743–762. https://doi.org/10.1002/joc.6686

Wiedinmyer, C., Kimura, Y., McDonald-Buller, E. C., Emmons, L. K., Buchholz, R. R., Tang, W., Seto, K., Joseph, M. B., Barsanti, K. C., Carlton, A. G., & Yokelson, R. (n.d.). *The Fire Inventory from NCAR version 2.5: An updated global fire emissions model for climate and chemistry applications*. Retrieved March 4, 2025, from https://repository.library.noaa.gov/view/noaa/58425

Writer, G. (2018, November 26). In Mount Everest Region, World's Highest Glaciers Are Melting. *Inside Climate News*. https://insideclimatenews.org/news/26112018/mount-everest-photos-world-highest-glacier-climate-change-khombu-icefall-climbing-route/

Xu, H., Ren, Y., Zhang, W., Meng, W., Yun, X., Yu, X., Li, J., Zhang, Y., Shen, G., Ma, J., Li, B., Cheng, H., Wang, X., Wan, Y., & Tao, S. (2021). Updated Global Black Carbon Emissions from 1960 to 2017: Improvements, Trends, and Drivers. *Environmental Science & Technology*, *55*(12), 7869–7879. https://doi.org/10.1021/acs.est.1c03117

Yasunari, T. J., Tan, Q., Lau, K.-M., Bonasoni, P., Marinoni, A., Laj, P., Ménégoz, M., Takemura, T., & Chin, M. (2013). Estimated range of black carbon dry deposition and the related snow albedo reduction over Himalayan glaciers

during dry pre-monsoon periods. *Atmospheric Environment*, *78*, 259–267. https://doi.org/10.1016/j.atmosenv.2012.03.031

You, C., & Xu, C. (2022). Himalayan glaciers threatened by frequent wildfires. *Nature Geoscience*, *15*(12), 956–957. https://doi.org/10.1038/s41561-022-01076-0

You, C., Yao, T., Xu, B., Xu, C., Zhao, H., & Song, L. (2016). Effects of sources, transport, and postdepositional processes on levoglucosan records in southeastern Tibetan glaciers. *Journal of Geophysical Research: Atmospheres*, *121*(14), 8701–8711. https://doi.org/10.1002/2016JD024904

Zeller, L., McGrath, D., McCoy, S. W., & Jacquet, J. (2024). Seasonal to decadal dynamics of supraglacial lakes on debris-covered glaciers in the Khumbu region, Nepal. *The Cryosphere*, *18*(2), 525–541. https://doi.org/10.5194/tc-18-525-2024

Zhang, R., Wang, H., Qian, Y., Rasch, P. J., Easter, R. C., Ma, P.-L., Singh, B., Huang, J., & Fu, Q. (2015). Quantifying sources, transport, deposition, and radiative forcing of black carbon over the Himalayas and Tibetan Plateau. *Atmospheric Chemistry and Physics*, *15*(11), 6205–6223. https://doi.org/10.5194/acp-15-6205-2015

ANNEX A :

Calculation of Potential Black Carbon (BC) Emissions from Wildfires Along the HYSPLIT Trajectory

Table 0 1 BC Emission Calculation for biomass burning along the Trajectory for the month of March2021

S.No	Area in Sq.km	Vegetation Type	Area_ha	Reduced area (overestimation)	Emission in tonnes (Lfire)
1	0.52	Agri and Crop Residue	52.01	39.01	0.13
2	1.00	Agri and Crop Residue	100.31	75.23	0.25
3	0.38	Agri and Crop Residue	38.03	28.52	0.09
4	0.37	Agri and Crop Residue	37.00	27.75	0.09
5	0.38	Agri and Crop Residue	38.03	28.52	0.09
6	0.55	Agri and Crop Residue	54.77	41.08	0.13
7	0.38	Agri and Crop Residue	38.03	28.52	0.09
8	0.93	Agri and Crop Residue	92.78	69.58	0.23
9	0.59	Agri and Crop Residue	59.45	44.59	0.15
10	0.44	Agri and Crop Residue	44.12	33.09	0.11
11	0.95	Agri and Crop Residue	95.48	71.61	0.23
12	0.40	Agri and Crop Residue	39.95	29.96	0.10
13	0.96	Agri and Crop Residue	95.81	71.86	0.23
14	0.52	Savanna and Grassland	52.47	39.35	0.04
15	0.37	Savanna and Grassland	37.00	27.75	0.03
16	0.45	Agri and Crop Residue	44.95	33.71	0.11
17	1.24	Savanna and Grassland	123.62	92.72	0.09
18	0.34	Tropical Forest	34.17	25.63	0.39
19	0.34	Tropical Forest	34.17	25.62	0.39
20	0.94	Tropical Forest	93.73	70.30	1.08
21	0.34	Tropical Forest	34.17	25.62	0.39
22	0.34	Savanna and Grassland	34.16	25.62	0.02
23	0.46	Agri and Crop Residue	45.91	34.43	0.11
24	0.68	Agri and Crop Residue	68.21	51.16	0.17
25	0.36	Agri and Crop Residue	35.99	26.99	0.09
26	0.68	Savanna and Grassland	68.43	51.32	0.05

S.No	Area in Sq.km	Vegetation Type	Area_ha	Reduced area (overestimation)	Emission in tonnes (Lfire)
27	0.49	Agri and Crop Residue	49.14	36.85	0.12
28	1.83	Tropical Forest	183.22	137.41	2.12
29	0.75	Savanna and Grassland	75.38	56.54	0.05
30	0.45	Savanna and Grassland	45.08	33.81	0.03
31	0.51	Savanna and Grassland	51.35	38.51	0.04
32	0.52	Savanna and Grassland	52.20	39.15	0.04
33	0.91	Tropical Forest	91.39	68.54	1.06
34	0.44	Tropical Forest	44.11	33.09	0.51
35	1.34	Savanna and Grassland	133.51	100.13	0.10
36	0.36	Tropical Forest	35.99	26.99	0.42
37	0.48	Tropical Forest	48.05	36.04	0.55
38	0.73	Savanna and Grassland	73.33	54.99	0.05
39	0.69	Savanna and Grassland	69.03	51.77	0.05
40	0.72	Tropical Forest	71.73	53.80	0.83
41	0.49	Savanna and Grassland	49.13	36.85	0.04
42	0.89	Savanna and Grassland	88.59	66.44	0.06
43	0.75	Savanna and Grassland	74.70	56.02	0.05
44	1.32	Tropical Forest	132.37	99.27	1.53
45	0.75	Savanna and Grassland	75.36	56.52	0.05
46	0.80	Tropical Forest	80.32	60.24	0.93
47	0.92	Agri and Crop Residue	92.10	69.07	0.23
48	0.34	Savanna and Grassland	34.12	25.59	0.02
49	0.84	Tropical Forest	84.29	63.22	0.97
50	0.56	Agri and Crop Residue	55.80	41.85	0.14
51	0.53	Savanna and Grassland	53.04	39.78	0.04
52	0.37	Tropical Forest	36.99	27.74	0.43
53	0.62	Agri and Crop Residue	61.94	46.45	0.15
54	1.52	Agri and Crop Residue	151.52	113.64	0.37

S.No	Area in Sq.km	Vegetation Type	Area_ha	Reduced area (overestimation)	Emission in tonnes (Lfire)
55	0.58	Savanna and Grassland	58.23	43.67	0.04
56	0.38	Agri and Crop Residue	37.89	28.42	0.09
57	0.56	Savanna and Grassland	55.93	41.95	0.04
58	0.95	Tropical Forest	95.05	71.29	1.10
59	1.04	Savanna and Grassland	103.92	77.94	0.07
60	1.16	Tropical Forest	116.15	87.11	1.34
61	0.63	Tropical Forest	63.24	47.43	0.73
62	1.10	Savanna and Grassland	109.68	82.26	0.08
63	0.50	Savanna and Grassland	50.00	37.50	0.04
64	0.52	Savanna and Grassland	52.18	39.14	0.04
65	0.63	Agri and Crop Residue	63.20	47.40	0.15
66	0.57	Agri and Crop Residue	57.22	42.91	0.14
67	0.76	Agri and Crop Residue	76.23	57.17	0.19
68	0.50	Agri and Crop Residue	49.77	37.33	0.12
69	0.50	Agri and Crop Residue	49.77	37.32	0.12
70	0.57	Agri and Crop Residue	57.22	42.92	0.14
71	0.51	Savanna and Grassland	51.09	38.32	0.04
72	0.43	Agri and Crop Residue	42.75	32.06	0.10
73	1.02	Agri and Crop Residue	101.82	76.36	0.25
74	0.75	Tropical Forest	74.81	56.11	0.86
75	1.32	Agri and Crop Residue	131.99	98.99	0.32
76	1.15	Agri and Crop Residue	115.29	86.47	0.28
77	0.62	Tropical Forest	61.76	46.32	0.71
78	0.37	Tropical Forest	36.87	27.66	0.43
79	0.60	Tropical Forest	60.48	45.36	0.70
80	0.83	Agri and Crop Residue	82.73	62.05	0.20
81	1.09	Agri and Crop Residue	109.14	81.85	0.27
82	0.48	Agri and Crop Residue	48.38	36.28	0.12

S.No	Area in Sq.km	Vegetation Type	Area_ha	Reduced area (overestimation)	Emission in tonnes (Lfire)
83	0.37	Agri and Crop Residue	36.87	27.65	0.09
84	0.58	Agri and Crop Residue	58.05	43.54	0.14
85	0.51	Agri and Crop Residue	51.18	38.39	0.13
86	0.60	Agri and Crop Residue	59.54	44.65	0.15
87	0.69	Agri and Crop Residue	68.83	51.62	0.17
88	0.34	Agri and Crop Residue	34.05	25.54	0.08
89	0.46	Agri and Crop Residue	45.80	34.35	0.11
90	0.50	Agri and Crop Residue	49.74	37.30	0.12
91	0.47	Agri and Crop Residue	47.20	35.40	0.12
92	0.62	Agri and Crop Residue	61.68	46.26	0.15
93	0.51	Agri and Crop Residue	50.54	37.91	0.12
94	1.16	Agri and Crop Residue	115.51	86.64	0.28
95	0.39	Agri and Crop Residue	38.79	29.09	0.09
96	0.34	Agri and Crop Residue	34.05	25.54	0.08
97	0.52	Agri and Crop Residue	51.88	38.91	0.13
98	0.58	Agri and Crop Residue	58.05	43.54	0.14
99	1.03	Agri and Crop Residue	102.76	77.07	0.25
100	1.06	Agri and Crop Residue	105.69	79.27	0.26
101	0.55	Agri and Crop Residue	54.97	41.23	0.13
102	1.10	Agri and Crop Residue	109.53	82.14	0.27
103	0.55	Agri and Crop Residue	54.97	41.23	0.13
104	0.88	Agri and Crop Residue	87.94	65.95	0.22
105	0.75	Agri and Crop Residue	75.13	56.35	0.18
106	0.70	Agri and Crop Residue	69.91	52.43	0.17
107	0.37	Agri and Crop Residue	36.88	27.66	0.09
108	0.52	Agri and Crop Residue	51.91	38.93	0.13
109	0.72	Agri and Crop Residue	71.99	53.99	0.18
110	0.50	Agri and Crop Residue	49.78	37.33	0.12

S.No	Area in Sq.km	Vegetation Type	Area_ha	Reduced area (overestimation)	Emission in tonnes (Lfire)
111	0.50	Agri and Crop Residue	49.78	37.34	0.12
112	0.49	Agri and Crop Residue	49.02	36.77	0.12
113	0.52	Agri and Crop Residue	51.91	38.94	0.13
114	1.03	Agri and Crop Residue	102.80	77.10	0.25
115	0.73	Agri and Crop Residue	73.35	55.01	0.18
116	0.45	Savanna and Grassland	44.80	33.60	0.03
117	0.36	Savanna and Grassland	35.89	26.92	0.03
Total SUM	77.40	**Total Sum**	7704.23	5778.17	29.69

Table 0 1 BC Emission Calculation for biomass burning along the Trajectory for the month of April 2021

S.No	Area in Sq.km	Vegetation Type	Area_ha	Reduced area (overestimation)	Emission in tonnes (Lfire)
1	0.77	Temperate Forest	76.79	76.79	0.54
2	0.41	Agri and Crop Residue	41.13	41.13	0.13
3	0.49	Agri and Crop Residue	49.22	49.22	0.16
4	0.78	Agri and Crop Residue	77.55	77.55	0.25
5	0.62	Agri and Crop Residue	61.98	61.98	0.20
6	0.63	Agri and Crop Residue	62.97	62.97	0.21
7	0.36	Agri and Crop Residue	35.91	35.91	0.12
8	0.49	Agri and Crop Residue	49.04	49.04	0.16
9	4.52	Agri and Crop Residue	451.70	451.70	1.47
10	1.13	Agri and Crop Residue	113.36	113.36	0.37
11	0.73	Agri and Crop Residue	72.55	72.55	0.24
12	1.07	Agri and Crop Residue	106.98	106.98	0.35
13	0.34	Agri and Crop Residue	34.11	34.11	0.11
14	0.65	Agri and Crop Residue	64.86	64.86	0.21
15	0.60	Agri and Crop Residue	60.19	60.19	0.20
16	0.37	Agri and Crop Residue	36.92	36.92	0.12
17	0.54	Agri and Crop Residue	54.27	54.27	0.18
18	0.95	Agri and Crop Residue	95.37	95.37	0.31
19	0.48	Agri and Crop Residue	47.96	47.96	0.16
20	4.02	Agri and Crop Residue	401.57	401.57	1.31
21	0.52	Agri and Crop Residue	52.35	52.35	0.17
22	0.66	Agri and Crop Residue	66.34	66.34	0.22
23	0.85	Agri and Crop Residue	85.12	85.12	0.28
24	1.24	Agri and Crop Residue	124.32	124.32	0.41
25	2.32	Agri and Crop Residue	232.30	232.30	0.76
26	0.57	Agri and Crop Residue	56.61	56.61	0.18

S.No	Area in Sq.km	Vegetation Type	Area_ha	Reduced area (overestimation)	Emission in tonnes (Lfire)
27	0.64	Agri and Crop Residue	64.23	64.23	0.21
28	3.13	Agri and Crop Residue	312.67	312.67	1.02
29	0.33	Agri and Crop Residue	33.17	33.17	0.11
30	1.67	Agri and Crop Residue	166.97	166.97	0.54
31	0.43	Agri and Crop Residue	42.90	42.90	0.14
32	0.55	Agri and Crop Residue	55.33	55.33	0.18
33	1.00	Agri and Crop Residue	100.03	100.03	0.33
34	0.71	Agri and Crop Residue	71.47	71.47	0.23
35	1.82	Agri and Crop Residue	181.53	181.53	0.59
36	0.46	Agri and Crop Residue	45.83	45.83	0.15
37	0.53	Agri and Crop Residue	53.48	53.48	0.17
38	0.43	Agri and Crop Residue	42.91	42.91	0.14
39	0.62	Agri and Crop Residue	61.98	61.98	0.20
40	0.52	Agri and Crop Residue	51.91	51.91	0.17
41	0.44	Agri and Crop Residue	43.88	43.88	0.14
42	1.16	Agri and Crop Residue	115.80	115.80	0.38
43	2.98	Agri and Crop Residue	297.67	297.67	0.97
44	0.48	Agri and Crop Residue	47.96	47.96	0.16
45	0.39	Agri and Crop Residue	38.84	38.84	0.13
46	0.96	Agri and Crop Residue	95.82	95.82	0.31
47	1.31	Agri and Crop Residue	131.39	131.39	0.43
48	0.63	Agri and Crop Residue	62.96	62.96	0.21
49	1.58	Agri and Crop Residue	157.76	157.76	0.51
50	0.63	Agri and Crop Residue	62.92	62.92	0.21
51	0.63	Agri and Crop Residue	62.97	62.97	0.21
52	0.33	Agri and Crop Residue	33.21	33.21	0.11
53	2.49	Agri and Crop Residue	248.56	248.56	0.81
54	0.86	Agri and Crop Residue	85.81	85.81	0.28

S.No	Area in Sq.km	Vegetation Type	Area_ha	Reduced area (overestimation)	Emission in tonnes (Lfire)
55	3.27	Agri and Crop Residue	327.12	327.12	1.07
56	0.34	Agri and Crop Residue	34.11	34.11	0.11
57	0.50	Agri and Crop Residue	49.78	49.78	0.16
58	1.11	Agri and Crop Residue	110.72	110.72	0.36
59	1.19	Agri and Crop Residue	118.82	118.82	0.39
60	0.61	Agri and Crop Residue	60.60	60.60	0.20
61	0.65	Agri and Crop Residue	65.34	65.34	0.21
62	0.45	Agri and Crop Residue	44.84	44.84	0.15
63	0.63	Agri and Crop Residue	62.96	62.96	0.21
64	0.46	Agri and Crop Residue	45.84	45.84	0.15
65	0.50	Agri and Crop Residue	49.88	49.88	0.16
66	0.38	Agri and Crop Residue	37.93	37.93	0.12
67	0.45	Agri and Crop Residue	44.84	44.84	0.15
68	1.81	Agri and Crop Residue	180.90	180.90	0.59
69	0.46	Agri and Crop Residue	45.83	45.83	0.15
70	0.53	Tropical Forest	53.34	53.34	0.82
71	0.87	Agri and Crop Residue	86.86	86.86	0.28
72	0.61	Agri and Crop Residue	60.53	60.53	0.20
73	0.49	Agri and Crop Residue	49.02	49.02	0.16
74	0.84	Agri and Crop Residue	84.02	84.02	0.27
75	0.84	Savanna and Grassland	84.17	84.17	0.08
76	0.33	Agri and Crop Residue	33.22	33.22	0.11
77	1.86	Agri and Crop Residue	185.52	185.52	0.61
78	0.66	Agri and Crop Residue	66.34	66.34	0.22
79	2.10	Agri and Crop Residue	209.63	209.63	0.68
80	0.81	Agri and Crop Residue	81.18	81.18	0.26
81	0.41	Agri and Crop Residue	40.95	40.95	0.13
82	0.33	Agri and Crop Residue	33.21	33.21	0.11

S.No	Area in Sq.km	Vegetation Type	Area_ha	Reduced area (overestimation)	Emission in tonnes (Lfire)
83	0.49	Agri and Crop Residue	49.00	49.00	0.16
84	1.67	Agri and Crop Residue	167.18	167.18	0.55
85	0.43	Agri and Crop Residue	42.90	42.90	0.14
86	0.89	Agri and Crop Residue	89.41	89.41	0.29
87	3.13	Agri and Crop Residue	312.57	312.57	1.02
88	0.78	Agri and Crop Residue	77.81	77.81	0.25
89	0.64	Agri and Crop Residue	64.22	64.22	0.21
90	0.42	Agri and Crop Residue	41.85	41.85	0.14
91	0.64	Agri and Crop Residue	63.88	63.88	0.21
92	1.82	Agri and Crop Residue	182.33	182.33	0.60
93	0.54	Agri and Crop Residue	54.10	54.10	0.18
94	0.59	Agri and Crop Residue	59.31	59.31	0.19
95	0.49	Agri and Crop Residue	48.99	48.99	0.16
96	1.04	Agri and Crop Residue	103.73	103.73	0.34
97	1.80	Agri and Crop Residue	179.73	179.73	0.59
98	1.50	Agri and Crop Residue	149.97	149.97	0.49
99	1.21	Agri and Crop Residue	121.35	121.35	0.40
100	0.39	Agri and Crop Residue	38.85	38.85	0.13
101	0.48	Agri and Crop Residue	47.96	47.96	0.16
102	0.54	Agri and Crop Residue	54.10	54.10	0.18
103	0.87	Agri and Crop Residue	86.99	86.99	0.28
104	0.53	Tropical Forest	52.51	52.51	0.81
105	0.84	Agri and Crop Residue	84.29	84.29	0.28
106	0.60	Agri and Crop Residue	60.49	60.49	0.20
107	0.49	Agri and Crop Residue	49.04	49.04	0.16
108	1.03	Tropical Forest	102.54	102.54	1.58
109	0.41	Agri and Crop Residue	40.95	40.95	0.13
110	0.52	Savanna and Grassland	52.20	52.20	0.05

S.No	Area in Sq.km	Vegetation Type	Area_ha	Reduced area (overestimation)	Emission in tonnes (Lfire)
111	0.52	Agri and Crop Residue	52.03	52.03	0.17
112	0.89	Savanna and Grassland	88.67	88.67	0.09
113	1.16	Agri and Crop Residue	115.58	115.58	0.38
114	0.73	Agri and Crop Residue	72.55	72.55	0.24
115	0.68	Tropical Forest	68.36	68.36	1.05
116	1.00	Agri and Crop Residue	100.01	100.01	0.33
117	1.23	Savanna and Grassland	123.46	123.46	0.12
118	0.83	Savanna and Grassland	82.87	82.87	0.08
119	0.52	Agri and Crop Residue	51.81	51.81	0.17
120	0.52	Agri and Crop Residue	52.34	52.34	0.17
121	0.56	Agri and Crop Residue	56.42	56.42	0.18
122	0.33	Agri and Crop Residue	33.22	33.22	0.11
123	0.49	Agri and Crop Residue	49.00	49.00	0.16
124	0.56	Agri and Crop Residue	56.42	56.42	0.18
125	0.33	Savanna and Grassland	33.23	33.23	0.03
126	0.74	Agri and Crop Residue	74.02	74.02	0.24
127	0.54	Tropical Forest	54.15	54.15	0.83
128	1.19	Agri and Crop Residue	119.24	119.24	0.39
129	2.07	Tropical Forest	206.51	206.51	3.18
130	1.60	Agri and Crop Residue	159.76	159.76	0.52
131	2.41	Agri and Crop Residue	240.79	240.79	0.79
132	0.55	Savanna and Grassland	55.44	55.44	0.05
133	0.63	Savanna and Grassland	63.26	63.26	0.06
134	2.39	Savanna and Grassland	238.97	238.97	0.23
135	0.42	Tropical Forest	41.96	41.96	0.65
136	0.52	Tropical Forest	52.15	52.15	0.80
137	0.57	Agri and Crop Residue	57.22	57.22	0.19
138	0.69	Agri and Crop Residue	68.90	68.90	0.22

S.No	Area in Sq.km	Vegetation Type	Area_ha	Reduced area (overestimation)	Emission in tonnes (Lfire)
139	0.49	Agri and Crop Residue	49.04	49.04	0.16
140	1.40	Tropical Forest	139.56	139.56	2.15
141	2.59	Savanna and Grassland	259.10	259.10	0.25
142	0.62	Savanna and Grassland	62.30	62.30	0.06
143	0.79	Temperate Forest	79.27	79.27	0.55
144	1.00	Agri and Crop Residue	100.01	100.01	0.33
145	1.17	Savanna and Grassland	116.68	116.68	0.11
146	1.26	Savanna and Grassland	126.27	126.27	0.12
147	0.52	Savanna and Grassland	52.20	52.20	0.05
148	1.14	Agri and Crop Residue	113.93	113.93	0.37
149	0.56	Agri and Crop Residue	56.40	56.40	0.18
150	0.67	Agri and Crop Residue	66.72	66.72	0.22
151	0.45	Agri and Crop Residue	44.83	44.83	0.15
152	0.49	Agri and Crop Residue	48.98	48.98	0.16
153	0.74	Agri and Crop Residue	73.56	73.56	0.24
154	0.47	Agri and Crop Residue	46.93	46.93	0.15
155	0.51	Agri and Crop Residue	51.20	51.20	0.17
156	0.95	Agri and Crop Residue	94.85	94.85	0.31
157	0.47	Tropical Forest	47.37	47.37	0.73
158	0.47	Agri and Crop Residue	47.20	47.20	0.15
159	0.48	Agri and Crop Residue	47.96	47.96	0.16
160	0.78	Agri and Crop Residue	78.31	78.31	0.26
161	0.45	Agri and Crop Residue	44.82	44.82	0.15
162	0.33	Tropical Forest	33.34	33.34	0.51
163	0.46	Agri and Crop Residue	45.83	45.83	0.15
164	0.54	Savanna and Grassland	54.43	54.43	0.05
165	0.66	Agri and Crop Residue	66.33	66.33	0.22
166	0.57	Agri and Crop Residue	57.22	57.22	0.19

S.No	Area in Sq.km	Vegetation Type	Area_ha	Reduced area (overestimation)	Emission in tonnes (Lfire)
167	0.94	Agri and Crop Residue	94.21	94.21	0.31
168	0.57	Agri and Crop Residue	57.22	57.22	0.19
169	0.92	Agri and Crop Residue	92.47	92.47	0.30
170	0.57	Agri and Crop Residue	57.29	57.29	0.19
171	1.50	Agri and Crop Residue	149.65	149.65	0.49
172	0.49	Agri and Crop Residue	49.01	49.01	0.16
173	0.92	Agri and Crop Residue	91.75	91.75	0.30
174	1.34	Tropical Forest	133.60	133.60	2.06
175	2.60	Agri and Crop Residue	260.07	260.07	0.85
176	0.55	Agri and Crop Residue	54.57	54.57	0.18
177	0.55	Agri and Crop Residue	54.57	54.57	0.18
178	1.43	Agri and Crop Residue	142.74	142.74	0.47
179	0.54	Tropical Forest	54.44	54.44	0.84
180	0.64	Agri and Crop Residue	63.88	63.88	0.21
181	0.53	Boreal Forest	52.61	52.61	0.42
182	0.89	Agri and Crop Residue	89.22	89.22	0.29
183	0.64	Agri and Crop Residue	64.21	64.21	0.21
184	0.48	Agri and Crop Residue	47.96	47.96	0.16
185	0.42	Agri and Crop Residue	41.79	41.79	0.14
186	0.63	Agri and Crop Residue	62.90	62.90	0.21
187	0.73	Agri and Crop Residue	72.54	72.54	0.24
188	0.33	Savanna and Grassland	33.20	33.20	0.03
189	0.54	Agri and Crop Residue	54.10	54.10	0.18
190	0.69	Agri and Crop Residue	68.86	68.86	0.22
191	1.26	Savanna and Grassland	125.81	125.81	0.12
192	0.44	Boreal Forest	44.12	44.12	0.35
193	0.45	Agri and Crop Residue	44.81	44.81	0.15
194	0.52	Agri and Crop Residue	52.29	52.29	0.17

S.No	Area in Sq.km	Vegetation Type	Area_ha	Reduced area (overestimation)	Emission in tonnes (Lfire)
195	0.39	Tropical Forest	38.84	38.84	0.60
196	1.25	Tropical Forest	125.47	125.47	1.93
197	0.63	Tropical Forest	62.90	62.90	0.97
198	0.45	Agri and Crop Residue	44.81	44.81	0.15
199	0.63	Tropical Forest	62.92	62.92	0.97
200	0.52	Tropical Forest	51.92	51.92	0.80
201	0.66	Savanna and Grassland	66.34	66.34	0.06
202	0.52	Savanna and Grassland	51.92	51.92	0.05
203	1.34	Agri and Crop Residue	134.25	134.25	0.44
204	0.55	Agri and Crop Residue	54.57	54.57	0.18
205	1.29	Agri and Crop Residue	128.97	128.97	0.42
206	3.64	Agri and Crop Residue	363.91	363.91	1.19
207	0.42	Agri and Crop Residue	41.80	41.80	0.14
208	0.78	Agri and Crop Residue	77.50	77.50	0.25
209	0.54	Agri and Crop Residue	54.08	54.08	0.18
210	0.78	Agri and Crop Residue	77.50	77.50	0.25
211	0.55	Agri and Crop Residue	54.95	54.95	0.18
212	1.35	Tropical Forest	135.39	135.39	2.08
213	0.34	Agri and Crop Residue	34.06	34.06	0.11
214	0.49	Agri and Crop Residue	48.95	48.95	0.16
215	0.43	Agri and Crop Residue	42.76	42.76	0.14
216	1.81	Tropical Forest	181.28	181.28	2.79
217	0.78	Tropical Forest	77.69	77.69	1.20
218	0.59	Tropical Forest	59.26	59.26	0.91
219	0.48	Agri and Crop Residue	48.38	48.38	0.16
220	0.72	Savanna and Grassland	71.61	71.61	0.07
221	0.68	Agri and Crop Residue	68.03	68.03	0.22
222	0.83	Agri and Crop Residue	82.76	82.76	0.27

S.No	Area in Sq.km	Vegetation Type	Area_ha	Reduced area (overestimation)	Emission in tonnes (Lfire)
223	2.76	Tropical Forest	275.70	275.70	4.24
224	0.62	Agri and Crop Residue	61.65	61.65	0.20
225	1.16	Agri and Crop Residue	116.28	116.28	0.38
226	1.65	Agri and Crop Residue	165.37	165.37	0.54
227	0.82	Agri and Crop Residue	81.74	81.74	0.27
228	1.32	Agri and Crop Residue	131.96	131.96	0.43
229	1.00	Agri and Crop Residue	100.13	100.13	0.33
230	0.85	Agri and Crop Residue	84.63	84.63	0.28
231	0.49	Agri and Crop Residue	48.98	48.98	0.16
232	0.91	Agri and Crop Residue	91.18	91.18	0.30
233	0.60	Agri and Crop Residue	60.49	60.49	0.20
234	0.46	Agri and Crop Residue	45.82	45.82	0.15
235	0.52	Agri and Crop Residue	51.88	51.88	0.17
236	0.43	Agri and Crop Residue	42.75	42.75	0.14
237	0.55	Agri and Crop Residue	54.96	54.96	0.18
238	0.55	Agri and Crop Residue	54.96	54.96	0.18
239	1.04	Agri and Crop Residue	104.26	104.26	0.34
240	1.12	Agri and Crop Residue	112.18	112.18	0.37
241	0.50	Agri and Crop Residue	49.74	49.74	0.16
242	0.52	Agri and Crop Residue	51.91	51.91	0.17
243	3.26	Agri and Crop Residue	325.96	325.96	1.06
244	0.82	Agri and Crop Residue	81.72	81.72	0.27
245	0.73	Agri and Crop Residue	73.36	73.36	0.24
246	0.64	Agri and Crop Residue	63.98	63.98	0.21
247	0.91	Agri and Crop Residue	91.16	91.16	0.30
248	0.57	Agri and Crop Residue	56.88	56.88	0.19
249	0.70	Agri and Crop Residue	69.89	69.89	0.23
		Total Sum	21882.38	21882.38	93.82

Table 0 1 BC Emission Calculation for biomass burning along the Trajectory for the month of March2021

S.No	Area in SqKm	Vegetation Type	Area_ha	L_fire_tonnes	Emission
1	0.846	Savanna and Grassland	84.56	0.14	0.143919
2	0.931	Savanna and Grassland	93.10	0.16	0.158457
3	0.671	Savanna and Grassland	67.09	0.11	0.114195
		Total SUM	244.754		0.416571

Table A: Values for EF, Mf , Cf for various types of Vegetation

Vegetation types	**Emission Factor (g/kg)·**	**Mass of Fuel (tonne/hectare)**	**Combustion Factor(unitless)**	**Mass of Fuel * Cf**	
Tropical Forest	0.52	82.222	0.36	29.6	For Dry Tropical
Temperate Forest	0.56	27.77777778	0.45	12.5	
Boreal Forest	0.2	116.471	0.34	39.6	
Savanna and Grassland	0.37	3.514	0.74	2.6	
Agri and Crop Residue	0.51	8	0.8	6.4	

Emission Factor =The Fire Inventory from NCAR version 2.5: an updated global fire emissions model for climate and chemistry applications
Combustion Factor =2019 Refinement to the 2006 IPCC Guidelines for National Greenhouse Gas Inventories
Mass of Fuel = Emission factors for open and domestic biomass burning for use in atmospheric models (Vander Werf et.al(2010)

IOE Graduate Conference

Certificate of Participation

THIS CERTIFICATE IS AWARDED TO

Aashutosh Paudel

in recognition of an invaluable contribution as

PAPER PRESENTER

at the 16th IOE Graduate Conference

Organized by Tribhuvan University, IOE, Thapathali Campus in association with IOE, Office of the Dean held from April 18-20, 2025 at Thapathali Campus, Kathmandu, Nepal.

Dr. Raj Kumar Chaulagain
Convener
16th IOE Graduate Conference

Dr. Khem Gyanwali
Campus Chief
Thapathali Campus

Prof. Dr. Sushil Bahadur Bajracharya
Dean
Institute of Engineering

त्रिभुवन विश्वविद्यालय
Tribhuvan University
इन्जिनियरिङ्ग अध्ययन संस्थान
Institute of Engineering
थापाथली क्याम्पस
THAPATHALI CAMPUS
Accredited By University Grants Commission (UGC) Nepal, 2024

GPO Box- 280, Thapathali, Kathmandu
Tel: 01-5339766
E-mail: info@tcioe.edu.np
Website: www.tcioe.edu.np
गोश्वारा पो. नं. २८०, थापाथली, काठमाडौं
फोन: ०१-५३३५७६६

Date: April 21, 2025

To Whom It May Concern:

This is to certify that the paper titled **"Tracing the Potential Transport Pathways of Wildfire-Related Air Masses to the Khumbu Glacier using HYSPLIT Backward Trajectories"** (Submission# **105**) submitted by **Aashutosh Paudel** as the first author, which had been accepted for presentation after the peer-review process, has successfully been presented at the 16th IOE Graduate Conference held during April 18 - 20, 2025. Kindly note that the final revision of the papers and publication process of the conference proceedings is still underway and hence inclusion of the accepted manuscript in the conference proceedings is contingent upon timely response to further edits during the publication process.

INSTITUTE OF ENGINEERING
16th IOE Graduate Conference, 2025
THAPATHALI CAMPUS

Dr. Raj Kumar Chaulagain,
Convener,
16th IOE Graduate Conference

Tracing the Potential Transport Pathways of Wildfire-Related Air Masses to the Khumbu Glacier Using HYSPLIT Backward Trajectories

Aashutosh Paudel [a], Dhiraj Pradhananga [b]

Department of Applied Sciences and Chemical Engineering,Pulchowk Campus, Institute of Engineering, Tribhuvan University, Kathmandu, 44600, Nepal
Department of Meteorology , Tri-Chandra Multiple Campus, Tribhuvan University, Kathmandu Nepal
[a] 079msccd001.aashutosh@pcampus.edu.np

Abstract
Forests are critical for carbon sequestration, biodiversity conservation, and ecosystem regulation. Still, wildfires' black carbon (BC) can travel great distances to Himalayan glaciers, accelerating their melt and impacting regional climate and water supplies. This study employs HYSPLIT backward trajectory analysis for 120 hours from the Khumbu Glacier, tracking possible wildfire events along the trajectory with a focus on the year 2021 and a 500-meter planetary boundary layer (PBL). Results indicate that pre-monsoon southwesterly airflows facilitate long-range BC transport from biomass-burning locations in South Asia, with peak contributions occurring between March and May. During the monsoon season (June-September), increased precipitation and wet scavenging reduce BC deposition. However, post-monsoon months (October-December) witness a resurgence in BC transport, notably from the Indo-Gangetic Plain, where stable air conditions and widespread biomass burning lead to increased deposition hazards. These findings emphasize the significance of air circulation in influencing BC transport and its implications for glacier melt in the Himalayas. This study explores the transport pathways of wildfire-derived BC to the Khumbu Glacier during the pre-monsoon season using HYSPLIT backward trajectory analysis. This technique enhances understanding of how regional and long-transport wildfire emissions contribute to BC accumulation in the Khumbu region.

Keywords
HYSPLIT, Backward trajectory, Black Carbon, Wildfires

1. Introduction

BC emissions primarily originate from the incomplete combustion of biomass (forest fires, grass burning, etc.), biofuels (firewood, charcoal, etc.), and fossil fuels (coal, petroleum products) [1]. When BC deposits onto snow and ice, it reduces their albedo, accelerating melting[2]. BC is thought to be the second-largest human contributor to global warming after CO_2 because of its high absorption of light at visible and infrared wavelengths[3]. BC remains suspended in the atmosphere for approximately one week before being removed through both dry and wet deposition [4]. The Dry deposition is typically smaller in magnitude compared to wet deposition[5][6]. Wet deposition is the primary process for removing black carbon, responsible for over 90% of its total deposition in the Arctic [7]. The role of forest fires in snow and glacier melt is gaining greater recognition [8]. According to [9] real-time observations and simulation studies significant BC transport to the snow-capped Everest region. Since 2006, observations at the Nepal Climate Observatory at Pyramid (NCO-P), situated at 5079 m above sea level, have confirmed that aerosols, including BC, can be effectively transported from their sources to high-altitude regions in the Himalayan regions[10][11]. Surface glacier melt was affected by upwind wildfire activity by reducing surface albedo due to soot deposition on the glacier and by altering atmospheric conditions above the glacier through smoke[12]. Emissions from wildfires, particularly crown fires in the forest canopy, can easily rise to altitudes above 5 km, reaching up to 8-9 km in the mid-troposphere above the forest crown. Between 2000 and 2019, the Khumbu region experienced an approximate 34% expansion in the area of its glacial lakes, along with an estimated 42% rise in the total volume of liquid water contained within these lakes[13]. The Khumbu Glacier, the highest in the world, is receding at about 30 meters per year[14]. This study aims to determine how much BC from wildfires has accelerated the melting of the Khumbu Glacier. The annual cycle can be divided into four distinct climatic periods instead of the traditional seasonal classifications winter (December to February), pre-monsoon (March to May), the Southwest monsoon (June to September), and post-monsoon (October to November)[15].We thus define the period "March-end of May" as pre-monsoon, and the period "end of May–September" as monsoon season[16][17][18].

2. Methodology

2.1 Study Area

The Khumbu region is situated in northeastern Nepal, within the Solukhumbu district of Koshi Pradesh, covering around 1,148 km^2 square kilometers (443 $miles^2$) and bordering Tibet to the north. Encircled by the majestic Himalayas, the region is defined by snow-capped peaks, including Everest, Lhotse, Nuptse, and Ama Dablam, which dominate the landscape. Khumbu Glacier (27.970) stretches approximately 17 km in length and covers an area of about 27 km², which includes its detached tributary glaciers, Changri Nup and Changri Sharthey concluded that the concentrations of BC in the Khumbu Valley exhibit a seasonal pattern, with lower levels

during the post-monsoon and winter seasons, and higher levels during the pre-monsoon, reaching peak concentrations just before the monsoon begins[19][20][21]. In the Khumbu region, the climate features a summer monsoon season when almost all of the annual rainfall, about 587 ± 34 mm, occurs. The winters are cold and dry with little precipitation[22].

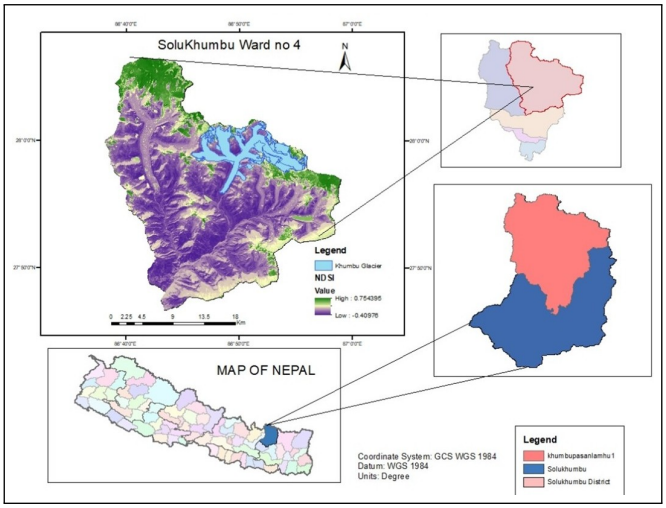

Figure 1: Location of the Study Area

2.2 The HYSPLIT Back Trajectories

The Air Resources Laboratory's Hybrid Single-Particle Lagrangian Integrated Trajectory (HYSPLIT) model is a full-fledged system for simulating both simple air parcel trajectories and complex dispersion and deposition scenarios[23].The model uses a combination of the Lagrangian and Eulerian approaches, with the former assuming air parcel advection and diffusion from a starting point and the latter observing a fixed three-dimensional grid across time[24].This work employs the HYSPLIT model with the Lagrangian technique to calculate backward trajectories.

The HYSPLIT Ready Atmospheric Transfer Modeling System (https://www.ready.noaa.gov/HYSPLIT_traj.php) provides an online tool to calculate trajectories using global meteorological data. Data sources include GDAS with 1° spatial resolution (2006-present) and 0.5° (09/2007-06/2019), GFS with 0.25° resolution (06/2019-present), and NCEP/NCAR Reanalysis (from 1948-present). The data used for this investigation is the 1° spatial resolution. While the vertical velocity of GDAS with 0.25° must be determined by vertically integrating the horizontal velocity, the vertical motion of the trajectory produced by GDAS with 1°can is computed directly from the model output vertical wind velocity[25]. Data objects with greater variability are grouped in distinct clusters, whereas clustering brings similar data objects together based on similarity[26]. This study groups comparable data using clustering rather than classification. By identifying distinct trends in atmospheric transport, this clustering technique improves the study and offers a greater understanding of air parcel movements and their possible causes.

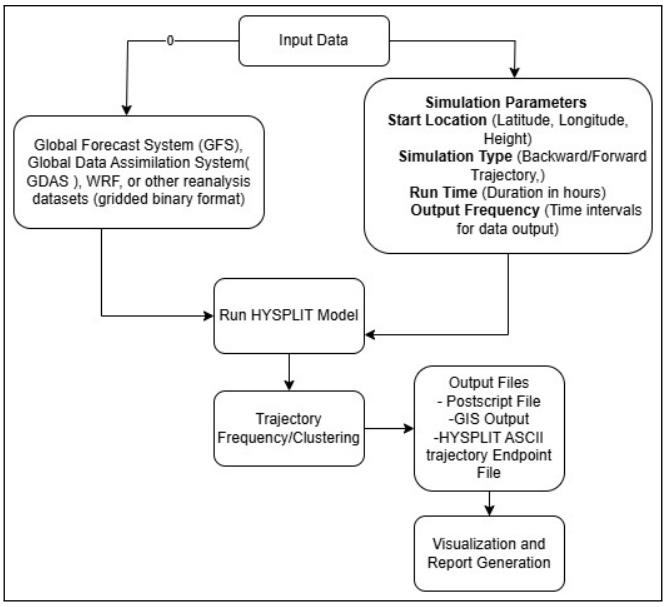

Figure 2: HYSPLIT model simulation

As shown in Figure 2, the HYSPLIT model simulation demonstrates the HYSPLIT model formulation method for trajectory analysis.It starts with input data, which can be meteorological datasets such as the Global Forecast System (GFS), Global Data Assimilation System (GDAS), or Weather Research and Forecasting (WRF) model, all in gridded binary format.The user then sets the simulation parameters, including the starting point (latitude, longitude, and height), simulation type (backward or forward trajectory), run time (hours), and output frequency.

Once these parameters are established, the HYSPLIT model is run, resulting in atmospheric trajectory simulation.The obtained trajectories go through frequency or clustering analysis, which aids in finding dominant transport channels. The model then generates output files in various forms, including PostScript, GIS outputs, and HYSPLIT ASCII. The Planetary Boundary layer was taken 500m above ground level. At 500 m above ground, within the Himalayan and Tibetan Plateau boundary layer, anthropogenic emissions increase significantly, as winter boundary layer heights typically range from 500 to 1000 m[27].

2.3 Wildfire and Black Carbon Emissions

Wildfire smoke can drift to distant mountain ranges that darken glacier surfaces, which leads to increased ice melting by up to 10% compared to simulations where the impacts of fire activity were removed[28]. The fire season, which runs from March to June, accounts for 86.3% of all recorded fires, with the highest activity occurring in April, representing 43.6% of the total, followed by March at 16.31% and May at 15.63%[17].Annually, in the Study done in the Yala Glacier,[3]. The atmospheric BC contribution from Nepal and India combined accounted for approximately 69% (ranging between 64% and 74% depending on the season). This was followed by contributions of 22% from China, 3% from Bangladesh, 2% from Pakistan, and 1% from Bhutan, with the remaining contributions coming from nearby regions[3]. Following wildfire events, BC concentrations in glacier snow and ice

have been recorded at levels higher than 20 ng/g. This suggests that wildfires have played a substantial role in accelerating glacier melt in the Himalayas, contributing to the overall retreat of these glaciers[29].Because solar radiation is the primary source of heat for surface melting on nearly all mountain glaciers, their sensitivity to black carbon-induced changes in surface reflectance is critically important for their survival[30]. According to a study done by [31], results suggest the potential advection and deposition of BC and OC aerosols in the downwind direction from Uttarakhand to Nepal, as well as over the upper Himalayan glaciated region.The fundamental formula from the IPCC Guidelines can be used to determine the black carbon emissions from wildfires[1].

$$L_{\text{fire}} = A \times M_B \times C_f \times G_{ef} \times 10^{-3}$$

Where:

- A = Area affected by fire, in square kilometers;
- M_B = Mass of biomass burned, in tons;
- C_f = Conversion factor for the type of fire;
- G_{ef} = Emission factor for black carbon (BC) from the fire;
- 10^{-3} = Scaling factor to adjust units.

The emission factors can be calculated using the study "Emission Factors for Open and Domestic Biomass Burning for Use in Atmospheric Models" [4]. Using these equations the BC emissions from various fires along the track. This approach allows for a more exact assessment of wildfire contributions to BC transport and deposition over the Khumbu Glacier.

3. Result and Discussions

3.1 Monthly Variations in BC Transport and Deposition

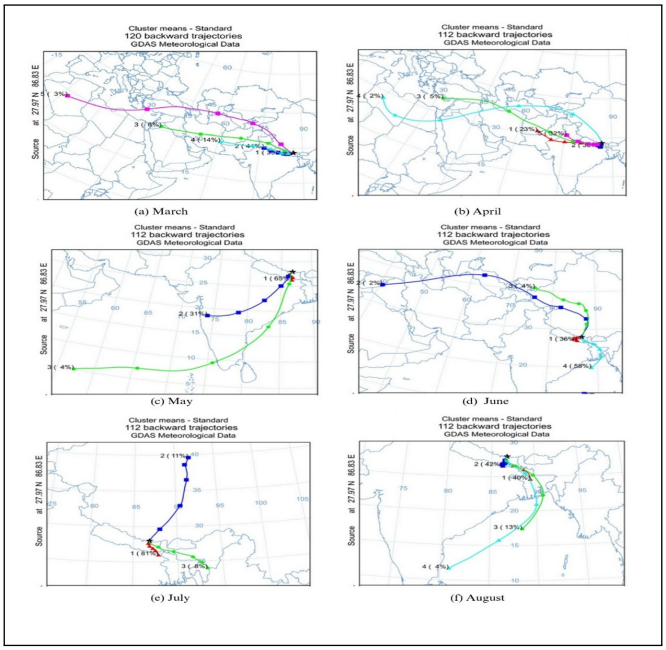

Figure 3: Potential Trajectories from March to August

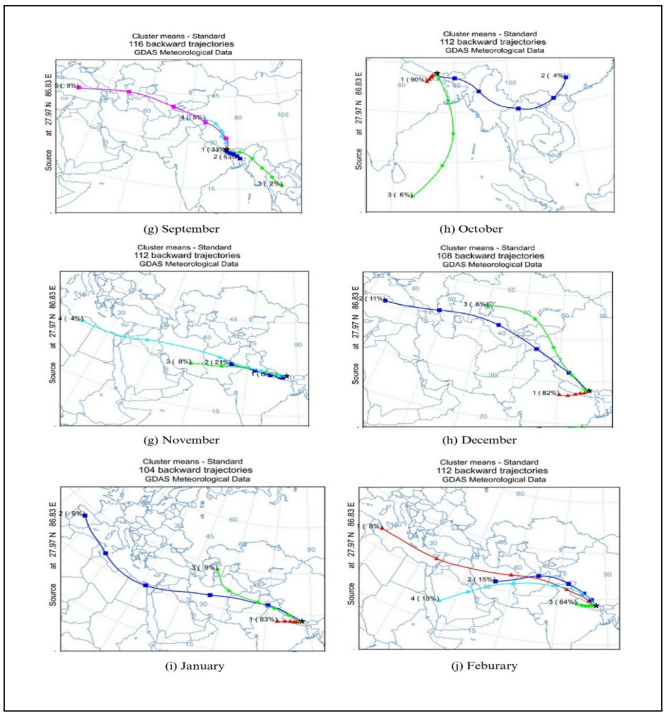

Figure 4: Potential Trajectories from September to Feburary

The HYSPLIT model was used to simulate the monthly trajectories of black carbon particles transported to the Khumbu Glacier, originating from forest fire emissions. The following sections analyze the seasonal variability in air parcel transport patterns and their implications for black carbon deposition. During March, the backward trajectory analysis indicates that air masses reaching the Khumbu Glacier primarily originate from the southwest, with significant influence from forest fire emissions in the lowland regions where the Dominant Cluster (43%) suggests strong air mass movement from a primary source following smaller clusters (33%,14%,6%,3%) shows the pre-monsoon atmospheric circulation facilitates the long-range transport of aerosols. April exhibits similar trajectory patterns, with stronger southwesterly airflows due to the increasing influence of pre-monsoon convective activity. The rising temperatures and intensified biomass burning in South Asia may have contributed to an elevated black carbon load. In May, brings a noticeable shift, with air parcels arriving from the south. The pre-monsoon period is characterized by heightened transport potential, as increased surface heating enhances atmospheric instability. This results in deeper vertical mixing and a broader spatial extent of pollutant transport.The onset of the monsoon season in June brings dispersed patterns in air parcel origins. Trajectories predominantly come from the Bay of Bengal with a dominant cluster of 58% indicating a potential dilution effect due to monsoonal precipitation. This may reduce the efficiency of black carbon deposition over the glacier, despite ongoing emissions from regional fire activity of 36%. July and August are characterized by a strong monsoonal influence, with air masses primarily originating from the Bay of Bengal and Indian Ocean. Heavy precipitation associated with the monsoon reduces atmospheric black carbon concentrations, leading to minimal deposition over the glacier. The wet scavenging effect dominates during this period. As the monsoon begins to retreat in September, there is a gradual

re-emergence of southwesterly airflows. The weakening of precipitation allows for increased aerosol transport, potentially leading to a resurgence in black carbon deposition over the glacier.October marks the transition to the post-monsoon season, with trajectories once again showing a dominant southwest influence. The drying of vegetation and resurgence of biomass burning events contribute to elevated black carbon emissions, increasing deposition risks in the Himalayan region.During November and December, air parcel trajectories indicate a strong influx from the Indo-Gangetic Plain with 83% and 64% of dominant clusters in each month, a region known for extensive agricultural burning. The stable atmospheric conditions favor pollutant accumulation, leading to significant black carbon transport toward the Khumbu Glacier.

3.2 Trajectory Frequency

Every six hours, the trajectory frequency will begin a trajectory from a single point in space and height, add up the frequency at which the trajectory crossed a grid cell, and then normalize by the total number of trajectories or endpoints. We should note that trajectory may intersect a grid cell once or multiple times.The blue contour highlights areas contributing the highest BC concentrations reaching the receptor region. Additional contours represent varying transport probabilities, providing insight into dominant atmospheric pathways. This visualization underscores the importance of targeted regional mitigation measures to address BC sources and reduce deposition impacts on the glacier.

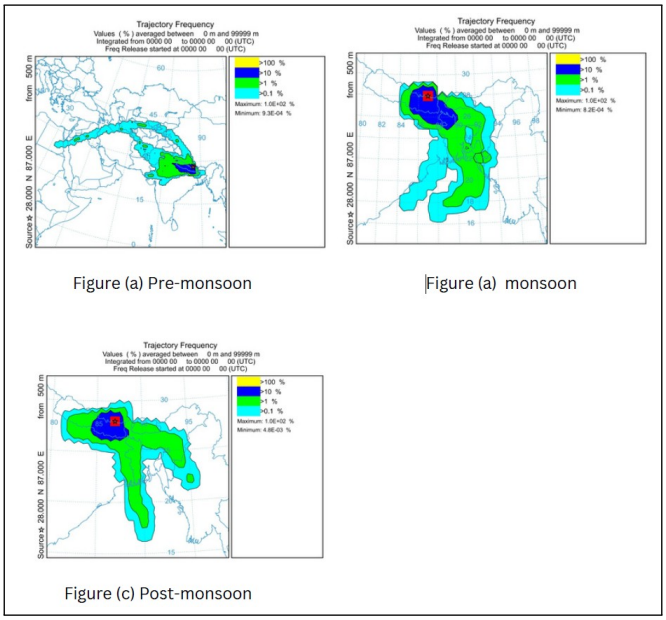

Figure 5: HYSPLIT frequency plot of five-day backward trajectories every 6 h at the Khumbu Glacier from 500 m agl in year 2021

We should note that trajectory may intersect a grid cell once or multiple times. The blue contour highlights areas contributing the highest BC concentrations reaching the receptor region. Additional contours represent varying transport probabilities, providing insight into dominant atmospheric pathways. This visualization underscores the importance of targeted regional mitigation measures to address BC sources and reduce deposition impacts on the glacier.

4. Conclusions and Recommendations

4.1 Conclusions

This trajectory frequency analysis highlights the dominant seasonal transport pathways of aerosols, black carbon, and dust affecting the Khumbu region.Understanding these transport mechanisms is crucial for assessing the Himalayas' air quality, climate dynamics, and glacial melting processes. These findings emphasize the need for emission control measures in major upwind regions to mitigate the impacts of long-range transported pollutants on the high-altitude cryosphere.To mitigate these impacts, urgent interventions are required at both national and transboundary levels.

4.2 Recommendations

To reduce black carbon (BC) inputs to the Khumbu Glacier, regional coordination among Nepal, India, China, Bangladesh, and Bhutan should be increased, with a focus on transboundary air quality monitoring and stricter biomass burning regulations.Improved wildfire management programs, such as controlled burning, early detection devices, and real-time satellite surveillance, can assist minimize emissions. Furthermore, growing research on BC source attribution using models like WRF-Chem.

Acknowledgments

The authors sincerely thank the program coordinator of the Department of Applied Sciences and Chemical Engineering, IOE, Pulchowk Campus, for all of the help, time, effort, and direction. The writers are also deeply appreciative of all the instructors who have consistently offered guidance and assistance during this process. The first author concludes by thanking his friends for contributing their thoughts and recommendations for the study.

References

[1] Sergey Kostrykin, Anastasia Revokatova, Alexey Chernenkov, Veronika Ginzburg, Polina Polumieva, and Maria Zelenova. Black carbon emissions from the siberian fires 2019: Modelling of the atmospheric transport and possible impact on the radiation balance in the arctic region. *Atmosphere*, 12(7), 2021.

[2] H.-W. Jacobi, S. Lim, M. Ménégoz, P. Ginot, P. Laj, P. Bonasoni, P. Stocchi, A. Marinoni, and Y. Arnaud. Black carbon in snow in the upper himalayan khumbu valley, nepal: observations and modeling of the impact on snow albedo, melting, and radiative forcing. *The Cryosphere*, 9(4):1685–1699, 2015.

[3] Chaman Gul, Parth Sarathi Mahapatra, Shichang Kang, Praveen Kumar Singh, Xiaokang Wu, Cenlin He, Rajesh Kumar, Mukesh Rai, Yangyang Xu, and Siva Praveen Puppala. Black carbon concentration in the central himalayas: Impact on glacier melt and potential source contribution. *Environmental Pollution*, 275:116544, 2021.

[4] S. K. Akagi, R. J. Yokelson, C. Wiedinmyer, M. J. Alvarado, J. S. Reid, T. Karl, J. D. Crounse, and P. O. Wennberg. Emission factors for open and domestic biomass burning for use in atmospheric models. *Atmospheric Chemistry and Physics*, 11(9):4039–4072, 2011.

[5] Jianjun He, Sunling Gong, Ye Yu, Lijuan Yu, Lin Wu, Hongjun Mao, Congbo Song, Suping Zhao, Hongli Liu, Xiaoyu Li, and Ruipeng Li. Air pollution characteristics and their relation to meteorological conditions during 2014–2015 in major chinese cities. *Environmental Pollution*, 223:484–496, 2017.

[6] H. Han, Y. Wu, J. Liu, T. Zhao, B. Zhuang, H. Wang, Y. Li, H. Chen, Y. Zhu, H. Liu, Q. Wang, S. Li, T. Wang, M. Xie, and M. Li. Impacts of atmospheric transport and biomass burning on the inter-annual variation in black carbon aerosols over the tibetan plateau. *Atmospheric Chemistry and Physics*, 20(21):13591–13610, 2020.

[7] Ting-Feng Dou and Cun-De Xiao. An overview of black carbon deposition and its radiative forcing over the arctic. *Advances in Climate Change Research*, 7(3):115–122, 2016. Including special topic on atmospheric black carbon and its effects on cryosphere.

[8] Susan Kaspari, S McKenzie Skiles, Ian Delaney, Daniel Dixon, and Thomas H Painter. Accelerated glacier melt on snow dome, mount olympus, washington, usa, due to deposition of black carbon and mineral dust from wildfire. *Journal of Geophysical Research: Atmospheres*, 120(7):2793–2807, 2015.

[9] X. Chen, S. Kang, Z. Cong, J. Yang, and Y. Ma. Concentration, temporal variation, and sources of black carbon in the mt. everest region retrieved by real-time observation and simulation. *Atmospheric Chemistry and Physics*, 18(17):12859–12875, 2018.

[10] A Marinoni, P Cristofanelli, Paolo Laj, R Duchi, F Calzolari, S Decesari, K Sellegri, E Vuillermoz, GP Verza, P Villani, et al. Aerosol mass and black carbon concentrations, a two year record at nco-p (5079 m, southern himalayas). *Atmospheric Chemistry and Physics*, 10(17):8551–8562, 2010.

[11] Paolo Bonasoni, Paolo Laj, Angela Marinoni, Michael Sprenger, Federico Angelini, Jgor Arduini, U Bonafè, F Calzolari, T Colombo, Stefano Decesari, et al. Atmospheric brown clouds in the himalayas: first two years of continuous observations at the nepal climate observatory-pyramid (5079 m). *Atmospheric Chemistry and Physics*, 10(15):7515–7531, 2010.

[12] Caroline Aubry-Wake, André Bertoncini, and John W Pomeroy. Fire and ice: The impact of wildfire-affected albedo and irradiance on glacier melt. *Earth's Future*, 10(4):e2022EF002685, 2022.

[13] Umanga Pandit. *Temporal Analysis of Potentially Dangerous Glacial Lakes (PDGLs) in Nepal: Assessing the Seasonal Glacial Melt Inflow into the Thulagi Glacier Lake (Dona Lake)*. PhD thesis, Kathmandu University, 2024.

[14] Kunda Dixit. In mount everest region, world's highest glaciers are melting, November 26 2018. Accessed: 2025-02-15.

[15] Gianni Tartari, Gianpietro Verza, and Laura Bertolami. Meteorological data at the pyramid observatory laboratory (khumbu valley, sagarmatha national park, nepal). *Mem. Ist. Ital. Idrobiol*, 57:23–40, 1998.

[16] P. Bonasoni, P. Laj, A. Marinoni, M. Sprenger, F. Angelini, J. Arduini, U. Bonafè, F. Calzolari, T. Colombo, S. Decesari, C. Di Biagio, A. G. di Sarra, F. Evangelisti, R. Duchi, MC. Facchini, S. Fuzzi, G. P. Gobbi, M. Maione, A. Panday, F. Roccato, K. Sellegri, H. Venzac, GP. Verza, P. Villani, E. Vuillermoz, and P. Cristofanelli. Atmospheric brown clouds in the himalayas: first two years of continuous observations at the nepal climate observatory-pyramid (5079 m). *Atmospheric Chemistry and Physics*, 10(15):7515–7531, 2010.

[17] Krishna Prasad Vadrevu, Evan Ellicott, Louis Giglio, KVS Badarinath, Eric Vermote, Chris Justice, and William KM Lau. Vegetation fires in the himalayan region–aerosol load, black carbon emissions and smoke plume heights. *Atmospheric Environment*, 47:241–251, 2012.

[18] Chao You and Chao Xu. Himalayan glaciers threatened by frequent wildfires. *Nature Geoscience*, 15(12):956–957, 2022.

[19] Christian Vincent, Patrick Wagnon, Joseph M Shea, Walter W Immerzeel, Philip Kraaijenbrink, Dibas Shrestha, Alvaro Soruco, Yves Arnaud, Fanny Brun, Etienne Berthier, et al. Reduced melt on debris-covered glaciers: investigations from changri nup glacier, nepal. *The Cryosphere*, 10(4):1845–1858, 2016.

[20] Morgan J Gibson, Tristram DL Irvine-Fynn, Patrick Wagnon, Ann V Rowan, Duncan J Quincey, Rachel Homer, and Neil F Glasser. Variations in near-surface debris temperature through the summer monsoon on khumbu glacier, nepal himalaya. *Earth Surface Processes and Landforms*, 43(13):2698–2714, 2018.

[21] H-W Jacobi, S Lim, M Ménégoz, Patrick Ginot, P Laj, P Bonasoni, P Stocchi, A Marinoni, and Yves Arnaud. Black carbon in snow in the upper himalayan khumbu valley, nepal: observations and modeling of the impact on snow albedo, melting, and radiative forcing. *The Cryosphere*, 9(4):1685–1699, 2015.

[22] Lucas Zeller, Daniel McGrath, Scott W McCoy, and Jonathan Jacquet. Seasonal to decadal dynamics of supraglacial lakes on debris-covered glaciers in the khumbu region, nepal. *The Cryosphere*, 18(2):525–541, 2024.

[23] R. R. Draxler and G. D. Rolph. Hysplit (hybrid single-particle lagrangian integrated trajectory) model access via noaa arl ready website, 2010. NOAA Air Resources Laboratory, Silver Spring, MD. Accessed: 2025-02-15.

[24] Jessica Castagna, Alfonso Senatore, Mariantonia Bencardino, Francesco D'Amore, Francesca Sprovieri, Nicola Pirrone, and Giuseppe Mendicino. Multiscale assessment of the impact on air quality of an intense wildfire season in southern italy. *Science of The Total Environment*, 761:143271, 2021.

[25] Lin Su, Zibing Yuan, Jimmy C.H. Fung, and Alexis K.H. Lau. A comparison of hysplit backward trajectories generated from two gdas datasets. *Science of The Total Environment*, 506-507:527–537, 2015.

[26] Likai Cui, Xiaoquan Song, and Guoqiang Zhong. Comparative analysis of three methods for hysplit atmospheric trajectories clustering. *Atmosphere*, 12(6), 2021.

[27] Kirpa Ram and M.M. Sarin. Spatio-temporal variability in atmospheric abundances of ec, oc and wsoc over northern india. *Journal of Aerosol Science*, 41(1):88–98, 2010. Special Issue for the 9th International Conference on Carbonaceous Particles in the Atmosphere.

[28] C. Aubry-Wake, A. Bertoncini, and J. W. Pomeroy. Fire and ice: The impact of wildfire-affected albedo and irradiance on glacier melt. *Earth's Future*, 10(4):e2022EF002685, 2022.

[29] Chao You, Tandong Yao, Baiqing Xu, Chao Xu, Huabiao Zhao, and Lili Song. Effects of sources, transport, and postdepositional processes on levoglucosan records in southeastern tibetan glaciers. *Journal of Geophysical Research: Atmospheres*, 121(14):8701–8711, 2016.

[30] Andrew J Hodson. Understanding the dynamics of black carbon and associated contaminants in glacial systems. *Wiley Interdisciplinary Reviews: Water*, 1(2):141–149, 2014.

[31] Kunal Bali, Amit Kumar Mishra, and Sachchidanand Singh. Impact of anomalous forest fire on aerosol radiative forcing and snow cover over himalayan region. *Atmospheric Environment*, 150:264–275, 2017.

9% Overall Similarity

The combined total of all matches, including overlapping sources, for each database.

Filtered from the Report

- Bibliography
- Quoted Text
- Small Matches (less than 10 words)

Match Groups

44 Not Cited or Quoted 5%
Matches with neither in-text citation nor quotation marks

29 Missing Quotations 4%
Matches that are still very similar to source material

0 Missing Citation 0%
Matches that have quotation marks, but no in-text citation

0 Cited and Quoted 0%
Matches with in-text citation present, but no quotation marks

Top Sources

6% Internet sources
6% Publications
0% Submitted works (Student Papers)

Integrity Flags

0 Integrity Flags for Review

No suspicious text manipulations found.

Our system's algorithms look deeply at a document for any inconsistencies that would set it apart from a normal submission. If we notice something strange, we flag it for you to review.

A Flag is not necessarily an indicator of a problem. However, we'd recommend you focus your attention there for further review.

Match Groups

- **44** Not Cited or Quoted 5%
  Matches with neither in-text citation nor quotation marks
- **29** Missing Quotations 4%
  Matches that are still very similar to source material
- **0** Missing Citation 0%
  Matches that have quotation marks, but no in-text citation
- **0** Cited and Quoted 0%
  Matches with in-text citation present, but no quotation marks

Top Sources

6% Internet sources
6% Publications
0% Submitted works (Student Papers)

Top Sources

The sources with the highest number of matches within the submission. Overlapping sources will not be displayed.

1	Internet	ready.arl.noaa.gov 1%
2	Publication	Chaman Gul, Parth Sarathi Mahapatra, Shichang Kang, Praveen Kumar Singh et a... <1%
3	Internet	www.researchgate.net <1%
4	Internet	data.klima.tu-berlin.de <1%
5	Internet	tc.copernicus.org <1%
6	Internet	www.science.gov <1%
7	Publication	Jessica Castagna, Alfonso Senatore, Mariantonia Bencardino, Francesco D'Amore ... <1%
8	Publication	Bali, Kunal, Amit Kumar Mishra, and Sachchidanand Singh. "Impact of anomalous... <1%
9	Publication	Xintong Chen, Shichang Kang, Zhiyuan Cong, Junhua Yang, Yaoming Ma. "Concen... <1%
10	Publication	K. Sandeep, A.S. Panicker, Alok Sagar Gautam, G. Beig, Naveen Gandhi, Sanjeev S, ... <1%

11 Internet
elibrary.tucl.edu.np <1%

12 Internet
argon.ess.washington.edu <1%

13 Internet
acp.copernicus.org <1%

14 Publication
Hodson, Andrew J.. "Understanding the dynamics of black carbon and associated ... <1%

15 Publication
Saurabh Yadav, Panuganti C. S. Devara, S. M. Sonbawne, B. S. Murthy, S. Tiwari, S. ... <1%

16 Internet
journals.plos.org <1%

17 Publication
Chao You, Chao Xu. "Himalayan glaciers threatened by frequent wildfires", Natur... <1%

18 Publication
Praveen Kumar Singh, Bhupesh Adhikary, Xintong Chen, Shichang Kang et al. "Va... <1%

19 Internet
law.resource.org <1%

20 Publication
Sergey Kostrykin, Anastasia Revokatova, Alexey Chernenkov, Veronika Ginzburg, ... <1%

21 Internet
progearthplanetsci.springeropen.com <1%

22 Publication
Panicker, A.S., Sung-Hwa Park, Dong-In Lee, Dong-Chul Kim, Woon-Seon Jung, San... <1%

23 Publication
V. A. Ginzburg, S. V. Kostrykin, A. P. Revokatova, A. G. Ryaboshapko, A. S. Pastukh... <1%

24 Internet
insideclimatenews.org <1%

25 Internet

www.gofc-gold.uni-jena.de <1%

26 Publication

Oleg Tomshin, Vladimir Solovyev. "Features of the Extreme Fire Season of 2021 in ... <1%

27 Internet

downloads.hindawi.com <1%

28 Publication

Kira Thiel, Anselm Arndt, Puyu Wang, Huilin Li, Zhongqin Li, Christoph Schneider. ... <1%

29 Internet

essay.utwente.nl <1%

30 Internet

www.iasta.org.in <1%

31 Internet

www.mdpi.com <1%

32 Internet

www.ncbi.nlm.nih.gov <1%

33 Internet

aaqr.org <1%

34 Publication

Chaman Gul, Cenlin He, Shichang Kang, Yangyang Xu et al. "Measured black carb... <1%

35 Publication

Fengxiang Guo, Jiayue Sun, Die Hu. "Surface energy balance-based surface urban ... <1%

36 Publication

John Hulth, Cecilie Rolstad, Karoline Trondsen, Ragnhild Wedøe Rødby. "Surface ... <1%

37 Publication

K.L. Chan. "Biomass burning sources and their contributions to the local air qualit... <1%

38 Publication

M.A. Hernández-Ceballos, M. Sangiorgi, B. García-Puerta, M. Montero, C. Trueba. "... <1%

39 Internet

developers.google.com <1%

40 Internet

hikingbees.com <1%

41 Internet

www.ipcc.ch <1%

42 Internet

www.researchandmarkets.com <1%

43 Internet

www3.epa.gov <1%